



Calhoun: The NPS Institutional Archive

Theses and Dissertations

Thesis Collection

1957-06

Angular distribution of protons from the Co(59) (d.p.)Co(60) reaction

Jarrell, Donald Lee

Massachusetts Institute of Technology, 1957.

<http://hdl.handle.net/10945/26379>



Calhoun is a project of the Dudley Knox Library at NPS, furthering the precepts and goals of open government and government transparency. All information contained herein has been approved for release by the NPS Public Affairs Officer.

Dudley Knox Library / Naval Postgraduate School
411 Dyer Road / 1 University Circle
Monterey, California USA 93943

<http://www.nps.edu/library>

**ANGULAR DISTRIBUTION OF PROTONS
FROM THE $\text{Co}^{59}(\text{d}, \text{p})\text{Co}^{60}$ REACTION**

**Donald Lee Jarrell
and
Cornell Carpenter Angleman**

ANGULAR DISTRIBUTION OF PROTONS
FROM THE $\text{Co}^{59}(\text{d},\text{p})\text{Co}^{60}$ REACTION

by

Donald Lee Jarrell
B. S., United States Naval Academy
(1950)

and

Cornell Carpenter Angleman
B. S., United States Naval Academy
(1950)

SUBMITTED IN PARTIAL FULFILLMENT OF
THE REQUIREMENTS FOR THE DEGREE OF

MASTER OF SCIENCE

at the

MASSACHUSETTS INSTITUTE OF TECHNOLOGY

June 1957

ANGULAR DISTRIBUTIONS OF PROTONS FROM THE

$\text{Co}^{59}(\text{d},\text{p})\text{Co}^{60}$ REACTION

by

Donald Lee Jarrell
Lieutenant, U. S. Navy

and

Cornell Carpenter Angleman
Lieutenant, U. S. Navy

Submitted to the Department of Physics on May 20, 1957
in partial fulfillment of the degree of

MASTER OF SCIENCE

ABSTRACT

The MIT-ONR electrostatic accelerator and broad-range magnetic spectrograph have been used to investigate the $\text{Co}^{59}(\text{d},\text{p})\text{Co}^{60}$ reaction by bombarding a thin target of cobalt on Formvar with 6.0-Mev deuterons. An analysis of the proton groups for sixteen reaction angles between 10 and 110 degrees determined the angular distribution of the cross section and the Q-values for sixty levels of Co^{60} up to 3.7-Mev excitation. The ground-level Q-value was determined to be 5.262 ± 0.011 Mev. Some of the levels observed have not been previously reported, and the Q-values of the other levels are in agreement with those previously observed by (d,p) and (n, γ) reactions. One previously reported level at a Q of 2.659 Mev was not observed. The present values remove some small discrepancies between those of the (d,p) and (n, γ) reactions.

From the angular distributions of this work, the reaction was observed to proceed predominantly by stripping. They have been compared with the predictions of Butler's stripping theory in order to assign values of ℓ_n , the orbital angular momentum of the captured neutron, to thirty-seven levels. It was observed that most of the distributions required superposition of curves corresponding to two values of ℓ_n . Results obtained endorse the recently assigned values of $J = 5^+$ for the ground level and $J = 2^+$ for the metastable state, instead of the previously reported values of 4^+ and 1^+ , respectively.

Thesis Supervisor: Harald A. Enge

Title: Assistant Professor of Physics

35887

ANALYSIS OF THE DATA

CO₂ (5.2) NO₂ (5.2)

by

Donald Lee Jorrell
Lieutenant, U. S. Navy

and

Correll Carpenter
Lieutenant, U. S. Navy

Submitted to the Department of Physics on May 10, 1957
in partial fulfillment of the degree of

MASTER OF SCIENCE

ABSTRACT

The KIV-ONE spectroscopic apparatus and associated magnetic spectrometer have been used to investigate the $^{235}\text{U}(n,f)$ reaction by bombarding a thin target of cobalt in a vacuum with 0.045 Mev neutrons. An analysis of the proton groups for various reaction angles between 10 and 110 degrees determined the angular distribution of the cross section and the α -values for alpha levels of Co⁵⁷ in the 0.011 Mev. Some of the levels observed have not been previously reported, and the α -values of the other levels are in excellent agreement with those previously observed by (1,2) and (3,4) reactions. The cross section reported level at 1.15 Mev was not observed. The cross section values show small discrepancies between those of the (0,0) and (0,1) reactions.

From the angular distribution of this work, the reaction was observed to proceed predominantly by stripping. This has been compared with the prediction of Butler's stripping theory in order to obtain values of α , the orbital angular momentum of the captured neutron, for thirty-seven levels. It was observed that most of the distributions required assignment of values corresponding to $\alpha = 0$ or $\alpha = 1$. Results obtained indicate the reaction is a stripping reaction. The α values for the ground level and $\alpha = 1$ for the other levels were, respectively, instead of the previously reported values of $\alpha = 0$ and $\alpha = 1$, respectively.

Physics Department, Cornell University
Ithaca, New York

ACKNOWLEDGMENTS

The authors wish to express their appreciation and thanks to all of the members of the High Voltage Laboratory for their friendly assistance and cooperation, without which this work could not have been accomplished.

We are indebted to Professors W. W. Buechner and H. A. Enge for proposing this investigation. Professor Enge was a most patient and helpful adviser. We wish to express our thanks to Dr. C. H. Paris, Mr. A. Sperduto, and Mr. M. Mazari for their kind consideration of our many questions.

We should like to thank Mrs. Grace Rowe for the careful preparation of the numerous graphs in the thesis, Miss Estelle Freedman and Mr. W. A. Tripp for the tedious job of counting the tracks on the photographic plates, and Mr. E. W. Nickerson for his advice and assistance with mechanical problems.

Finally, we wish to thank Mrs. Mary E. White for her excellent preparation of the manuscript.

MEMORANDUM

The subject is the request for information and data in all of the records of the High School regarding the health condition and cooperation of students with the school and home.

We are indebted to Mr. J. H. Brown and Mr. A. L. Brown for providing this information. Mr. J. H. Brown and Mr. A. L. Brown are both helpful and willing to assist in the work of the school. Mr. J. H. Brown and Mr. A. L. Brown are both helpful and willing to assist in the work of the school.

It should be noted that the work of the school is not only a matter of the school but also a matter of the community. The work of the school is not only a matter of the school but also a matter of the community. The work of the school is not only a matter of the school but also a matter of the community.

Finally, we wish to thank Mr. J. H. Brown and Mr. A. L. Brown for their assistance in the work of the school.

TABLE OF CONTENTS

	Page Number
I. INTRODUCTION	1
II. APPARATUS	6
III. EXPERIMENTAL PROCEDURE	14
IV. RESULTS	24
PROBABLE ERRORS	24
DISCUSSION OF Q-VALUES AND COMPARISON WITH PREVIOUS WORK	28
STRIPPING THEORY	39
ANGULAR DISTRIBUTIONS	42
V. CONCLUSIONS	80
BIBLIOGRAPHY	

TABLE OF CONTENTS

Page
Number

i

I. INTRODUCTION

ii

II. STATEMENT

iii

III. EXPLANATION OF THE

iv

IV. RESULTS

v

CONCLUSIONS

vi

REMARKS ON THE RESULTS
OBTAINED BY THE METHOD

vii

APPENDIX

viii

EXPLANATION OF THE

ix

V. SUMMARY

INDEX

I. INTRODUCTION

The MIT-ONR electrostatic accelerator is being used in a program of study of deuteron stripping reactions. This reaction is a valuable tool in nuclear spectroscopy as an aid in the determination of the angular momentum and parity of ground and excited levels of various nuclides.

The element cobalt has been the object of several studies of the beta-ray and gamma-ray decay of its isotopes. Charged-particle studies of Co^{59} by proton bombardment¹ and of Co^{60} through the $\text{Co}^{59}(\text{d},\text{p})\text{Co}^{60}$ reaction² have been done at the High Voltage Laboratory of the Massachusetts Institute of Technology.

We have chosen the investigation of the angular distribution of protons from the $\text{Co}^{59}(\text{d},\text{p})\text{Co}^{60}$ reaction in an effort to resolve an uncertainty in the Q-value for the ground level of Co^{60} , to determine more fully the excited levels of Co^{60} , and to furnish more information on the angular momentum and parity of these excited levels.

The work of Bartholomew and Kinsey³ results in a Q-value for the ground level of 5.260 ± 0.007 Mev, determined by subtracting the binding energy of the deuteron from their highest energy gamma ray. The $\text{Co}^{59}(\text{d},\text{p})\text{Co}^{60}$ work of Foglesong and Foxwell² gave a Q-value of 5.283 ± 0.008 Mev, a difference of 23 kev.

On the basis of the "shell model," ${}_{27}^{59}\text{Co}_{32}$ has a single "hole" in the proton $1f_{7/2}$ shell, and the position of the four neutrons above the $1f_{7/2}$ shell is somewhat in doubt. The states

1. INTRODUCTION

The fitting of a statistical model to a set of data is a process of trial and error. The model is chosen on the basis of a preliminary examination of the data. The model is then fitted to the data and the results are compared with the original data. If the model is not satisfactory, a new model is chosen and the process is repeated.

The first step in the fitting of a statistical model is the choice of a model. The model is chosen on the basis of a preliminary examination of the data. The model is then fitted to the data and the results are compared with the original data. If the model is not satisfactory, a new model is chosen and the process is repeated.

The second step in the fitting of a statistical model is the choice of a model. The model is chosen on the basis of a preliminary examination of the data. The model is then fitted to the data and the results are compared with the original data. If the model is not satisfactory, a new model is chosen and the process is repeated.

The third step in the fitting of a statistical model is the choice of a model. The model is chosen on the basis of a preliminary examination of the data. The model is then fitted to the data and the results are compared with the original data. If the model is not satisfactory, a new model is chosen and the process is repeated.

The fourth step in the fitting of a statistical model is the choice of a model. The model is chosen on the basis of a preliminary examination of the data. The model is then fitted to the data and the results are compared with the original data. If the model is not satisfactory, a new model is chosen and the process is repeated.

$2p_{3/2}$ and $1f_{5/2}$ lie very close together.⁴ Whether the addition of a neutron to an odd one in the $2p_{3/2}$ state would cause the pair to jump from the $2p_{3/2}$ state to the $1f_{5/2}$ state depends on the magnitude of the difference of the pairing energies $P_{f_{5/2}} - P_{p_{3/2}}$ relative to the level distance $\epsilon_{f_{5/2}} - \epsilon_{p_{3/2}}$. It is possible to show⁴ that the order of filling these levels might proceed by three different schemes for configurations of 1, 2, 3, 4, 5, and 6 neutrons:

- a. $(p_{3/2})^1; (f_{5/2})^2; (p_{3/2})^1(f_{5/2})^2; (f_{5/2})^4; (p_{3/2})^1(f_{5/2})^4; (f_{5/2})^6.$
- b. $(p_{3/2})^1; (p_{3/2})^2; (p_{3/2})^3; (p_{3/2})^4; (p_{3/2})^3(f_{5/2})^2; (p_{3/2})^4(f_{5/2})^2.$
- c. $(p_{3/2})^1; (p_{3/2})^2; (p_{3/2})^3; (p_{3/2})^4; (p_{3/2})^4(f_{5/2})^1; (p_{3/2})^4(f_{5/2})^2.$

The experimental evidence for the magnetic moments of Co^{58} ⁵ and Co^{60} ^{6,7} compared with the calculated magnetic moments⁴ indicate the assignments of the thirty-first neutron in Co^{58} to the $f_{5/2}$ state and the thirty-third neutron in Co^{60} to the $p_{3/2}$ state, with three neutrons in the $p_{3/2}$ state and two neutrons in the $f_{5/2}$ state. Thus, it would seem that the neutrons fill in the following manner for three, four, and five neutrons:

$$(p_{3/2})^2(f_{5/2})^1; (p_{3/2})^2(f_{5/2})^2; (p_{3/2})^3(f_{5/2})^2.$$

This is not in accord with the schemes mentioned above but would seem to be a reasonable interpretation of data available.

A survey of present data on the angular momentum and parities of Co^{60} is presented in Figure 1. The 1.48-Mev beta ray from the ground level of Co^{60} to the 1.33-Mev level of Ni^{61} was first reported by Keister and Schmidt⁸ to have a shape corresponding to $\Delta J = 2$, no, and hence led to the angular momentum and parity assignments of 4^+ and 1^+ to the ground and metastable levels, respectively, in contrast to the previously reported values of 5^+ and 2^+ .⁹ More recent work by Dobrowolski et al⁶, using the method of paramagnetic resonance to measure the angular momentum and magnetic moment, and by Wolfson¹⁰ on the 1.48-Mev beta ray, obtaining $\Delta J = 3$, no, leads to confirmation of the values of 5^+ and 2^+ .

The use of the deuteron stripping reaction as a means of assigning values of angular momentum to various energy levels of a nucleus is based on the pronounced maxima in a forward direction of the emergent particle. These maxima may be characterized by values of l_n , the orbital angular momentum of the captured nucleon. The angle at which a maximum occurs is a measure of the l_n value. Knowledge of the angular momentum and parity of the initial nucleus, together with the observed l_n value, will determine the parity of the residual nucleus and allowed values of the angular momentum.

Several theories accounting for the stripping maxima in the intermediate energy region have been published, notably by Butler¹¹, Bhatia et al¹², Daitch and French¹³, Friedman and Tobocman¹⁴, and others. In this investigation, an angular distribution formula from the noncoulomb stripping theory of Friedman and Tobocman¹⁴ is used,

A survey of several data on the regular minimum and maximum values of α is presented in Figure 1. The 1.5-day data are from the former level of α and the 1.5-day level of α are from the latter level of α . It is seen that a slight correspondence is observed between the two levels of α and the 1.5-day data are slightly higher than the 1.5-day data. The 1.5-day data are slightly higher than the 1.5-day data.

The use of the constant angular velocity as a means of

the conclusion regarding theory of vitamins and tobacco¹¹ is good, others. In this investigation, as regular distribution occurs from intake of 21¹², 1000 and 1000¹³, 1000 and 1000¹⁴, and 1000 and 1000¹⁵ cigarettes per day, it is evident that the

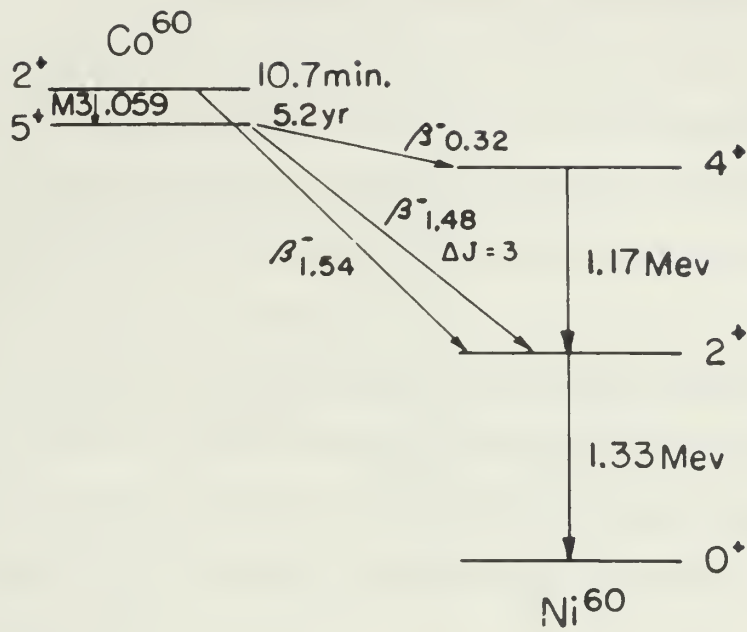


Figure 1

ENERGY LEVEL DIAGRAM SHOWING
DECAY SCHEME OF Co⁶⁰

(Ref. 6, 7, 9, 10)

together with tables and graphs prepared by Enge and Graue¹⁵ for numerical calculations of the theoretical angular distribution curves.

The use of the MIT-ONR electrostatic generator and the broad-range magnetic spectrograph enabled us to investigate the Q-values and angular distributions of protons from the $\text{Co}^{59}(\text{d},\text{p})\text{Co}^{60}$ reaction simultaneously. The investigation was carried out at energies of 6.01 and 6.18 Mev. The proton groups associated with the ground and excited levels were observed at seventeen angles between 5 and 110 degrees.

Sixty Q-values, corresponding to the ground level and fifty-nine excited levels of Co^{60} , were determined. Angular distribution curves and values of l_n for the ground level and twenty-five excited levels were calculated. Tentative assignments of l_n were given to eleven other levels.

calculated with tables and graphs prepared by W. G. and G. W. for
numerical calculations of the theoretical angular distribution
curves.

The use of the BETHE electronic energy loss formula and the
presented angular distribution curves enabled us to investigate the
g-values and angular distributions of protons from the
 ^{60}Co source. The investigation was per-
formed at energies of 0.01 and 0.1 MeV. The proton source was
related with the ground and excited levels were observed at various
angles between 2 and 110 degrees.

Eighty g-values, corresponding to the ground level and fifty-
nine excited levels of ^{60}Co , were determined. Angular distribu-
tion curves and values of μ for the ground level and twenty-five
excited levels were calculated. Tentative assignments of μ were
given to eleven other levels.

II. APPARATUS

The major equipment used in this investigation consisted of the MIT-ONR electrostatic accelerator¹⁶ and the associated deflecting magnet, a collimating slit system, target chamber, and the broad-range magnetic spectrograph¹⁷.

The major characteristic of a Van de Graaff generator used as a particle accelerator is the small energy spread possible (approximately 0.1 percent). The MIT-ONR generator has a range of normal operation of 5.0 to 7.5 Mev with a beam intensity upwards of 0.3 microamperes.

The physical features of the accelerator are shown in Figure 2. The energy of the particle beam is defined and controlled by the collimating slit system and the deflecting magnet. The particles are accelerated downward into the deflecting magnet and are then deflected through a 90-degree arc which has a radius of 60 centimeters by a given magnetic field which determines the momentum allowed to pass through the magnet.

By means of adjustable shims at the entrance and exit faces of the magnet, the beam was focused on a set of defining slits placed 185 centimeters from the exit face of the magnet¹⁶. The slit jaws are insulated, and the currents collected on them are used to control a corona current to the generator terminal, thus providing voltage control.

The particle beam then enters the target chamber (Figure 3) and provides a sharply defined beam impinging on a fixed position

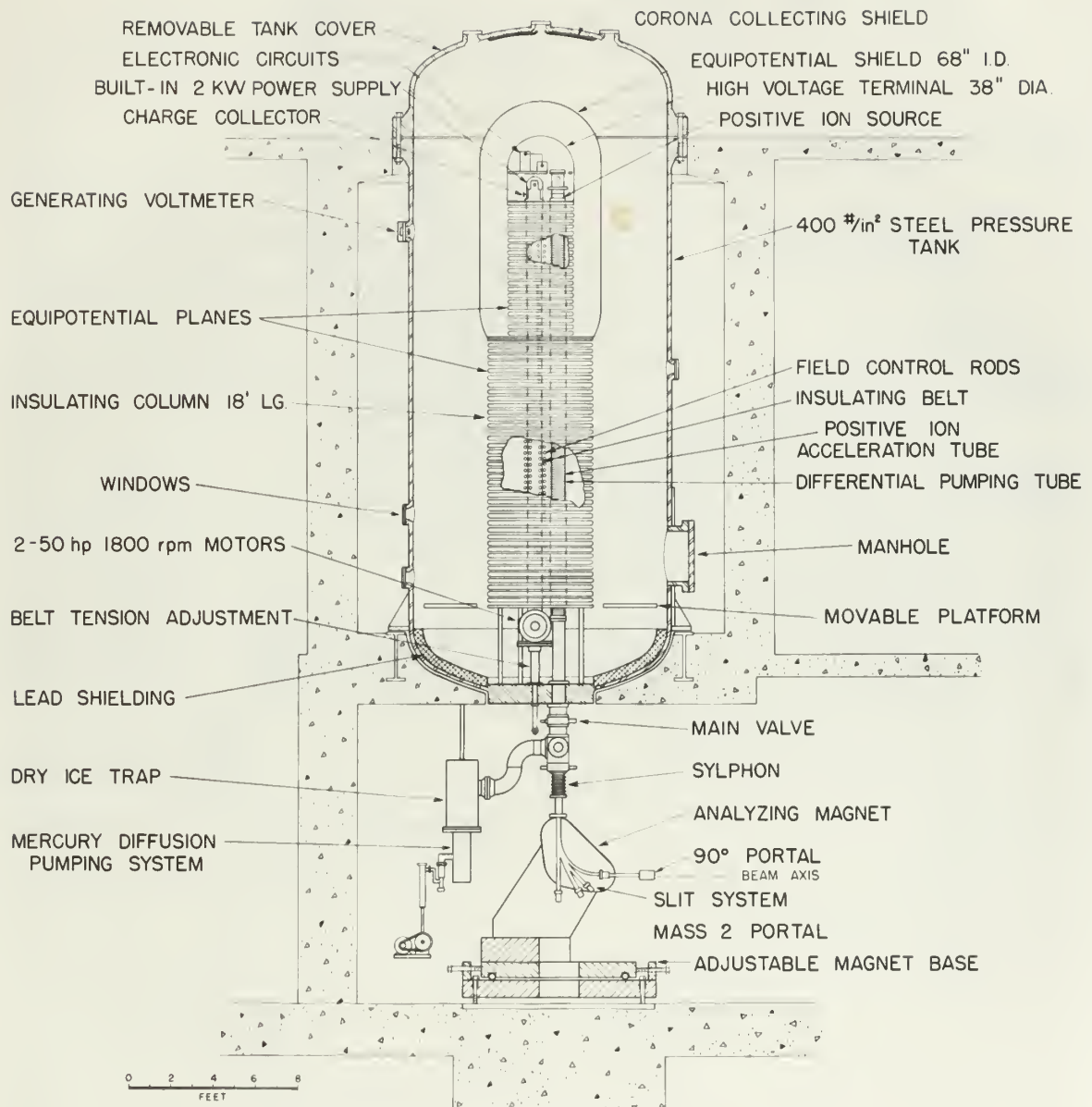
The following information was obtained from the records of the Bureau of Prisons, Washington, D.C., and the Department of Justice, Office of the Inspector General, Washington, D.C.

The paper is devoted to a study of the properties of the solutions of the system of equations (1) for the case of a periodic motion of the body. The results of the calculations are presented in the form of graphs and tables. The calculations were performed on a BESM-6 computer.

The medical features of the condition are given in Table 1. The group of 10 patients was divided into two subgroups: 5 patients with the following features: (1) the condition was present at birth; (2) the condition was present at birth; (3) the condition was present at birth; (4) the condition was present at birth; (5) the condition was present at birth.

[illegible]

and provides a strongly defined non-binding in a fixed position.



POSITIVE ION ACCELERATOR FOR M.I.T.

Figure 2

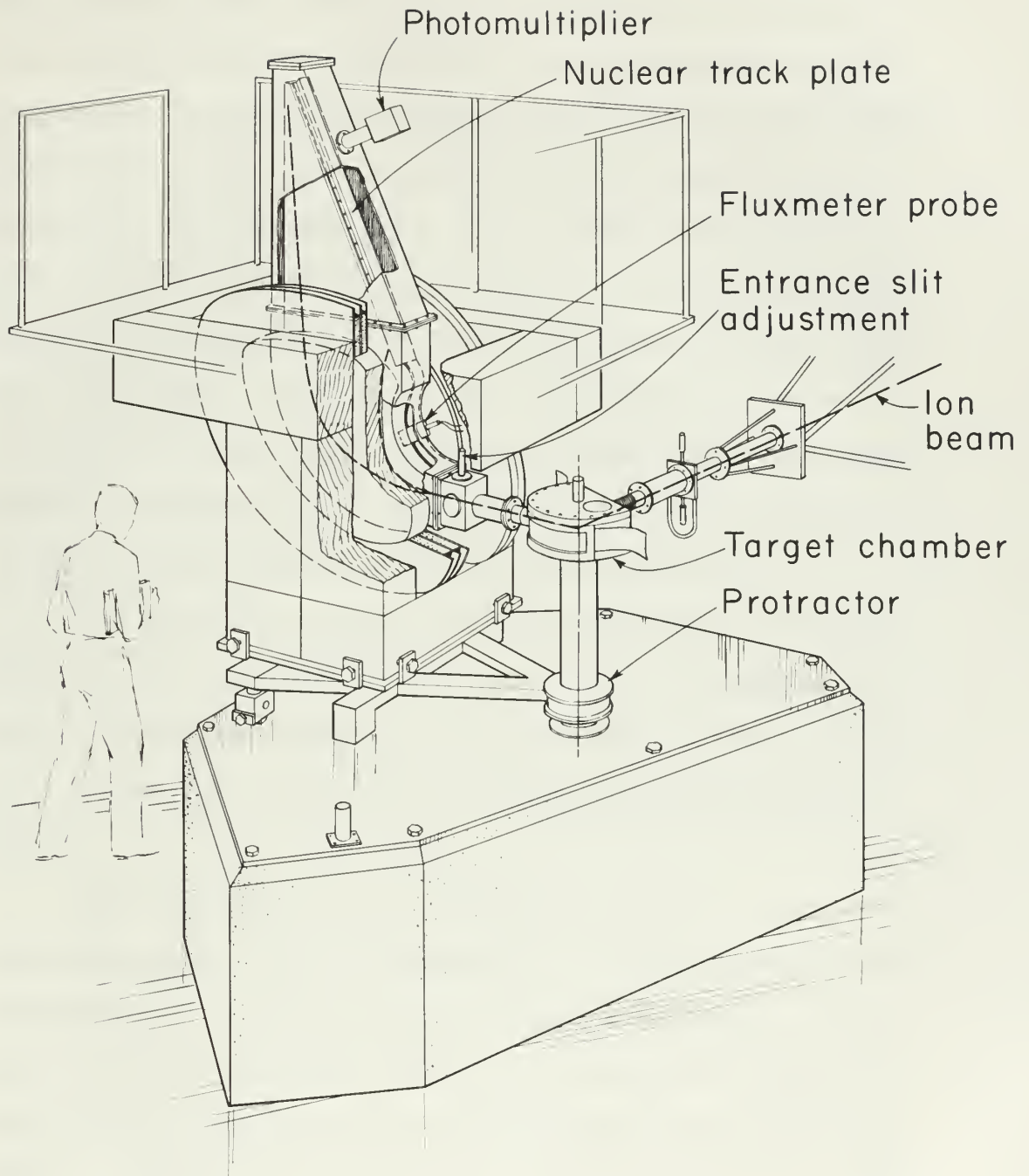


Figure 3

on the target. The particles from the target which emerge into the acceptance angle of the broad-range magnetic spectrograph are deflected with a radius proportional to their momentum. They are recorded on three ten-inch long Eastman NTA 25-micron photographic plates positioned at the top of the spectrograph, as shown in Figure 3. The photographic plates are contained in a plateholder and conform to a hyperbolic focal surface. They are indexed when in the plateholder by a set of razor-edged slits illuminated from below which give a set of sharp lines approximately 7 centimeters apart for the entire length of the photographic plate. These slits provide a reference for a measure of distance along the plates used when the particle tracks are counted after an exposure.

The magnetic spectrograph may be rotated about a vertical axis through the point at which the beam hits the target. Angles from 0 to 130 degrees with respect to the beam line from the accelerator may be used with a position error of less than 10 minutes of arc¹⁸.

The solid angle of the spectrograph has been shown to be independent of the angle of observation. It is defined by an entrance aperture to the spectrograph and by an 8-millimeter wide slit in front of the focal surface. The aperture angle may be varied, but is used for normal work with a half-angle of about $2\frac{1}{2}$ degrees. The solid angle on the focal surface is about 3.4×10^{-4} steradian for a given peak at a distance along the plate of 52 centimeters. Since particles of different momenta are magnetically

on the target. The position from the target was varied from
the maximum angle of the beam-throwing mechanism to the
deflected with a certain proportion to their number. They are
recorded on five two-inch long scales the distance between

plates provided at the top of the apparatus, as shown in
Figure 3. The photographic plates are mounted in a glass
and contain a hypodermic local surface. The one shown was
in the plateholder by a set of four-edges with dimensions from
below which give a set of four lines approximately 7 centimeters
apart for the entire length of the photographic plate. These also
provide a reference for a change in distance along the plates and
that the points shown are mounted after an exposure.

The magnetic photograph may be rotated about a vertical
axis through the point at which the beam hits the target. Hence
from 0 to 180 degrees with respect to the beam from the source
refer may be used with a position error of less than 10 minutes of

arc.

The solid angle of the photograph has been shown to be
independent of the angle of observation. It is defined by an ex-
treme aperture in the photograph and is an independent value
with the front of the local surface. The aperture angle may be
varied, but the normal with a half-angle of about 15
degrees. The solid angle to the local surface is about 1.5 x 10⁻⁴
steradians for a given area at a distance along the beam of 10 cm.
Hence, since portions of different size are separately

deflected through different radii, they are recorded at different points on the focal surface. Since each position on the photographic plates corresponds to a different distance traveled by the particles, the solid angle varies with position on the plate. This variation is corrected for by using the experimental curve given by Browne and Buechner¹⁷.

The magnetic fields in the deflecting and spectrograph magnets are determined by a nuclear resonance technique, using the known gyromagnetic ratio of the Li^7 nucleus. This consists of measuring the Larmor precession frequency using resonance induction of Li^7 or of a proton in an aqueous solution of LiCl . The LiCl is contained in a small glass capsule positioned in the pole gap of the magnets. A secondary frequency standard is used for the frequency measurement and is calibrated against the broadcast frequency standard of the Bureau of Standards station WWV.

Thin targets are necessary in charged-particle work, since sharply defined groups of reaction particles result, thus taking advantage of the resolving power of the apparatus. The work of Fogleson and Foxwell² was done at 90 degrees on a comparatively thick cobalt layer evaporated onto platinum sheet. The present work, using transmission through the target for all angles less than 90 degrees, required the use of a thin cobalt layer on thin Formvar film.

Circular (about 1-inch diameter) target frames were covered with four double layers of Formvar. The thickness of the Formvar was measured by means of an alpha-particle thickness gauge developed

by Enge, Wahlig, and Aanderaa¹⁹. The average thickness was found to be about 13 mils air equivalent.

Co⁵⁹ in the form of cobalt sponge obtained from Johnson, Matthey and Company, London, was evaporated under vacuum in a steel tank using a tungsten crucible. The tungsten was in strip form one-quarter inch wide and 20 mils in thickness; the strip was ground down in a small area to about 10-mils thickness to form a "boat." By passing a current through the tungsten strip, the cobalt was heated to a temperature above the melting point and allowed to evaporate. The evaporation was allowed to proceed until no cobalt remained in the boat. The temperature had to be controlled to within quite narrow limits in order to achieve evaporation but yet not destroy the Formvar backing by excessive heat. Some fifteen evaporation attempts were made before securing the necessary number of targets. After evaporation, the thickness of the cobalt was measured by measuring the thickness of the cobalt plus Formvar and subtracting the thickness of the Formvar.

The targets were placed in the target chamber shown in Figure 3. This chamber is insulated from ground and has small apertures for the entrance of the particle beam and for the exit of emergent particles into the spectrograph. The secondary electrons from nearby energy-analyzing slits are prevented from entering by insulating the entrance aperture from the target chamber and biasing to -300 volts. The amount of particle charge collected

in the target chamber is measured by a combined current integrator and sensitive microammeter²⁰, with an accuracy better than 1 percent for the beam currents used.

In order to reduce the surface contamination buildup and to insure better heat removal, the targets were placed in a rotating target mount²¹. This consists of a geared target holder driven with a flexible shaft by a D. C. motor. Magnetic coupling is used to transmit drive power through the lid of the target chamber. Speed of rotation is approximately one revolution per second.

After the photographic plates are exposed and developed, they are counted by mounting them on an accurate traveling stage and observing the tracks by use of a binocular microscope, with a Leitz dark-field illuminator source. For normal track size and intensity, a 20X objective is used, defining a one-half millimeter square. For very dense peaks or short tracks, a 43X objective is used which defines a field of view of about one-quarter millimeter square. The number of particle tracks across the exposed strip is plotted against distance along the plates. The position of the point at one-third the peak height on the high-energy side of the peak has been used as a measure of the position of a group²². The distance is measured to an accuracy of ± 0.1 millimeter or better. With the distance known, the corresponding value of ρ , the radius of curvature of a given peak, is found from the calibration curve. This is multiplied by B, the known magnetic field of the spectrograph. This gives the value $B\rho$, the momentum of the particle, and, since the type of particle is

and, in the case of the *Chrysomelidae*, the *Chrysomelidae* are the most common group of insects found on the leaves of the plants. The *Chrysomelidae* are the most common group of insects found on the leaves of the plants. The *Chrysomelidae* are the most common group of insects found on the leaves of the plants.

[illegible][illegible]

an answer of ± 0.1 millimeter or better. With the following values
a measure of the position of $\pm 10\mu$. The distance is measured in
the peak height on the right-hand side of the wave and used as
distance along the axis. The position of the peak on the left-hand

the corresponding value of ρ , the radius of curvature of a given curve, is found from the information given. This is indicated by 2, the second numeric label of the photographs. This gives the value for the curvature of the particle, and, since the time of capture is

known, use may be made of tables of $B\rho$ versus energy²³ to find the energy of the emergent particles.

Calibration of the magnetic spectrograph¹⁷ is based on the accurately known momentum of polonium alpha particles. A polonium-coated silver wire is placed accurately in the target chamber in the same position as the beam spot on the target. Then exposures are made at various values of field strength of the spectrograph. This places the alpha particles at different positions along the photographic plate and provides the relation between distance along the plate versus radius of curvature. The value of 331.59 kilogauss centimeters for polonium alpha particles is used. The calibration error is found to be about ± 0.04 percent in particle energy.

known, and we are sure of finding it in every case.

Copyright © 1999 by John Wiley & Sons, Inc.

add the number 12 72

Source: *U.S. Census Bureau, Statistical Abstract of the United States, 1967*

THESE RESULTS WERE REPRODUCED BY OTHER RESEARCHERS.

Agreement will be given if it is in the best interests of the child.

This journal has been published by the American Psychological Association or one of its allied publishers. This article is intended solely for the personal use of the individual user and is not to be disseminated broadly.

biochemicals like the protein and amino acids

the photo shows evidence of a possible

Copyright © 2004 by John Wiley & Sons, Inc.

provided error is taken to be ± 0.01 percent in weight.

1999, 2000, 2001, 2002, 2003, 2004, 2005, 2006, 2007, 2008, 2009, 2010, 2011, 2012, 2013, 2014, 2015, 2016, 2017, 2018, 2019, 2020, 2021, 2022, 2023, 2024, 2025, 2026, 2027, 2028, 2029, 2030, 2031, 2032, 2033, 2034, 2035, 2036, 2037, 2038, 2039, 2040, 2041, 2042, 2043, 2044, 2045, 2046, 2047, 2048, 2049, 2050, 2051, 2052, 2053, 2054, 2055, 2056, 2057, 2058, 2059, 2060, 2061, 2062, 2063, 2064, 2065, 2066, 2067, 2068, 2069, 2070, 2071, 2072, 2073, 2074, 2075, 2076, 2077, 2078, 2079, 2080, 2081, 2082, 2083, 2084, 2085, 2086, 2087, 2088, 2089, 2090, 2091, 2092, 2093, 2094, 2095, 2096, 2097, 2098, 2099, 2100, 2101, 2102, 2103, 2104, 2105, 2106, 2107, 2108, 2109, 2110, 2111, 2112, 2113, 2114, 2115, 2116, 2117, 2118, 2119, 2120, 2121, 2122, 2123, 2124, 2125, 2126, 2127, 2128, 2129, 2130, 2131, 2132, 2133, 2134, 2135, 2136, 2137, 2138, 2139, 2140, 2141, 2142, 2143, 2144, 2145, 2146, 2147, 2148, 2149, 2150, 2151, 2152, 2153, 2154, 2155, 2156, 2157, 2158, 2159, 2160, 2161, 2162, 2163, 2164, 2165, 2166, 2167, 2168, 2169, 2170, 2171, 2172, 2173, 2174, 2175, 2176, 2177, 2178, 2179, 2180, 2181, 2182, 2183, 2184, 2185, 2186, 2187, 2188, 2189, 2190, 2191, 2192, 2193, 2194, 2195, 2196, 2197, 2198, 2199, 2200, 2201, 2202, 2203, 2204, 2205, 2206, 2207, 2208, 2209, 2210, 2211, 2212, 2213, 2214, 2215, 2216, 2217, 2218, 2219, 2220, 2221, 2222, 2223, 2224, 2225, 2226, 2227, 2228, 2229, 2230, 2231, 2232, 2233, 2234, 2235, 2236, 2237, 2238, 2239, 2240, 2241, 2242, 2243, 2244, 2245, 2246, 2247, 2248, 2249, 2250, 2251, 2252, 2253, 2254, 2255, 2256, 2257, 2258, 2259, 2260, 2261, 2262, 2263, 2264, 2265, 2266, 2267, 2268, 2269, 2270, 2271, 2272, 2273, 2274, 2275, 2276, 2277, 2278, 2279, 2280, 2281, 2282, 2283, 2284, 2285, 2286, 2287, 2288, 2289, 2290, 2291, 2292, 2293, 2294, 2295, 2296, 2297, 2298, 2299, 2300, 2301, 2302, 2303, 2304, 2305, 2306, 2307, 2308, 2309, 2310, 2311, 2312, 2313, 2314, 2315, 2316, 2317, 2318, 2319, 2320, 2321, 2322, 2323, 2324, 2325, 2326, 2327, 2328, 2329, 2330, 2331, 2332, 2333, 2334, 2335, 2336, 2337, 2338, 2339, 2340, 2341, 2342, 2343, 2344, 2345, 2346, 2347, 2348, 2349, 2350, 2351, 2352, 2353, 2354, 2355, 2356, 2357, 2358, 2359, 2360, 2361, 2362, 2363, 2364, 2365, 2366, 2367, 2368, 2369, 2370, 2371, 2372, 2373, 2374, 2375, 2376, 2377, 2378, 2379, 2380, 2381, 2382, 2383, 2384, 2385, 2386, 2387, 2388, 2389, 2390, 2391, 2392, 2393, 2394, 2395, 2396, 2397, 2398, 2399, 2400, 2401, 2402, 2403, 2404, 2405, 2406, 2407, 2408, 2409, 2410, 2411, 2412, 2413, 2414, 2415, 2416, 2417, 2418, 2419, 2420, 2421, 2422, 2423, 2424, 2425, 2426, 2427, 2428, 2429, 2430, 2431, 2432, 2433, 2434, 2435, 2436, 2437, 2438, 2439, 2440, 2441, 2442, 2443, 2444, 2445, 2446, 2447, 2448, 2449, 2450, 2451, 2452, 2453, 2454, 2455, 2456, 2457, 2458, 2459, 2460, 2461, 2462, 2463, 2464, 2465, 2466, 2467, 2468, 2469, 2470, 2471, 2472, 2473, 2474, 2475, 2476, 2477, 2478, 2479, 2480, 2481, 2482, 2483, 2484, 2485, 2486, 2487, 2488, 2489, 2490, 2491, 2492, 2493, 2494, 2495, 2496, 2497, 2498, 2499, 2500, 2501, 2502, 2503, 2504, 2505, 2506, 2507, 2508, 2509, 2510, 2511, 2512, 2513, 2514, 2515, 2516, 2517, 2518, 2519, 2520, 2521, 2522, 2523, 2524, 2525, 2526, 2527, 2528, 2529, 2530, 2531, 2532, 2533, 2534, 2535, 2536, 2537, 2538, 2539, 2540, 2541, 2542, 2543, 2544, 2545, 2546, 2547, 2548, 2549, 2550, 2551, 2552, 2553, 2554, 2555, 2556, 2557, 2558, 2559, 2560, 2561, 2562, 2563, 2564, 2565, 2566, 2567, 2568, 2569, 2570, 2571, 2572, 2573, 2574, 2575, 2576, 2577, 2578, 2579, 2580, 2581, 2582, 2583, 2584, 2585, 2586, 2587, 2588, 2589, 2590, 2591, 2592, 2593, 2594, 2595, 2596, 2597, 2598, 2599, 2600, 2601, 2602, 2603, 2604, 2605, 2606, 2607, 2608, 2609, 2610, 2611, 2612, 2613, 2614, 2615, 2616, 2617, 2618, 2619, 2620, 2621, 2622, 2623, 2624, 2625, 2626, 2627, 2628, 2629, 2630, 2631, 2632, 2633, 2634, 2635, 2636, 2637, 2638, 2639, 2640, 2641, 2642, 2643, 2644, 2645, 2646, 2647, 2648, 2649, 2650, 2651, 2652, 2653, 2654, 2655, 2656, 2657, 2658, 2659, 2660, 2661, 2662, 2663, 2664, 2665, 2666, 2667, 2668, 2669, 2670, 2671, 2672, 2673, 2674, 2675, 2676, 2677, 2678, 2679, 2680, 26

III. EXPERIMENTAL PROCEDURE

The first step in the investigation after the targets were made consisted of bombarding a target with 6.5-Mev protons and analyzing the elastically scattered proton groups to determine the contaminants contained in the target and to measure the effective thickness of the cobalt coating. Elastic runs were made at 90 degrees, as shown in Table I. The results from one such bombardment are shown in Figure 4 and in Table I. For scattering at 90 degrees from a target initially at rest, nonrelativistically we use the following

$$m = \frac{E_{in} m_p + E_o m_p}{E_{in} - E_o}, \quad \begin{array}{l} \text{(where } m_p \text{ is the} \\ \text{mass of a proton)} \end{array}$$

to determine the mass of the scattering nuclei.

According to the manufacturer²³, Formvar contains 33 percent oxygen, 59.1 percent carbon, and 7.8 percent hydrogen (by weight) plus traces of sulfur and nitrogen. For use, Formvar is diluted with ethylene dichloride, which adds only chlorine to the list of contaminants contained in the backing. The calcium could possibly be present in the distilled water used in floating the Formvar films onto the target frame. The arsenic and silver are believed to be due to previous evaporated materials which were not completely removed from the evaporator.

It is noted that the analysis of contamination on one of a different group of targets showed less sodium and chlorine than in the first run, which may be due to better cleaning of the evaporator before making new targets, or may be a case of "sweat physics."

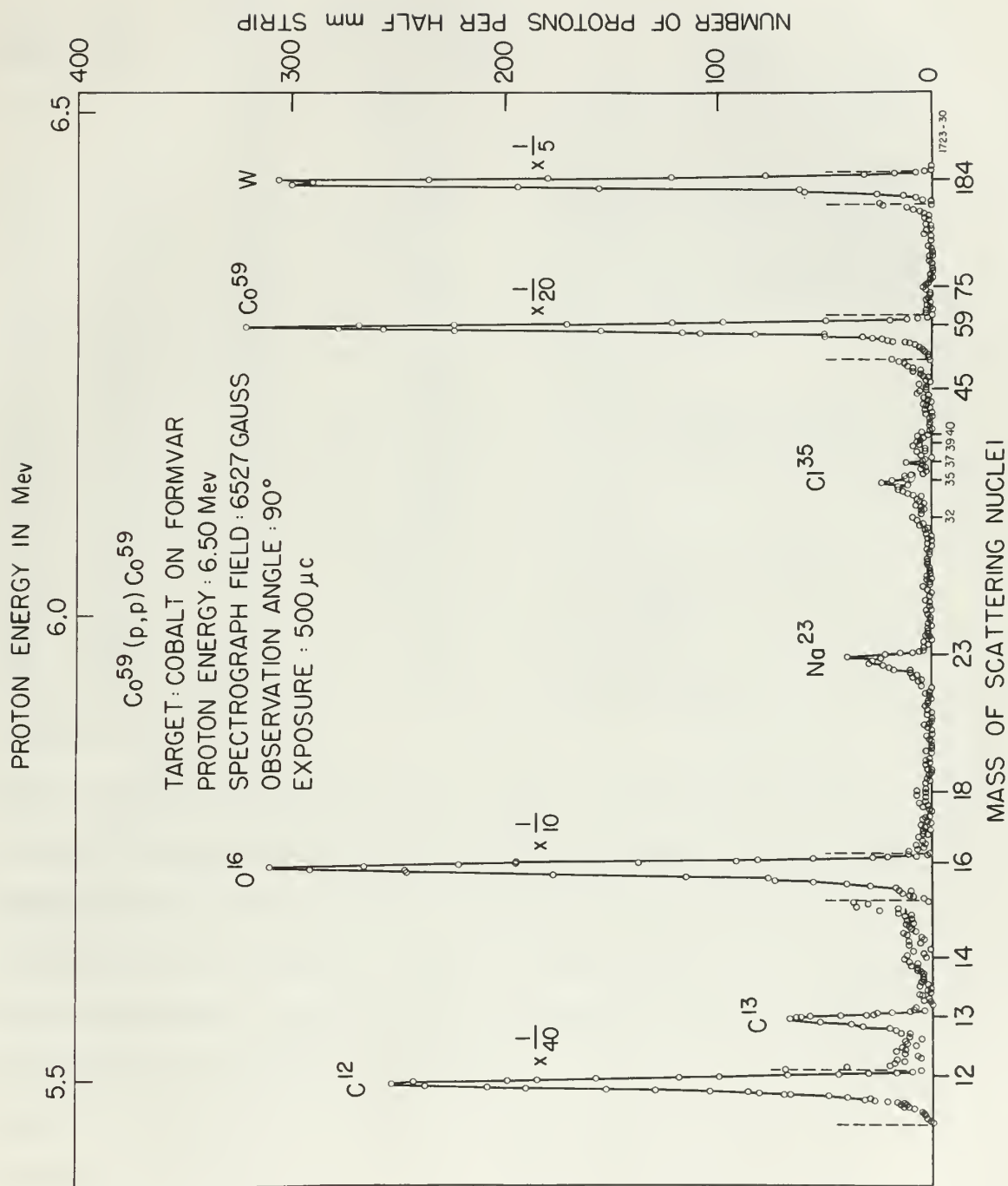


Figure 4

Table I. Mass Analysis of Cobalt Target on Formvar Backing

Element	Number Z	Significant Isotope A	No. Tracks in Peak $\div Z^2$ Rel. to Co ⁵⁹	Origin
C	6	12	3500.0	Backing and vacuum system
C	6	13	34.5	Backing and vacuum system
N	7	14	1.67	Backing and vacuum system
O	8	16	638.0	Backing and vacuum system
O	8	18	0.57	Backing and vacuum system
Na	11	23	4.7	Sweat Physics
S	16	32	1.58	Backing
Cl	17	35	0.57	Backing, Sweat Physics
Cl	17	37	0.23	Backing, Sweat Physics
K	19	39	0.14	?
Ca	20	40	0.11	Backing
Co	27	59	100.0	Evaporated material
As	33	75	0.03	Evaporator
Ag	47	107	0.3	Evaporator
W	74	184	4.0	Tungsten boat

Note: An estimate of the relative amount of each element present has been made by assuming (very incorrectly in general) Rutherford scattering. The number of tracks assigned to each element was divided by Z^2 and is given in the fourth column of Table I relative to the cobalt peak. Column 5 gives the assigned origin of these contaminants, as a matter of interest.

Table 1. Mass analysis of cobalt target on various binding

Element	Mass- number	Relative intensity A	Relative intensity B	Relative intensity C
Co	59	100	100	100
Fe	56	10	10	10
Ni	58	5	5	5
Cu	63	2	2	2
Zn	66	1	1	1
As	75	0.5	0.5	0.5
Se	78	0.3	0.3	0.3
Br	80	0.2	0.2	0.2
Kr	84	0.1	0.1	0.1
Rb	85	0.1	0.1	0.1
Sr	88	0.1	0.1	0.1
Y	89	0.1	0.1	0.1
Zr	90	0.1	0.1	0.1
Mo	96	0.1	0.1	0.1
Ag	108	0.1	0.1	0.1
Cd	114	0.1	0.1	0.1
In	115	0.1	0.1	0.1
Sn	119	0.1	0.1	0.1
Pb	208	0.1	0.1	0.1

Note: In addition to the relative intensity of each element present in the sample by assuming (very roughly) in general, the relative intensity of each element is divided by A^2 and is given in the fourth column of Table 1 relative to the cobalt peak. Column 5 gives the assigned value of each element, as a matter of interest.

In other words, prior to evaporating perspiration was left on the crucible, electrodes, and target frame supports because of handling. The greater apparent abundance of Na versus Cl may be caused by the effects of high deuteron bombarding energy.

Since the targets were quite fragile, we had to use a total of five targets from two different evaporations. The contaminants were checked for each group. Normalization of the different runs is described later.

The following procedure was employed in the angular distribution runs: We first determined the approximate barrier height of Co^{59} from the equation²⁴ $B \approx 0.76 \text{ } zZ^{2/3} \text{ Mev}$, and found it to be $\approx 6.8 \text{ Mev}$ for deuterons on cobalt. It was desirable to use a bombarding energy of roughly this value to minimize exposure time, but a value of 6.0 Mev was chosen because the accelerator was better stabilized at this energy; an important factor in long runs, such as were made.

The energy of the bombarding deuterons was established by setting up the desired magnetic field in the deflecting magnet. This energy was a constant throughout a set of angular runs, but the setting of the magnetic spectrograph field was changed every few angles to maintain an approximately constant position of the ground level proton peaks from Co^{59} on the photographic plate. This insured that the peaks had a constant solid angle throughout the run and thus removed the need for solid-angle correction in comparing the intensities of peaks at different angles. The exact

in other words, prior to separating completely and left on the
 movable, cylindrical, and tapered base supports because of bending.
 The greater amount of bending at its base it can be seen by the
 effects of this bending compressing energy.

Since the supports were quite flexible, as has been a point
 of the supports from two different observations. The observations
 were checked the same group. Observation of the different parts
 is described later.

The following procedure was followed in the engine design-
 ing process: we first determined the approximate bending energy
 of C_{22} from the equation $B = 0.75 \times 10^6$ and found it to
 be 0.6 for the design as usual. It was determined to use a
 bending energy of roughly this value to produce engine size,
 and a value of 0.6 for the design because the compression was being
 applied at this energy; in fact, the value is lower than, and is
 more than, the value of 0.6 for the design.

The energy at the combustion chamber was calculated by
 using up the stored energy that is the bending energy.
 This energy was a constant throughout a set of engine parts, and
 the engine at the combustion chamber that was shown was
 the engine as calculated as approximately constant position of the
 engine level from the base to the combustion chamber.
 This showed that the engine was a constant with slight variations.
 The run and time showed the same for the engine as shown in
 comparison the information of parts at different points. The data

energy of the deuteron beam was determined by an elastic deuteron exposure and by using the accurately known Q-value²⁵ (2.717 ± 0.007 Mev) for the $C^{12}(d,p)C^{13}$ reaction which appeared in all exposures.

The first series of angular distributions was made at an average deuteron energy of 6.009 Mev, and the exposures were 500 microcoulombs. The second series was made, through an error in setting up the deflecting magnet, at an average energy of 6.187 Mev, and with varied exposures. Table II summarizes these runs. The longer runs of the second series were designed to resolve better several weak peaks seen in the first series in order to determine their energy with greater accuracy. The higher energy of the second series shifted the position of the proton peaks a distance approximately two centimeters toward the high-energy end of the plates. The average deuteron current input to the target chamber was about 0.10 microamperes.

When making the (d,p) distribution runs, the photographic plates were covered with two layers of 1.5-mil aluminum foil to screen out alpha particles and deuterons. After exposure, the plates were developed and counted, as described previously. We plotted the number of protons per one-half millimeter strip versus distance along the plate, as shown by the example in Figure 5. The proton groups from cobalt were identified by observing the shift in position on the plate from one angle to another. The expected drift was calculated as an aid in identification. In each run, one or more of the proton groups were obscured by the large ground level

TABLE II. Summary of Targets and Exposure for Angular Distribution

<u>Angle</u>	<u>Exposure (μcoul.)</u>	<u>Target</u>	<u>Remarks</u>
10°	500	B 3	
15	500	B 3	
20	500	B 3	
25	500	B 3	
30	500	B 3	
35	500	B 3	
40	500	B 3	
45	500	B 3	
50	500	B 3	
55	500	B 3	
60	500	B 3	
70	500	B 3	
80	500	B 8	
90	500	B 8	
5	1000	A 3	Unusable-deuterons
15	1000	A 3	
25	1427	A 3	
30	1000	A 4	
45	1000	A 4	
90	1250	A 3	
100	1250	A 3	
110	1250	A 3	
15	500	B 6	First test run
45	250	A 4	Second test run

TABLE II. Summary of results and comments for various experiments

Run	Time (min)	Temp (°C)	Pressure (mm Hg)
10	10	100	10
11	10	100	10
12	10	100	10
13	10	100	10
14	10	100	10
15	10	100	10
16	10	100	10
17	10	100	10
18	10	100	10
19	10	100	10
20	10	100	10
21	10	100	10
22	10	100	10
23	10	100	10
24	10	100	10
25	10	100	10
26	10	100	10
27	10	100	10
28	10	100	10
29	10	100	10
30	10	100	10
31	10	100	10
32	10	100	10
33	10	100	10
34	10	100	10
35	10	100	10
36	10	100	10
37	10	100	10
38	10	100	10
39	10	100	10
40	10	100	10
41	10	100	10
42	10	100	10
43	10	100	10
44	10	100	10
45	10	100	10
46	10	100	10
47	10	100	10
48	10	100	10
49	10	100	10
50	10	100	10
51	10	100	10
52	10	100	10
53	10	100	10
54	10	100	10
55	10	100	10
56	10	100	10
57	10	100	10
58	10	100	10
59	10	100	10
60	10	100	10
61	10	100	10
62	10	100	10
63	10	100	10
64	10	100	10
65	10	100	10
66	10	100	10
67	10	100	10
68	10	100	10
69	10	100	10
70	10	100	10
71	10	100	10
72	10	100	10
73	10	100	10
74	10	100	10
75	10	100	10
76	10	100	10
77	10	100	10
78	10	100	10
79	10	100	10
80	10	100	10
81	10	100	10
82	10	100	10
83	10	100	10
84	10	100	10
85	10	100	10
86	10	100	10
87	10	100	10
88	10	100	10
89	10	100	10
90	10	100	10
91	10	100	10
92	10	100	10
93	10	100	10
94	10	100	10
95	10	100	10
96	10	100	10
97	10	100	10
98	10	100	10
99	10	100	10
100	10	100	10

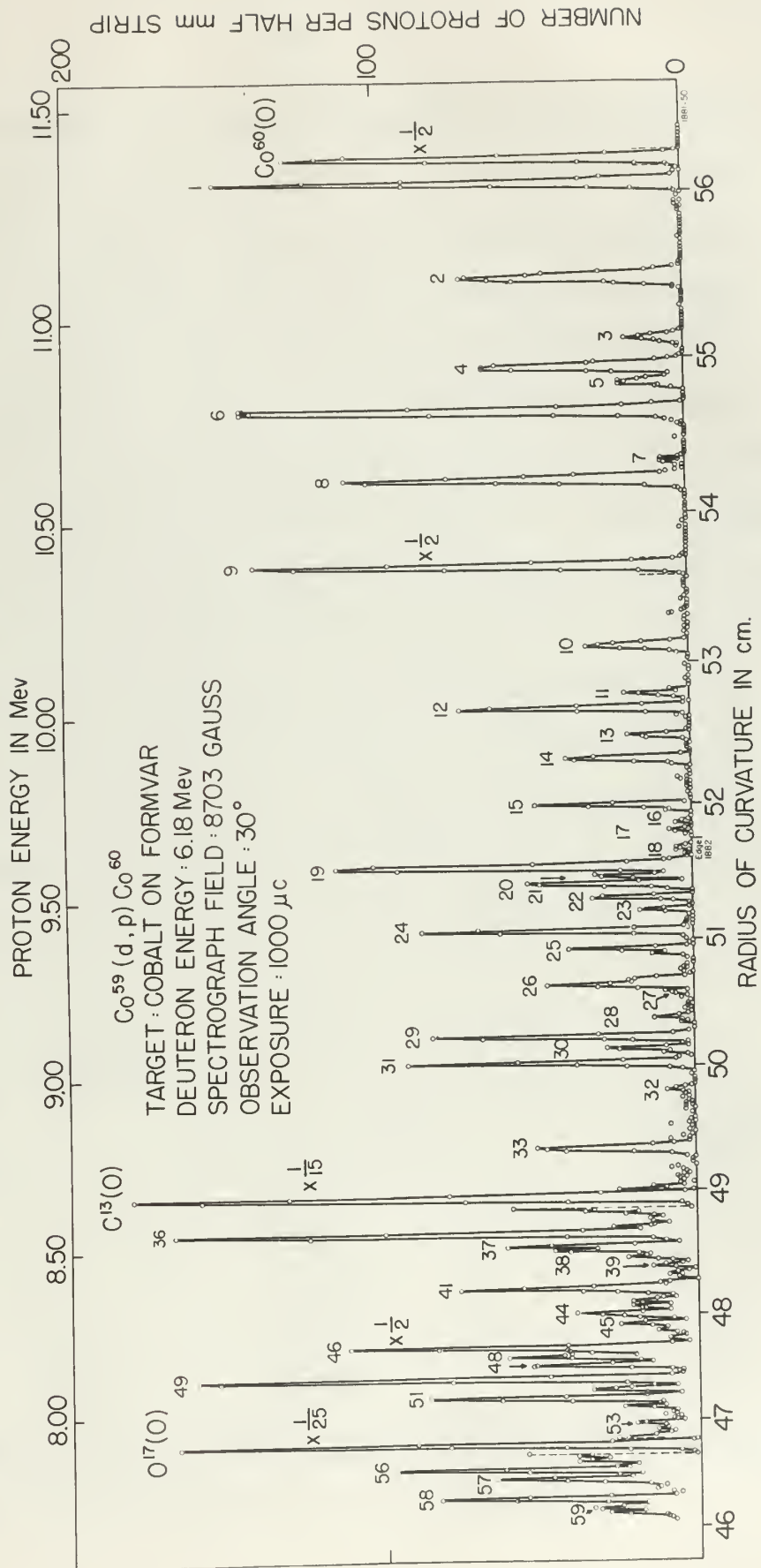


Figure 5

and first excited levels of the $O^{16}(d,p)O^{17}$ and $C^{12}(d,p)C^{13}$ reactions. Since these latter are light nuclei, the shift of peak position versus angle is greater for them than for the cobalt peaks. Hence, the cobalt peaks which had been obscured at one angle by carbon and oxygen could be seen at a different angle.

The data from the different runs were normalized in order to correct for the various thicknesses of cobalt and for the different amounts of exposure used. For the latter, the number of proton tracks in a peak was corrected to a 500 microcoulomb exposure by multiplying by the ratio of 500 over the actual exposure for the run. To determine the target thicknesses relative to the original one (B 3), the total number of proton tracks on the first plate (up to excited level No. 14) was corrected for the amount of exposure and then compared with the first plate of target B 3 at a common angle of exposure. The results are summarized in Table III:

TABLE III

Target Thickness Relative to Target B 3

<u>Target</u>	<u>Relative Thickness</u>	<u>Angle of Comparison</u>
A 3	0.9362	15°
A 4	0.7300	30° + 45°
B 6	0.7746	15
B 8	0.7203	90°

The reciprocal of the relative thickness was multiplied with the peak counts after normalization for exposure amount.

and first excited levels of the ^{235}U and ^{238}U isotopes. Since these levels are in the region of the first excited level, the width of the position versus angle is greater for them than for the other peaks. Hence, the relative peak widths had been measured at one angle by using the relative widths of the peaks as a reference value. The data from the different runs were corrected in order to correct for the various thicknesses of material and for the different amounts of exposure used. For the latter, the number of tracks in a peak was corrected to a 500 microcurie exposure or multiplying by the ratio of 500 over the actual exposure for the run. To determine the relative thicknesses relative to the original one (U 3), the total number of tracks from the first peak (no first excited level in U 3) was corrected for the number of tracks and then compared with the first peak of target 3 as a common angle of exposure. The results are presented in Table III.

TABLE III

Relative thickness relative to target 3

Target	Relative thickness	Angle of exposure
3	0.130	12°
4	0.130	120° + 180°
5	0.130	12°
6	0.130	120°

The thickness of the relative thickness was calculated with the same method after correction for exposure amount.

It was noted by comparison of corresponding peaks at the same angle on two different targets that random fluctuations of the proton counts were relatively high; that is, several peaks out of fifteen on the first plate would be two or three standard deviations off with respect to two guides: the same peak obtained from the other target and the expected value obtained by approximating a smooth angular distribution through the peak counts of adjacent angles. In normalizing to minimize this effect where more than one exposure had been made at the same angle (Table III), a weighted mean count was determined for each such angle.

The first step was to multiply the amount of exposure for a given target and angle by the relative target thickness to obtain a standardized exposure which would have produced the same number of proton tracks within the limits of fluctuation had the standard target been used. Then, for each angle a factor of 500, the standard exposure, was divided by the sum of all standardized exposures, including the standard one. This was then multiplied by the sum of all protons counted in the peak on all exposures regardless of target to give the mean count. Example:

<u>Target</u>	<u>No. Counts 1 Peak</u>	<u>Exposure</u>	<u>Relative Thickness</u>
Standard	1000	500	1
Other	600	500	0.50

The standardized exposure of the other target is 250 and the mean count = $(\frac{500}{500 + 250})(1000 + 600) = 1067$. The advantage of this

procedure over others which might produce the same result is the simplicity of using the unweighted summation of all counts at the same angle for each peak. It was felt that the error in the mean value due to the error in determining the relative target thickness would be much less than the random fluctuations seen in single counts.

[illegible]

IV. RESULTS

PROBABLE ERRORS

The probable error quoted for the Q -values and excitation energies is, strictly speaking, not probable error but uncertainty in energy. This difference in meaning is mentioned because the term "probable error" has a particular definition in the field of statistics which is not the meaning used in this paper. The statistically determined standard error is not the major consideration involved in the quoted error, but is rather the question of the accuracy of our values compared to the "true" values. This is then basically a question of how accurate a calibration has been made against the standard polonium alpha particle. The uncertainty consists of two types of errors, one random in nature and the other systematic. A detailed examination of the uncertainty of each level has not been made, but the general effects have been determined, and it is felt that the uncertainty quoted is reasonable.

The factors which may contribute to the random error are:

1. The spread in energy of the incident particles resulting from finite slit widths;
2. The finite width of the beam which illuminates a finite area on the target, not a point source;
3. The spread in energy of the emergent particles because of variations in target thickness; and
4. Small adjustments of the magnet current to compensate for drift.

IV. SUMMARY

PROBABLE ERROR

The probable error quoted for the 4-values and estimated
emphases is, strictly speaking, not probable error, but uncertainty
in energy. This difference in meaning is pointed out in the paper.
"Probable error" has a particular definition in the table of statis-
tics which is not the meaning used in this paper. The statistically
determined statistical error is not the major consideration involved in
the quoted error, but in rather the question of the accuracy of our
values compared to the "true" values. This is then basically a ques-
tion of how accurate a calibration has been made against the stan-
dard potential alpha particles. The uncertainty consists of two types
of error, one random in nature and the other systematic. A de-
tailed examination of the uncertainty of each level has not been
made, but the general effects have been determined, and it is felt
that the uncertainty quoted is reasonable.

The factors which may contribute to the random error are:

1. The spread in energy of the incident particles

resulting from finite slit widths;

2. The finite width of the beam when it strikes a

thinness near the target, not a point source;

3. The spread in energy of the emitted particles

because of variations in target thickness; and

4. Small adjustments of the magnet current to obtain

data for each.

Since each Q-value is the mean of three or four measurements (with one exception), it is possible to obtain an estimate of the random error by examination of the standard error of the mean values. The mean value is determined from

$$\bar{x} = \frac{1}{n} \sum_{i=1}^n x_i$$

where n is the number of observations. The standard error is then:

$$\sigma_{\bar{x}} = \left[\frac{\sum_{i=1}^n (x_i - \bar{x})^2}{n(n-1)} \right]^{\frac{1}{2}}$$

This procedure resulted in an average standard error throughout the range of Q-values reported of about 1.2 kev.

The systematic errors are of greater consequence and are in general a function of the energy of the emergent protons. These errors include the following:

1. The calibration error of the magnetic spectrograph, which includes the uncertainty in the Bp value of the polonium alpha particles;
2. Peak position and validity of the use of the one-third height position;
3. Since the energies of the protons and deuterons were measured after these particles had passed through the target, there is an error caused by the different energy losses suffered by protons and deuterons in the target. This difference in energy loss is partially

Since each observation is the sum of three or four measurements

(with one exception), it is possible to obtain an estimate of the random error by examination of the standard error of the mean values.

The mean value is determined from

$$\bar{x} = \frac{1}{n} \sum_{i=1}^n x_i$$

where n is the number of observations. The standard error is found

$$s = \sqrt{\frac{\sum_{i=1}^n (x_i - \bar{x})^2}{n(n-1)}}$$

This procedure resulted in an average standard error throughout the

study of 0.00015, repeated at about 1.5 per cent.

The standard error of the mean is found by dividing the standard error

by the square root of the number of observations. Thus

errors are the following:

1. The standard error of the magnetic measurement,

which includes the standard error of the value of the magnetic field

particles;

2. The standard error of the value of the magnetic field

which includes the standard error of the value of the magnetic field

particles. Since the standard error of the magnetic field is

measured after each particle has passed through the system, there is

an error caused by the different energy losses suffered by particles and

particles in the system. This difference is enough that it is relatively

canceled in the Q-equation. However, even though a small correction was made to compensate for the thickness of the cobalt when finding the deuteron energy, these losses cannot be accurately determined, since the exact path of each and every particle is not known; and

4. The effect of temperature on the fluxmeter circuits, which is random in part.

The targets used were continuously rotating and hence the effect of surface contamination was felt to be negligible in comparison with the above effects. The values assigned to each of these terms are shown in Table IV.

TABLE IV

Systematic Errors for Q-values

Errors given in percent of particle energy

1. Calibration error	0.04
2. Error caused by position of carbon and cobalt in target	0.02
3. Peak position and one-third height	0.03
4. Temperature coefficients in fluxmeter	<u>0.03</u>
Root of sum of squares	~ 0.06

The total uncertainty for a given Q-value was determined by first combining the random and systematic errors for one measurement of particle energy and then combining the various uncertainties in the Q-equation to obtain the total uncertainty in Q-value. This results in a very generous estimate of the total uncertainty in Q-value,

concerning the question, however, even though a small correction
 may be made to compensate for the difference of the mean line
 the deviation energy, these values cannot be accurately determined,
 since the mean path of each ion varies widely in length and
 4. The effect of temperature on the thickness of

cells, which is shown in Table IV.

The average mean was continuously varying and hence the effect
 of surface contamination was not so negligible in comparison with
 the above effects. The values obtained on each of these points are
 shown in Table IV.

TABLE IV

Gamma-ray source for calibration

Energy given in terms of relative energy

1. Calibration error	0.02
2. Error caused by position of source and source in target	0.05
3. Peak position and one-third width	0.02
4. Temperature fluctuations in detector	0.01
Total of sum of squares	0.05

The total uncertainty for a given value was obtained by
 first combining the random and systematic errors for the measurement
 of particle energy and then combining the various uncertainties in
 the question to obtain the total uncertainty in value. This re-
 sults in a very generous estimate of the total uncertainty in value,

since some of the systematic errors in the determination of the energies of the incident and emergent particles tend to cancel out. This particularly applies to the calibration error.

As an example, for the ground-state Q-value, the proton energy is about 11.4 Mev. This is found to have an error of ± 7 kev. The uncertainty in the deuteron energy required more calculation, since most of the deuteron energies were determined from the $C^{12}(d,p)C^{13}$ reaction, which has an uncertainty of ± 7 kev. The energy uncertainty of the deuteron is thus about ± 9 kev, which, combined with the proton uncertainty, gives an uncertainty in the Q-value of the ground level of about ± 11 kev.

The uncertainty in Q-value is given in the results as a constant ± 11 kev. This is due primarily to the larger expected error in peak position at lower proton energies where the peaks are closely spaced. This is an arbitrary assignment, but it is possible to make larger errors in peak position under these conditions.

The errors or uncertainties of the excitation energies are due to similar causes. The random error was determined by an examination of the standard errors of the mean values and was found to be about ± 4 kev. The systematic errors are approximately proportional to the excitation energy. In the calculation of the excitation energies, the results depend on the energy differences between groups recorded on the same plate and the systematic errors tend to cancel out. This has led to the assignment of a systematic error of ± 0.1 percent of the excitation energy. The total uncertainty is then the square root of the sums of the squares of the random and systematic errors.

some sort of the systematic errors in the determination of the value of the constants and systematic errors in the calculation of the results. This is especially true for the calculation of the results.

As an example, the standard error of the results is about ± 1.5 per cent.

This is found to have an error of ± 1 per cent. The

uncertainty in the constant energy required was calculated, since

most of the constant energies were determined from the $\frac{1}{2}(E_1 + E_2)$

relation, which has an uncertainty of ± 1 per cent. The energy required

of the constant is then about ± 2 per cent, which, combined with the error

uncertainty, gives an uncertainty in the value of the constant level

of about ± 1.5 per cent.

The uncertainty in the value of the results is about ± 1.5 per cent.

This is the result of the larger standard error

in the calculation of the constant energy required, since the results are directly

proportional to the constant energy required, and it is possible to have

larger errors in the calculation of the constant energy required.

The error in the calculation of the constant energy required is

so small that the error in the calculation of the constant energy required

of the standard error of the results is about ± 1.5 per cent.

The systematic errors are systematically proportional to the

uncertainty in the calculation of the constant energy required, since

the results are directly proportional to the constant energy required, and it is possible to have

larger errors in the calculation of the constant energy required.

The error in the calculation of the constant energy required is

so small that the error in the calculation of the constant energy required

of the standard error of the results is about ± 1.5 per cent.

DISCUSSION OF Q-VALUES AND COMPARISON WITH PREVIOUS WORK

The determination of the energy of a given particle group is done in the following manner. The calibration table is used to convert the third-height distance into ρ , the trajectory radius of the particle in the magnetic spectrograph. Knowing the value of the magnetic field B in kilogauss, we next find the "magnetic rigidity" of the particle, $B\rho$, and enter the tables calculated by Enge²³, where the following equation relating energy of a particle to its momentum has been solved for protons, deuterons, tritons, and alpha particles, for values of $B\rho$ from 10^5 to 6.5×10^5 gauss centimeters.

$$E_0 = m_0 c^2 \left[\left(1 + \left(\frac{ZeB\rho}{m_0 c} \right)^2 \right)^{\frac{1}{2}} - 1 \right]$$

where m_0 = rest mass of the particle.

The equation for the Q -value of a given reaction can be expressed in the following form:

$$Q = \frac{M_R + M_0}{M_R} E_0 - \frac{M_R - M_I}{M_R} E_I - 2 \cos \theta \frac{(M_I M_0 E_I E_0)^{\frac{1}{2}}}{M_R} + \delta_{rel}$$

where M_R = mass of residual nucleus

M_0 = mass of emitted particle

E_0 = energy of emitted particle

M_I = mass of incident particle

E_I = energy of incident particle

θ = reaction angle in laboratory coordinate.

DISCUSSION OF RESULTS

OVERALL AND PARTIAL RESULTS

The definition of the energy of a given particle group is given in the following manner. The definition here is used to convert the third-order distance into a two-body distance of the particle in the magnetic spectrum. Knowing the value of the magnetic field B in kilogauss, we can find the magnetic rigidity of the particle, qB , and when the value is related by $qB = mv/c$, where the following equation relating energy of a particle to its momentum has been solved for velocity, momentum, kinetic, and mass particles. For values of q from 10^2 to 0.5×10^5 gauss centimeters.

$$E = mc^2 \left[\left(1 + \left(\frac{qB}{mc} \right)^2 \right)^{1/2} - 1 \right]$$

where q = total mass of the particle.

The equation for the γ -value of a given reaction can be written in the following form:

$$\gamma = \frac{E_0 + E_1}{E_0} \left(1 - \frac{E_1}{E_0} \right) - \frac{E_1}{E_0} \left(1 - \frac{E_1}{E_0} \right) - \frac{E_1}{E_0} \left(1 - \frac{E_1}{E_0} \right) - \frac{E_1}{E_0} \left(1 - \frac{E_1}{E_0} \right)$$

where E_0 = mass of incident particle

E_1 = mass of emitted particle

E_2 = energy of emitted particle

E_3 = mass of incident particle

E_4 = energy of incident particle

γ = reaction angle in laboratory coordinate.

The term δ_{rel} is a small relativistic correction term and is approximately:

$$\delta_{\text{rel}} \approx \frac{1}{2M_R c^2} \left[E_I^2 + E_O^2 - E_R^2 - \cos \theta (M_I M_O E_I E_O)^{\frac{1}{2}} \left(\frac{E_I}{M_I} + \frac{E_O}{M_O} \right) \right]$$

where E_R , the energy of the residual nucleus, is found from

$$E_R = \frac{M_I}{M_R} E_I + \frac{M_O}{M_R} E_O - 2 \cos \theta \frac{(M_I M_O E_I E_O)^{\frac{1}{2}}}{M_R}.$$

To find the bombarding energy of a particle using elastic scattering, we set Q equal to zero and have

$$E_I = \frac{M_R + M_O}{M_R - M_I} E_O - 2 \cos \theta (M_I M_O E_I E_O)^{\frac{1}{2}} + \delta_{\text{rel}} \frac{M_R}{M_R - M_I}$$

Unless θ is equal to 90 degrees, we have a second-order equation; therefore, the method of successive approximations was employed in the solution of this equation. This technique was also employed when the deuteron energy was obtained from the $C^{12}(d,p)C^{13}$ reaction leading to the ground level of C^{13} .

The Q -values were computed from four exposures, the 45- and 60-degree exposures of the 6.009-Mev series, and the 25- and 30-degree exposures of the 6.187-Mev series. The exposures at 45 and 60 degrees were 500 μ coulomb and, in examining the results, we found several small peaks identified with Co^{60} were observed besides the large ones. The second set of exposures was given longer bombardment in order to obtain better counting statistics for small proton groups.

The term δ is a small correction to the main term ϵ

approximate

$$\left[\frac{1}{2} \frac{d^2}{dt^2} + \frac{1}{2} \frac{d^2}{dx^2} \right] \psi = \epsilon \psi$$

where ϵ is the energy of the system, known to be zero

$$\frac{1}{2} \frac{d^2}{dt^2} + \frac{1}{2} \frac{d^2}{dx^2} = \epsilon$$

to find the wavefunction ψ of a particle with energy

zero, we set $\epsilon = 0$ and have

$$\frac{1}{2} \frac{d^2}{dt^2} + \frac{1}{2} \frac{d^2}{dx^2} = 0$$

where ψ is equal to 0 at $t = 0$ and $x = 0$

that is, the wavefunction is zero at the origin and at $t = 0$

in the region of the system. This condition is also satisfied

when the wavefunction is zero at $t = 0$ and $x = 0$

leading to the general form of ψ

The wavefunction is zero at $t = 0$ and $x = 0$

degree of freedom of the system, and the $t = 0$ and $x = 0$

degrees of freedom of the system. The wavefunction is zero at $t = 0$ and $x = 0$

degrees of freedom of the system, and the $t = 0$ and $x = 0$

degrees of freedom of the system, and the $t = 0$ and $x = 0$

degrees of freedom of the system, and the $t = 0$ and $x = 0$

degrees of freedom of the system, and the $t = 0$ and $x = 0$

The 25- and 30-degree exposures were selected for computation to give the highest average intensity of all the peaks regardless of the shape of their angular distribution. The use of four separate exposures at different angles insured at least three separate determinations of the Q-value for each level, with but one exception. The average Q-value and excitation energy for the ground level and fifty-nine excited levels are given in Table V. Level number 54 is inclosed in parentheses to indicate that it is the mean of only two measurements and has a larger random error. This peak was consistently observed at other angles but was obscured by the O^{17} ground level on two of the four exposures used in determining Q-values.

In the computations for the Q-values, the relativity correction was less than 0.5 kev for the 25, 30, and 45-degree exposures, and was less than 0.8 kev for the 60-degree exposure. It has been included in the results for the 60-degree exposure.

A separate series of computations for the Q-value of the ground level at twelve different angles gave a Q of 5.262 ± 0.011 Mev. The maximum spread in these Q-values was 7 kev, with a standard random error of less than 2 kev.

The agreement for the Q-values of the excited levels was good on all exposures. The standard random error was found to be less than 4 kev for any level, and for most levels, it was less than 3 kev.

The 25- and 30-degree experiments were arranged in comparison to give the highest average intensity of all the pairs registered at the same at least within the experiment. The use of four separate exposures at different angles insured on each plate separate distributions of the reaction for each level, and no overlapping. The average reaction and correlation energy for the ground level and fifty-nine excited levels are given in Table V. Level number 26 is included in parentheses to indicate that it is the least of only two measurements and has a larger relative error. This level was also slightly observed at other angles but not included by the 25- ground level) as for all the four exposures used in determining it.

In the comparison for the reaction, the relatively narrow lines were taken into account for the 25, 30, and 35-degree exposures, and were taken into account for the 30-degree exposure. It was then included in the reaction for the 30-degree exposure. A separate series of calculations for the reaction of the ground level at various different angles gave a $\pm 0.002 \pm 0.001$ ev. The reaction spread in these levels was 7 ev, with a standard reaction error of less than 1 ev. The agreement for the reaction of the excited levels was good on all exposures. The standard reaction error was found to be less than 1 ev for all levels, and for each level, it was less than 1 ev.

TABLE V

Q-values for $\text{Co}^{59}(\text{d},\text{p})\text{Co}^{60}$ and Excitation Energies of Co^{60}

<u>Level</u>	<u>Q-value in Mev + 0.011</u>	<u>Excitation Energy in Mev</u>
Ground State	5.262	0
1	5.204	0.058 \pm 0.004
2	4.980	0.282 \pm 0.004
3	4.830	0.432 \pm 0.004
4	4.761	0.501 \pm 0.004
5	4.721	0.541 \pm 0.004
6	4.650	0.612 \pm 0.004
7	4.524	0.738 \pm 0.004
8	4.479	0.783 \pm 0.004
9	4.256	1.006 \pm 0.004
10	4.055	1.207 \pm 0.004
11	3.925	1.337 \pm 0.004
12	3.885	1.377 \pm 0.004
13	3.815	1.447 \pm 0.004
14	3.750	1.512 \pm 0.004
15	3.624	1.638 \pm 0.004
16	3.578	1.684 \pm 0.004
17	3.555	1.707 \pm 0.004
18	3.514	1.748 \pm 0.004
19	3.463	1.799 \pm 0.004
20	3.433	1.829 \pm 0.004

TABLE V

Calculated for $\alpha = 0.05$ and $\beta = 0.80$ for various values of ρ

Level	Calculated for $\alpha = 0.05$ and $\beta = 0.80$	Calculated for $\alpha = 0.05$ and $\beta = 0.80$
0	0.000	0.000
1	0.000	0.000
2	0.000	0.000
3	0.000	0.000
4	0.000	0.000
5	0.000	0.000
6	0.000	0.000
7	0.000	0.000
8	0.000	0.000
9	0.000	0.000
10	0.000	0.000
11	0.000	0.000
12	0.000	0.000
13	0.000	0.000
14	0.000	0.000
15	0.000	0.000
16	0.000	0.000
17	0.000	0.000
18	0.000	0.000
19	0.000	0.000
20	0.000	0.000

<u>Level</u>	<u>Q-value</u>	<u>Ex (Mev)</u>
21	3.412	1.850 \pm 0.004
22	3.375	1.887 \pm 0.004
23	3.339	1.923 \pm 0.004
24	3.283	1.979 \pm 0.004
25	3.231	2.031 \pm 0.005
26	3.131	2.131 \pm 0.005
27	3.112	2.150 \pm 0.005
28	3.045	2.217 \pm 0.005
29	2.988	2.274 \pm 0.005
30	2.952	2.310 \pm 0.005
31	2.914	2.348 \pm 0.005
32	2.835	2.427 \pm 0.005
33	2.671	2.591 \pm 0.005
34	2.528	2.734 \pm 0.005
35	2.500	2.762 \pm 0.005
36	2.417	2.845 \pm 0.005
37	2.378	2.884 \pm 0.005
38	2.363	2.899 \pm 0.005
39	2.320	2.942 \pm 0.005
40	2.295	2.967 \pm 0.005
41	2.252	3.010 \pm 0.005
42	2.214	3.048 \pm 0.005
43	2.197	3.065 \pm 0.005
44	2.176	3.086 \pm 0.005

Level	Value	Std. Dev.
14	1.140	1.140 ± 0.140
15	1.141	1.141 ± 0.141
16	1.142	1.142 ± 0.142
17	1.143	1.143 ± 0.143
18	1.144	1.144 ± 0.144
19	1.145	1.145 ± 0.145
20	1.146	1.146 ± 0.146
21	1.147	1.147 ± 0.147
22	1.148	1.148 ± 0.148
23	1.149	1.149 ± 0.149
24	1.150	1.150 ± 0.150
25	1.151	1.151 ± 0.151
26	1.152	1.152 ± 0.152
27	1.153	1.153 ± 0.153
28	1.154	1.154 ± 0.154
29	1.155	1.155 ± 0.155
30	1.156	1.156 ± 0.156
31	1.157	1.157 ± 0.157
32	1.158	1.158 ± 0.158
33	1.159	1.159 ± 0.159
34	1.160	1.160 ± 0.160
35	1.161	1.161 ± 0.161
36	1.162	1.162 ± 0.162
37	1.163	1.163 ± 0.163
38	1.164	1.164 ± 0.164
39	1.165	1.165 ± 0.165
40	1.166	1.166 ± 0.166
41	1.167	1.167 ± 0.167
42	1.168	1.168 ± 0.168
43	1.169	1.169 ± 0.169
44	1.170	1.170 ± 0.170
45	1.171	1.171 ± 0.171
46	1.172	1.172 ± 0.172
47	1.173	1.173 ± 0.173
48	1.174	1.174 ± 0.174
49	1.175	1.175 ± 0.175
50	1.176	1.176 ± 0.176
51	1.177	1.177 ± 0.177
52	1.178	1.178 ± 0.178
53	1.179	1.179 ± 0.179
54	1.180	1.180 ± 0.180
55	1.181	1.181 ± 0.181
56	1.182	1.182 ± 0.182
57	1.183	1.183 ± 0.183
58	1.184	1.184 ± 0.184
59	1.185	1.185 ± 0.185
60	1.186	1.186 ± 0.186
61	1.187	1.187 ± 0.187
62	1.188	1.188 ± 0.188
63	1.189	1.189 ± 0.189
64	1.190	1.190 ± 0.190
65	1.191	1.191 ± 0.191
66	1.192	1.192 ± 0.192
67	1.193	1.193 ± 0.193
68	1.194	1.194 ± 0.194
69	1.195	1.195 ± 0.195
70	1.196	1.196 ± 0.196
71	1.197	1.197 ± 0.197
72	1.198	1.198 ± 0.198
73	1.199	1.199 ± 0.199
74	1.200	1.200 ± 0.200
75	1.201	1.201 ± 0.201
76	1.202	1.202 ± 0.202
77	1.203	1.203 ± 0.203
78	1.204	1.204 ± 0.204
79	1.205	1.205 ± 0.205
80	1.206	1.206 ± 0.206
81	1.207	1.207 ± 0.207
82	1.208	1.208 ± 0.208
83	1.209	1.209 ± 0.209
84	1.210	1.210 ± 0.210
85	1.211	1.211 ± 0.211
86	1.212	1.212 ± 0.212
87	1.213	1.213 ± 0.213
88	1.214	1.214 ± 0.214
89	1.215	1.215 ± 0.215
90	1.216	1.216 ± 0.216
91	1.217	1.217 ± 0.217
92	1.218	1.218 ± 0.218
93	1.219	1.219 ± 0.219
94	1.220	1.220 ± 0.220
95	1.221	1.221 ± 0.221
96	1.222	1.222 ± 0.222
97	1.223	1.223 ± 0.223
98	1.224	1.224 ± 0.224
99	1.225	1.225 ± 0.225
100	1.226	1.226 ± 0.226

<u>Level</u>	<u>Q-Value</u>	<u>Ex (Mev)</u>
45	2.147	3.115 \pm 0.005
46	2.077	3.185 \pm 0.005
47	2.047	3.215 \pm 0.005
48	2.024	3.238 \pm 0.005
49	1.978	3.284 \pm 0.005
50	1.948	3.314 \pm 0.005
51	1.923	3.339 \pm 0.005
52	1.895	3.367 \pm 0.005
53	1.843	3.419 \pm 0.006
54	(1.798)	(3.464 \pm 0.006)
55	1.764	3.498 \pm 0.006
56	1.698	3.564 \pm 0.006
57	1.671	3.591 \pm 0.006
58	1.609	3.653 \pm 0.006
59	1.580	3.682 \pm 0.006

The excitation energy was found by subtracting the average Q-value of a level from the Q-value of the ground level. The average thus obtained was compared with the excitation energy determined for the individual exposures and agreement was again good.

The determination of energy levels was ended after fifty-nine levels had been measured. At levels above fifty-nine, the resolution of peaks is much poorer because of a larger background and closer spacing of proton groups. The beginning of this background may be

Level	Energy (eV)	Energy (eV)
1	1.100	1.100 ± 0.005
2	1.400	1.400 ± 0.005
3	1.600	1.600 ± 0.005
4	1.700	1.700 ± 0.005
5	1.800	1.800 ± 0.005
6	1.900	1.900 ± 0.005
7	2.000	2.000 ± 0.005
8	2.100	2.100 ± 0.005
9	2.200	2.200 ± 0.005
10	2.300	2.300 ± 0.005
11	2.400	2.400 ± 0.005
12	2.500	2.500 ± 0.005
13	2.600	2.600 ± 0.005
14	2.700	2.700 ± 0.005
15	2.800	2.800 ± 0.005
16	2.900	2.900 ± 0.005
17	3.000	3.000 ± 0.005
18	3.100	3.100 ± 0.005
19	3.200	3.200 ± 0.005
20	3.300	3.300 ± 0.005
21	3.400	3.400 ± 0.005
22	3.500	3.500 ± 0.005
23	3.600	3.600 ± 0.005
24	3.700	3.700 ± 0.005
25	3.800	3.800 ± 0.005
26	3.900	3.900 ± 0.005
27	4.000	4.000 ± 0.005
28	4.100	4.100 ± 0.005
29	4.200	4.200 ± 0.005
30	4.300	4.300 ± 0.005

The excitation energy was found by subtracting the average value of a level from the value of the next level. The values thus obtained are compared with the excitation energy calculated for the individual systems and systems are also found.

The determination of energy levels was aided after information levels had been measured. At levels above 100 eV, the excitation of levels is much lower because of a larger background and slight bending of proton groups. The bending of this background may be

seen in Figure 5 to the left of a radius of curvature of 48 cm. Figure 5 presents only that part of the data from the 30-degree exposure which was analyzed. It is noted that in the plot of the peaks in Figure 5, several peaks have half-widths greater than normal or display structure in the peak. Some of the effects noticed may be due to (d,p) reactions of the contaminant elements present, but several peaks display this at all angles of observation. In the latter cases, it is possible that the levels are closely spaced doublets, and the energy given is possibly in error because of this effect. More discussion of the effects of closely spaced doublets will be given in the discussion of the angular distribution curves. The peaks which are suspected of being doublets are numbers 2, 4, 10, 19, and 25. Level number 19 is particularly suspected of being a doublet, since pronounced double structure is shown at several angles.

It is interesting to compare the present results with the work of Foglesong and Foxwell² and with Bartholomew and Kinsey³. This comparison is presented in Table VI, listing both Q-values and excitation energies. It will be noted that the present work shows some fifty-nine levels in the region of excitation through 3.682 Mev, compared with the twenty-nine levels found by Foglesong and Foxwell. The agreement of the Q-value for the ground level in this investigation with that which is obtained from the work of Bartholomew and Kinsey is excellent. The Q-value of the ground level reported by Foglesong and Foxwell is 23 kev above that of Bartholomew and Kinsey and is 21 kev above that of the present investigation. This difference may have

mean in Figure 2 is the half of a number of numbers of 10 or
Figure 2 presents only part of the data from the 10-1000000
points which was analyzed. It is noted that in the case of the points
in Figure 2, several peaks have been indicated. These are shown by
dotted curves in the text. Some of the dotted curves are
due to (1,2) transitions of the mechanism elements involved, but are
not peaks. They are at all angles of observation. In the latter
case, it is possible that the levels are closely spaced doublets,
and the energy levels are possibly in error because of this effect.
The dimension of the effect of closely spaced doublets will be
given in the discussion of the angular distribution curves. The
peaks which are suggested of being doublets are numbers 9, 10, 11,
and 12. Level number 13 is particularly suggested of being a doublet,
also. The dotted curve in Figure 2 is shown at several angles.
It is interesting to compare the present results in the case
of hydrogen and deuterium, and also tritium and helium. The
comparison is presented in Table II, listing both 1-1000000 and 10-
100000000. It will be noted that the present work shows
fifty-nine levels in the region of excitation between 1.0000000 and
1.0000000. The twenty-nine levels found by Fitch and Fitch, and
Fitch and Fitch, are the same as the present work in this investigation
with that which is obtained from the work of Fitch and Fitch
is excellent. The 1-100000000 of the present work is reported by Fitch
and Fitch to be 13. The present work of Fitch and Fitch is 13
but above that of the present investigation. The difference may have

been caused by an effect noted by Strait et al²⁶ who observed that at high field strengths the iron of the magnet (the 180-degree annular magnet then used) was close to saturation and that the saturation did apparently cause appreciable errors in the energy measurements. The error in energy was of the order of 0.2 percent at values of B around 14,000 gauss. In the work of Foglesong and Foxwell, this represents an error of about 20 kev for a proton corresponding to the ground level and thus is very close to the observed difference. It should be possible to introduce a correction term in the form of a power series of the emergent particle energy²³. This correction would be zero at or above the field strength used for calibration with polonium alpha particles. A careful scrutiny of the Q-values of the present work and those of Foglesong and Foxwell shows that there is a correlation between the two which qualitatively agrees with the above argument. The values of Foglesong and Foxwell are generally higher through level number nine and from ten on agree within the limits of error except for number 48. If the difference in the Q-values for the ground level is subtracted from the excitation energy of the excited levels above nine, close agreement is again noticed. It should be noted that the present work covers part of a region which was obscured in the work of Foglesong and Foxwell. No level was found to correspond with a level at Q of 2.659 Mev.

[illegible]

TABLE VI

Comparison with Previous Results

Peak No	Present work		Foglesong + Foxwell ²		Bartholomew + Kinsey ³	
	Q-value (Mev)	Ex*(Mev)	Q-value (Mev)	Ex*(Mev)	Q-value (Mev)	Ex*(Mev)
Ground	5.262	0	5.283	0	5.260**	
1	5.204	0.058	5.223	0.060		
2	4.980	0.282	4.997	0.285		0.285
3	4.830	0.432	4.838	0.445		0.445
4	4.761	0.501	4.770	0.513		0.512
5	4.721	0.541	4.726	0.557		
6	4.650	0.612	4.661	0.622		0.619
7	4.524	0.738				
8	4.479	0.783	4.491	0.792		0.796
9	4.256	1.006	4.271	1.012		1.012
10	4.055	1.207	4.046	1.237		1.236
11	3.925	1.337				
12	3.885	1.377	3.889	1.394		1.376
13	3.815	1.447				
14	3.750	1.512	3.750	1.533		1.520
15	3.624	1.638	3.620	1.663		
16	3.578	1.684				
17	3.555	1.707				
18	3.514	1.748				1.760
19	3.463	1.799	3.458	1.825		
20	3.433	1.829				1.840

Order	Wavelength (nm)	Intensity (%)	Wavelength (nm)	Intensity (%)
1	210.0	100.0	210.0	100.0
2	215.0	95.0	215.0	95.0
3	220.0	90.0	220.0	90.0
4	225.0	85.0	225.0	85.0
5	230.0	80.0	230.0	80.0
6	235.0	75.0	235.0	75.0
7	240.0	70.0	240.0	70.0
8	245.0	65.0	245.0	65.0
9	250.0	60.0	250.0	60.0
10	255.0	55.0	255.0	55.0
11	260.0	50.0	260.0	50.0
12	265.0	45.0	265.0	45.0
13	270.0	40.0	270.0	40.0
14	275.0	35.0	275.0	35.0
15	280.0	30.0	280.0	30.0
16	285.0	25.0	285.0	25.0
17	290.0	20.0	290.0	20.0
18	295.0	15.0	295.0	15.0
19	300.0	10.0	300.0	10.0
20	305.0	5.0	305.0	5.0

<u>Peak</u>	<u>Q-value</u>	<u>Ex*(Mev)</u>	<u>Q-value</u>	<u>Ex*(Mev)</u>	<u>Q-value</u>	<u>Ex*(Mev)</u>
21	3.412	1.850				
22	3.375	1.887				
23	3.339	1.923				
24	3.283	1.979	3.278	2.005		
25	3.231	2.031	3.218	2.065		
26	3.131	2.131	3.129	2.154		2.135
27	3.112	2.150				
28	3.045	2.217				
29	2.988	2.274	2.988	2.295		
30	2.952	2.310				2.307
31	2.914	2.348	2.913	2.370		
32	2.835	2.427				
33	2.671	2.591	2.673	2.610		2.583
			2.659	2.624		
34	2.528	2.734				
35	2.500	2.762	2.497	2.786		
36	2.417	2.845	2.413	2.870		
37	2.378	2.884				
38	2.363	2.899	2.359	2.924		2.90
39	2.320	2.942				
40	2.295	2.967				
41	2.252	3.010	2.245	3.038		
42	2.214	3.048				
43	2.197	3.065				
44	2.176	3.086	2.163	3.120		

Point	Distance	Altitude	Distance	Altitude	Point
11	1.100	1.100			
12	1.100	1.100			
13	1.100	1.100			
14	1.100	1.100			
15	1.100	1.100			
16	1.100	1.100			
17	1.100	1.100			
18	1.100	1.100			
19	1.100	1.100			
20	1.100	1.100			
21	1.100	1.100			
22	1.100	1.100			
23	1.100	1.100			
24	1.100	1.100			
25	1.100	1.100			
26	1.100	1.100			
27	1.100	1.100			
28	1.100	1.100			
29	1.100	1.100			
30	1.100	1.100			
31	1.100	1.100			
32	1.100	1.100			
33	1.100	1.100			
34	1.100	1.100			
35	1.100	1.100			
36	1.100	1.100			
37	1.100	1.100			
38	1.100	1.100			
39	1.100	1.100			
40	1.100	1.100			
41	1.100	1.100			
42	1.100	1.100			
43	1.100	1.100			
44	1.100	1.100			
45	1.100	1.100			
46	1.100	1.100			
47	1.100	1.100			
48	1.100	1.100			
49	1.100	1.100			
50	1.100	1.100			

Peak	Q-value	Ex*(Mev)	Q-value	Ex*(Mev)	Q-value	Ex*(Mev)
45	2.147	3.115	2.145	3.138		3.12
46	2.077	3.185	2.075	3.208		
47	2.047	3.215				
48	2.024	3.238	1.995	3.288		
49	1.978	3.284	1.979	3.304		
50	1.948	3.314				3.30
51	1.923	3.339				
52	1.895	3.367				
53	1.843	3.419				
54	(1.798)	(3.464)				3.46
55	1.764	3.498				
56	1.698	3.564				
57	1.671	3.591				
58	1.609	3.653				
59	1.580	3.682				

** Obtained by subtracting the binding energy of the deuteron from their highest value gamma-ray energy.

The excitation energies reported by Bartholomew and Kinsey are found to be within the limits of error except for level number ten. This seems to confirm further the assumption that the gamma rays observed in their work originated in transitions to the ground state. Within the region obscured in the work of Foglesong and Foxwell, agreement with the 3.30-Mev and 3.46-Mev gamma rays is found to be good.

Peak	(0-75) sec	(75-150) sec	(150-225) sec	(225-300) sec
15	2.117	2.112	2.110	2.110
16	2.077	2.072	2.070	2.070
17	2.067	2.062	2.060	2.060
18	2.051	2.050	2.049	2.049
19	2.049	2.048	2.047	2.047
20	2.048	2.047	2.046	2.046
21	2.080	2.079	2.078	2.078
22	2.092	2.091	2.090	2.090
23	2.119	2.118	2.117	2.117
24	(2.170)	(2.169)	(2.168)	(2.168)
25	2.166	2.165	2.164	2.164
26	2.160	2.159	2.158	2.158
27	2.171	2.170	2.169	2.169
28	2.163	2.162	2.161	2.161
29	2.162	2.161	2.160	2.160

* Estimated by extrapolating the timing curve of the detector from their highest value frame-by-frame.

The maximum energies reported by instruments and timing are found to be within the limits of error except for level number two. This seems to explain further the assumption that the lower rays observed in their work originated in transitions to the ground state. Within the region observed in the work of Robinson and Fowler, agreement with the 1.30-1.35 MeV gamma rays is found to be good.

STRIPPING THEORY

The theory of deuteron stripping has been dealt with extensively^{11-14,27}. Therefore only a brief discussion of the principles will be given. A beam of monoenergetic incident particles can be represented in terms of plane waves, and the angular distribution of the emergent particles can be analyzed in terms of spherical harmonics. These harmonics are characterized by definite values of orbital angular momentum with respect to the nucleus. We can let the angular momentum of the incoming deuteron be $\overline{\ell}_d$ and its spin be \overline{S}_d . The angular momentum of the outgoing proton wave will be $\overline{\ell}_p$ and its spin \overline{S}_p . The captured neutron will have angular momentum $\overline{\ell}_n$ and spin \overline{S}_n . Let the target nucleus have angular momentum I and the residual nucleus have angular momentum J .

By conservation of total angular momentum, we find

$$\overline{I} + \overline{\ell}_d + \overline{S}_d = \overline{J} + \overline{\ell}_p + \overline{S}_p$$

Also, the difference in spin and angular momentum of the two nuclei is equal to that of the captured neutron:

$$\overline{J} - \overline{I} = \overline{\ell}_n + \overline{S}_n$$

Combining the above, we find:

$$\overline{\ell}_d - \overline{\ell}_p = \overline{\ell}_n + \overline{S}_n - (\overline{S}_d - \overline{S}_p).$$

NOTE: This discussion concerns only standard stripping theory and does not take into account the recently reported spin-flip stripping²⁸.

Since $\overline{S}_d = \overline{S}_p + \overline{S}_n$, and the spin of the proton does not change because it is not interacting with the nucleus, we find

$$\overline{l}_d - \overline{l}_p = \overline{l}_n + \Delta \overline{S}_n .$$

Thus, the values of $\overline{l}_d - \overline{l}_p$ are restricted by the conditions on \overline{l}_n . This gives rise to a description of the angular distribution of the emergent protons as a function of discrete values of \overline{l}_n , orbital angular momentum, with which the neutron enters the nucleus. The discrete values of \overline{l}_n are characterized by varying values of angle at which there is a maximum. Our calculations were based on the work of Friedman and Tobocman¹⁴, which is derived on the basis of four simplifying assumptions:

1. The coulomb interaction can be ignored;
2. The protons have no interaction with the target nucleus;
3. The deuteron fragments can be treated as free particles;
4. The deuteron wave function can be approximated by a plane wave.

The differential cross section for a (d,p) stripping process leading to a specific bound level of the residual nucleus in the center-of-mass coordinate system may be expressed in the following elementary form for convenience in calculation:¹⁵

where $\bar{E}_i = \bar{E}_i + \bar{E}_i$ and the sign of the system does not change

because it is not interacting with the medium, so that

$$\bar{E}_i = \bar{E}_i + \bar{E}_i$$

Thus, the value of $\bar{E}_i = \bar{E}_i$ are constant of the medium in \bar{E}_i .

This gives rise to a description of the angular distribution of the

emitted photons as a function of discrete values of \bar{E}_i , which

angular momentum, with which the medium enters the medium. The

discrete values of \bar{E}_i are characterized by varying values of angle

at which there is a maximum. Our calculations were based on the

work of Frenkel and Tatarskiy¹², which is derived on the basis of

four simplifying assumptions:

1. The optical interaction can be ignored;

2. The photon has no interaction with the

medium medium;

3. The electron frequency can be treated as

free particles;

4. The electron wave function can be approximated

by a plane wave.

The differential cross section has a $\langle A_{ij} \rangle$ averaging process

leading to a specific point level of the residual medium in the

center-of-mass coordinate system and is expressed in the following

equation for conversion in calculation¹²

$$\sigma(\theta_{\text{CMS}}) = (2J + 1) C D \sum_{\ell} \gamma_{\ell} B_{\ell}.$$

C is a constant for the level, calculated from the masses and energies of the particles in the reaction, the nuclear radius, and the angular momentum of the target nucleus. D is the deuteron factor which is determined from the approximate internal wave function of the deuteron. This is a function of angle and expresses the probability of the proton, neutron, and incident deuteron wave functions matching the correct internal wave function in the deuteron. γ_{ℓ} is the partial reduced width for each value of ℓ_n and its empirical determination will be discussed later. Finally, B_{ℓ} represents a term composed of spherical Bessel and Hankel functions.

$$\pi(\frac{1}{2}, \frac{1}{2}) = (2\pi + 1) \sum_{k=0}^{\infty} \frac{1}{k!} \pi_k$$

0 is a constant for the level, calculated from the mean and variance of the population in the analysis, the analysis table, and the analysis variance of the sample analysis. It is the analysis factor which is determined from the appropriate interval and divided by the distance. This is a function of sample size and represents the width of the error, distance, and distance between two functions within the error interval was divided by the distance. It is the partial reduced with the value of 10 and the constant 10. This will be discussed later. Finally, 10 represents a form composed of spectral, partial and partial functions.

ANGULAR DISTRIBUTIONS

The problem of finding the cross section for the stripping reaction was attacked by use of the alpha-particle thickness gauge mentioned previously to measure the thickness of cobalt on the Formvar film. Measurements were made before and after the cobalt was evaporated onto the Formvar. The difference in the two measurements gave the thickness of the cobalt in terms of the equivalent stopping power of air, in mils, for the alpha particles of polonium. The energy loss per centimeter of path for a substance is found from²⁴

$$\frac{dE}{dx} = \frac{4\pi e^4 z^2}{mV^2} NB,$$

where V = velocity of incident particle

N = number of atoms in target per cm^3

z = charge of incident particle

m = mass of electron

B , the "atomic stopping number," is found from

$$B = Z \ln \frac{2mV^2}{I},$$

where Z = charge of target, and

I = ionization potential of target.

The energy loss of the alpha particles is the same for each medium. The energy loss per centimeter of path is a constant for each medium; hence a simple constant ratio relating the energy loss in cobalt to that in air can be formed. Since the thickness of the cobalt

ANALYSIS OF THE PROBLEM

The problem of finding the wave number for the standing wave-
tion was attacked by use of the eigenvalue method. The eigenvalue
problem is solved by the method of separation of variables. The
eigenvalue problem is solved by the method of separation of variables.
The eigenvalue problem is solved by the method of separation of variables.
The eigenvalue problem is solved by the method of separation of variables.
The eigenvalue problem is solved by the method of separation of variables.
The eigenvalue problem is solved by the method of separation of variables.
The eigenvalue problem is solved by the method of separation of variables.
The eigenvalue problem is solved by the method of separation of variables.

$$\frac{d^2 \psi}{dx^2} + k^2 \psi = 0$$

where ψ = velocity of incident wave

k = wave number of incident wave

ψ = change of incident wave

ψ = wave of incident

ψ , the second standing wave, is found from

$$\frac{d^2 \psi}{dx^2} + k^2 \psi = 0$$

where ψ = change of wave, and

ψ = reflection potential of wave.

The energy loss of the wave is found by the method of

method. The energy loss per unit length of wave is a constant for

each medium; hence a single constant value exists for energy loss in

each medium. The energy loss per unit length of wave is a constant for

in mils of air equivalent is known, the thickness of cobalt can be determined by multiplying the ratio of the energy losses per centimeter of path times the air equivalent thickness. For an air equivalent thickness of 13 mils, this gave about 5.0×10^{-6} cm for the thickness of cobalt.

The half-width of a cobalt elastically scattered deuteron peak was computed from the Q-equation using the previously determined thickness of cobalt. A comparison with the observed half-width of the deuteron elastic peak at 90 degrees showed that the cobalt layer contributed 60 to 70 percent to the observed half-width. This seems to be reasonable, taking into account the angle between the target and the incident deuteron beam.

The approximate differential cross section for the (d,p) reaction is determined from the following expression:

$$\frac{d\sigma(d,p)}{d\Omega} = \frac{N_p}{N_{Co} dx IA \Omega} \frac{\text{cm}^2}{\text{Steradian}}$$

where N_p = number of proton tracks observed in the (d,p) peak

N_{Co} = number of atoms of cobalt per cubic centimeter of target

dx = the effective thickness of the cobalt layer in centimeters

IA = the number of incident deuterons measured by the current integrator

Ω = the solid angle subtended by the magnetic spectrograph at a distance of 52 centimeters along the plate, in steradians.

in air of air equivalent is known, the thickness of deposit can be determined by multiplying the ratio of the energy losses per unit-
 meter of path in air and air equivalent thickness. For an air equivalent thickness of 1.5 mls, this gives about 2.0×10^{-6} m for the thickness of deposit.

The half-width of a deposit electrically measured section was was computed from the deposition ratio and previously determined thickness of deposit. A comparison with the observed half-width of the detector electric peak at 90 degrees showed that the deposit layer contributed 60 to 70 percent to the observed half-width. This seems to be reasonable, taking into account the angle between the target and the incident deuteron beam.

The experiment differential cross section for the (d,p) reaction is determined from the following expression:

$$\frac{d\sigma}{d\Omega} = \frac{N_p}{N_d} \frac{N_c}{N_t} \frac{1}{\sin^2 \theta} \frac{1}{\Omega} \frac{dN}{d\Omega d\theta}$$

where N_p = number of proton tracks observed in the (d,p) count
 N_c = number of counts at center per solid angle of target
 θ = the effective thickness of the deposit layer in centimeters
 N_d = the number of incident deuterons measured by the current
 integrator
 Ω = the solid angle subtended by the magnetic spectrograph at a distance of 50 centimeters from the target, in steradians.

It was found advantageous to convert the constant term in the above expression into a conversion term equal to

$$0.02 \frac{\text{millibarns/steradian}}{\text{proton track}} .$$

This term, multiplied by the number of proton tracks observed, gives the value of cross section used in the results.

A comparison of observed elastic scattering at 90 degrees to the calculated Rutherford scattering was made. The differential elastic cross section was determined from the above expression, using the number of deuterons observed and was found to be about

25 $\frac{\text{nb}}{\text{steradian}}$ at 90 degrees. The Rutherford cross section was computed from the following expression²³

$$\frac{d\sigma_R}{d\Omega} = 5.2 \times 10^{-27} \left(\frac{Z_I Z_T}{E_I} \right)^2 \left[1 - \left(\frac{M_I}{M_T} \right)^2 \right]^{\frac{1}{2}} \frac{\text{cm}^2}{\text{steradian}}$$

where I and T refer to the incident and target nuclei. This gives a value of 109 millibarns per steradian at 90 degrees, about four times the observed elastic scattering.

In addition, a correction was made to all cross sections thus obtained and to each angle in order to convert from the laboratory system into the center-of-mass system for comparison with the theory. This was facilitated by figures in Enge and Graue¹⁵ and amounted to a small increase in each angle and a small reduction in cross sections below 90 degrees.

It was found experimentally that the observed rate in the above reaction is a composite law equal to

$$\frac{0.05}{\text{mole liter}^{-1} \text{ sec}^{-1}}$$

This law, indicated by the nature of the reaction observed, gives the value of the reaction rate in the reaction.

A comparison of observed kinetic results at 30 degrees

the calculated values for the reaction rate. The difference

between the two values was observed from the above equation, being

the number of molecules observed and was found to be about

2.5. The observed reaction rate was

found from the following equation

$$\frac{0.05}{\text{mole liter}^{-1} \text{ sec}^{-1}} = 2.5 \times 10^{-6} \left(\frac{1}{\text{mole liter}^{-1}} \right)^2 \left[1 - \left(\frac{1}{\text{mole liter}^{-1}} \right)^2 \right]$$

where 1 and 2 refer to the initial and final states. This gives a

value of the equilibrium constant of 30 degrees, about four times

the observed kinetic constant.

In addition, a correction was made to all cross section data

obtained and to each value in order to correct from the laboratory

values into the number-of-moles system for comparison with the theory.

This was facilitated by dividing in each case by 2.5 and rounded to a

value between 1.5 and 2.5, and a small reduction in cross section

below 30 degrees.

The solid angle on the photographic plate, as mentioned in Section II, is approximately 3.4×10^{-4} steradians at a plate distance of 52 centimeters. The relative solid angle curve of reference 17 can be used to correct for variation in solid angle as a function of distance along the plate. The data points and curves of angular distributions presented later in this section were not so corrected, but the correction term is listed in Table VII. This correction varies from 1.155 to 0.875 and has been used to obtain all the results reported in Table VII.

The paper by Enge and Graue¹⁵ presents the method of numerical calculations in detail with the aid of an example. The same procedure was used in the present work with the results for the twenty-six levels being shown in Figure 6 through 31.

Prior to fitting the theoretical curve to the experimental points which represent the angular distribution of the cross section, an arbitrary isotropic background cross section was subtracted from the value at each angle²⁷. The amount was determined by inspection of each level distribution at the angle where the curve is most nearly zero (that is, 90 to 110 degrees). The background cross sections for all reported levels are given in Table VII and are shown in Figures 32 and 33. Twenty-three levels with small cross sections could not be assigned a value of ℓ_n for one of two reasons. Some of these display an isotropic distribution which may be caused by compound-nucleus formation or by a stripping reaction with an $\ell_n > 3$

The solid angle of the anisotropic element was measured in Section II, by means of a solid angle of 25 centimeters. The relative solid angle of reference is not used to correct for variation in solid angle as a function of distance from the plate. The data points are given at regular intervals but the points presented later in this section were not so corrected, but the correction given is listed in Table VII. This correction varies from 1.1% to 0.8% and has been used to obtain all the results reported in Table VII.

The paper by ¹² ~~the author~~ ¹² presents the method of measuring calculations in detail with the aid of an example. The same procedure was used in the present work with the results for the twenty-five levels being shown in Figure 8 through 31.

Prior to fitting the theoretical curve to the experimental points which represent the regular distribution of the cross section, an arbitrary isotropic background cross section was subtracted from the value at each angle. The amount was determined by inspection of each level distribution at the angle where the curve is best nearly zero (about 90 to 110 degrees). The background cross section for all reported levels are given in Table VII and are shown in Figure 32 and 33. Twenty-five levels with small cross sections could not be assigned a value of $\frac{1}{2}$ for one of two reasons. Some of these display an isotropic distribution which may be caused by component-matrix correction or by a slight variation with an $\frac{1}{2}$.

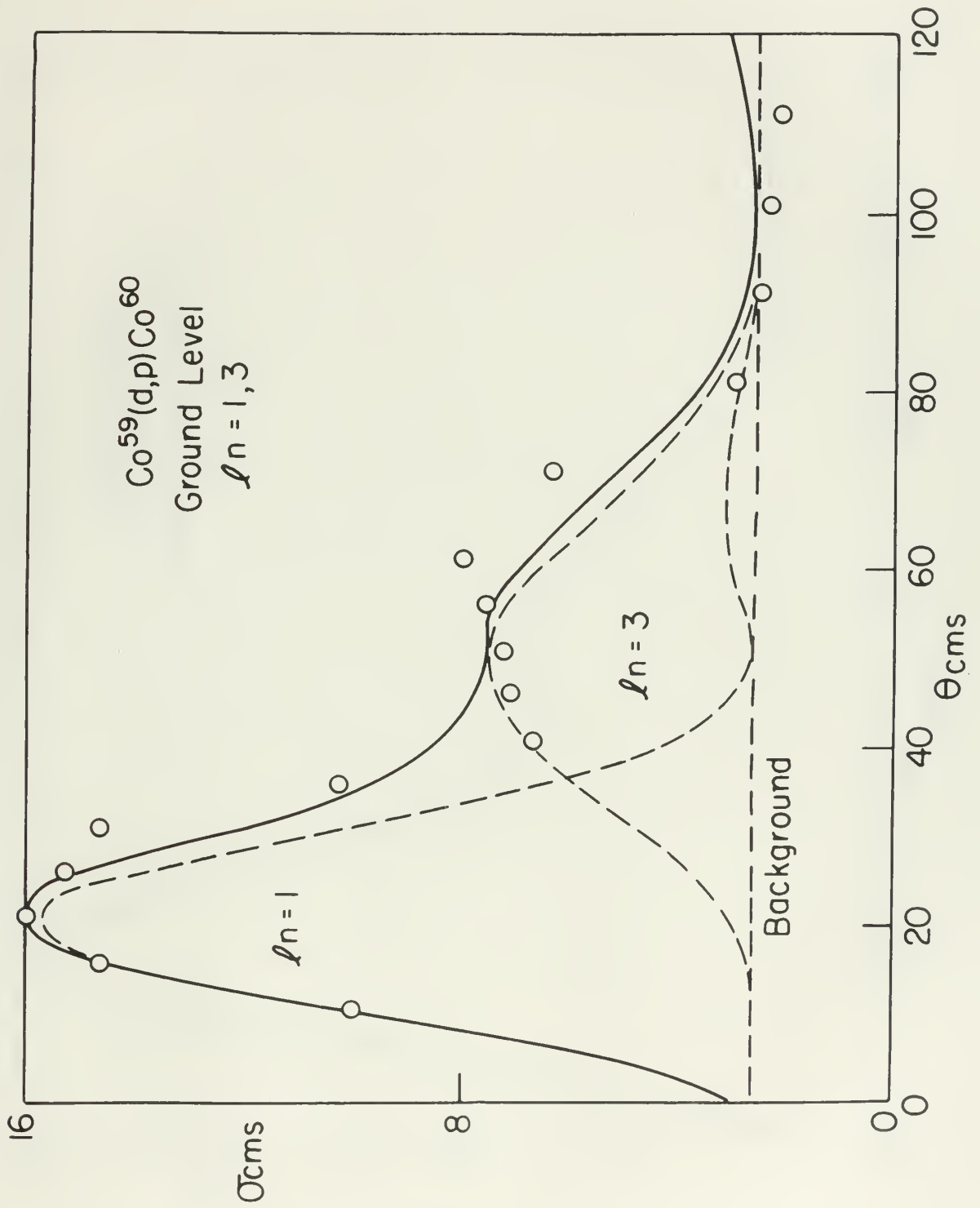


Figure 6

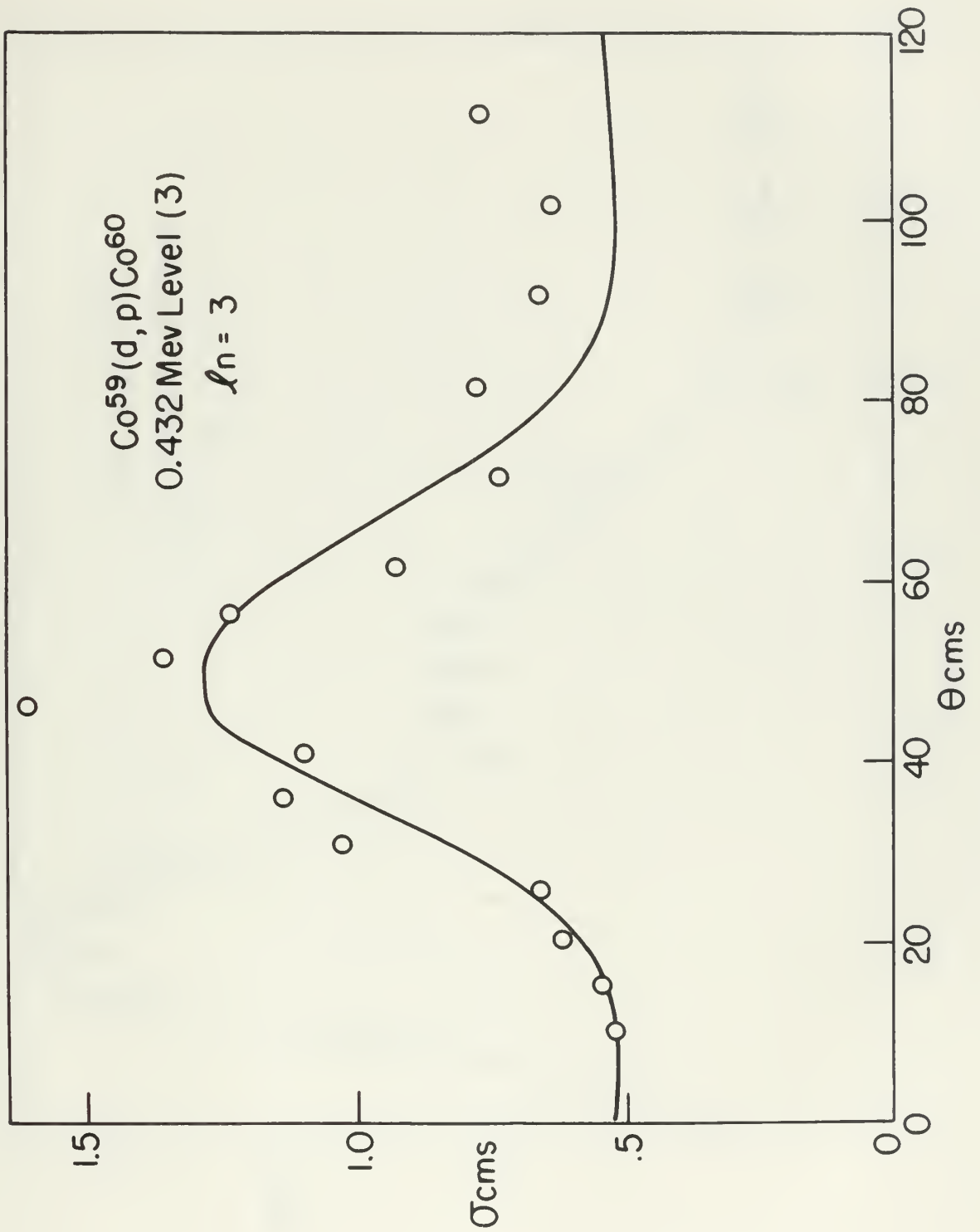


Figure 9

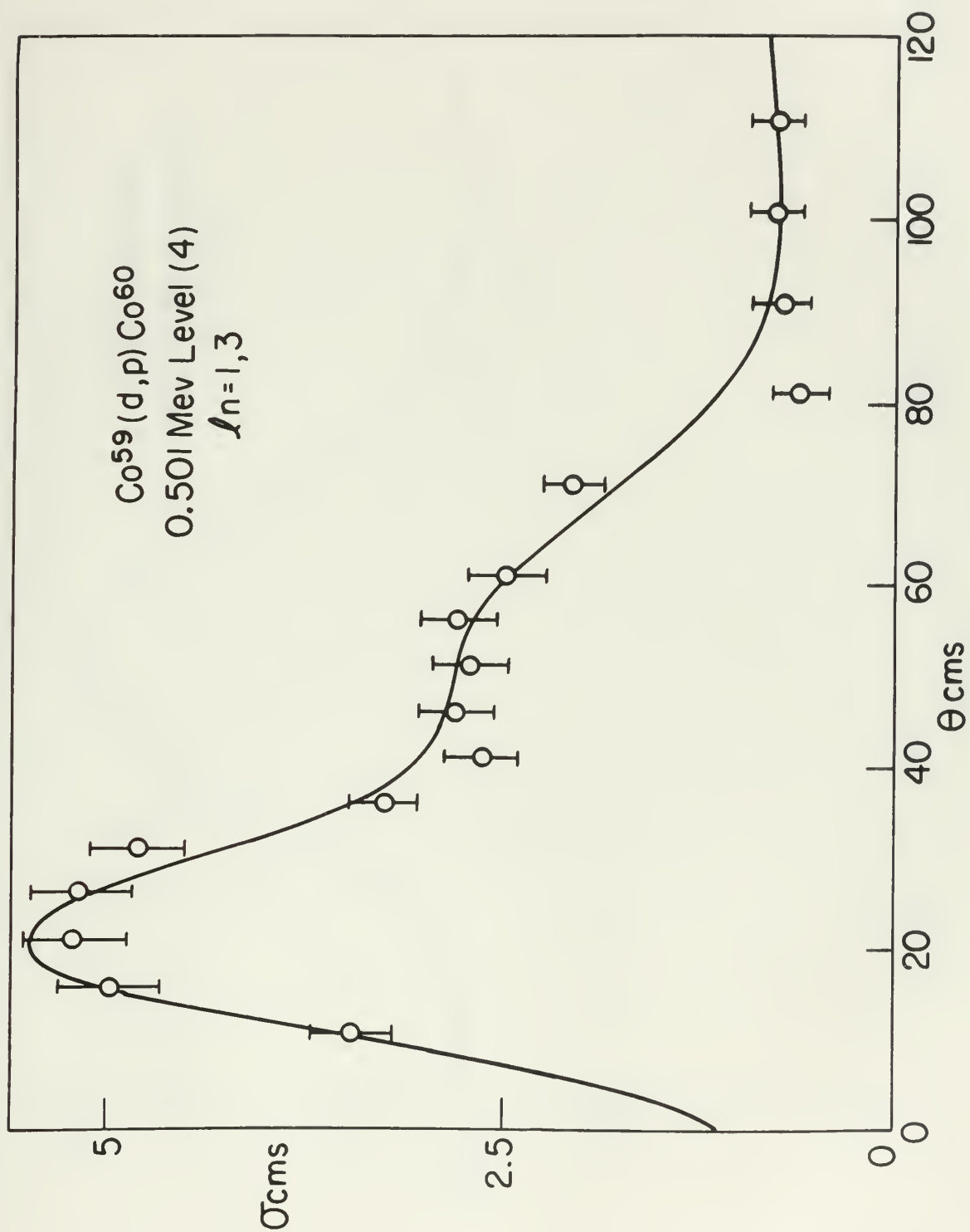


Figure 10

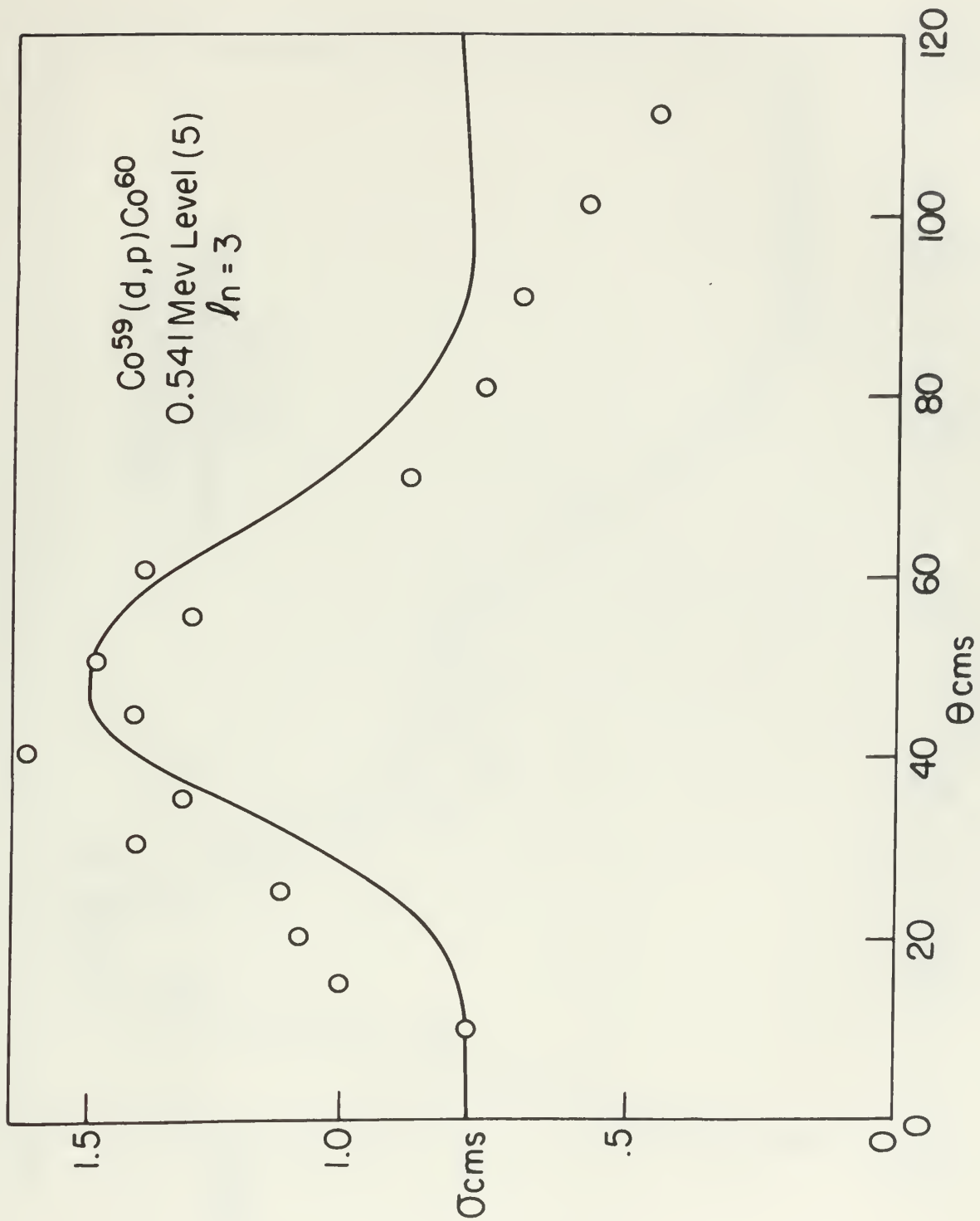


Figure 11

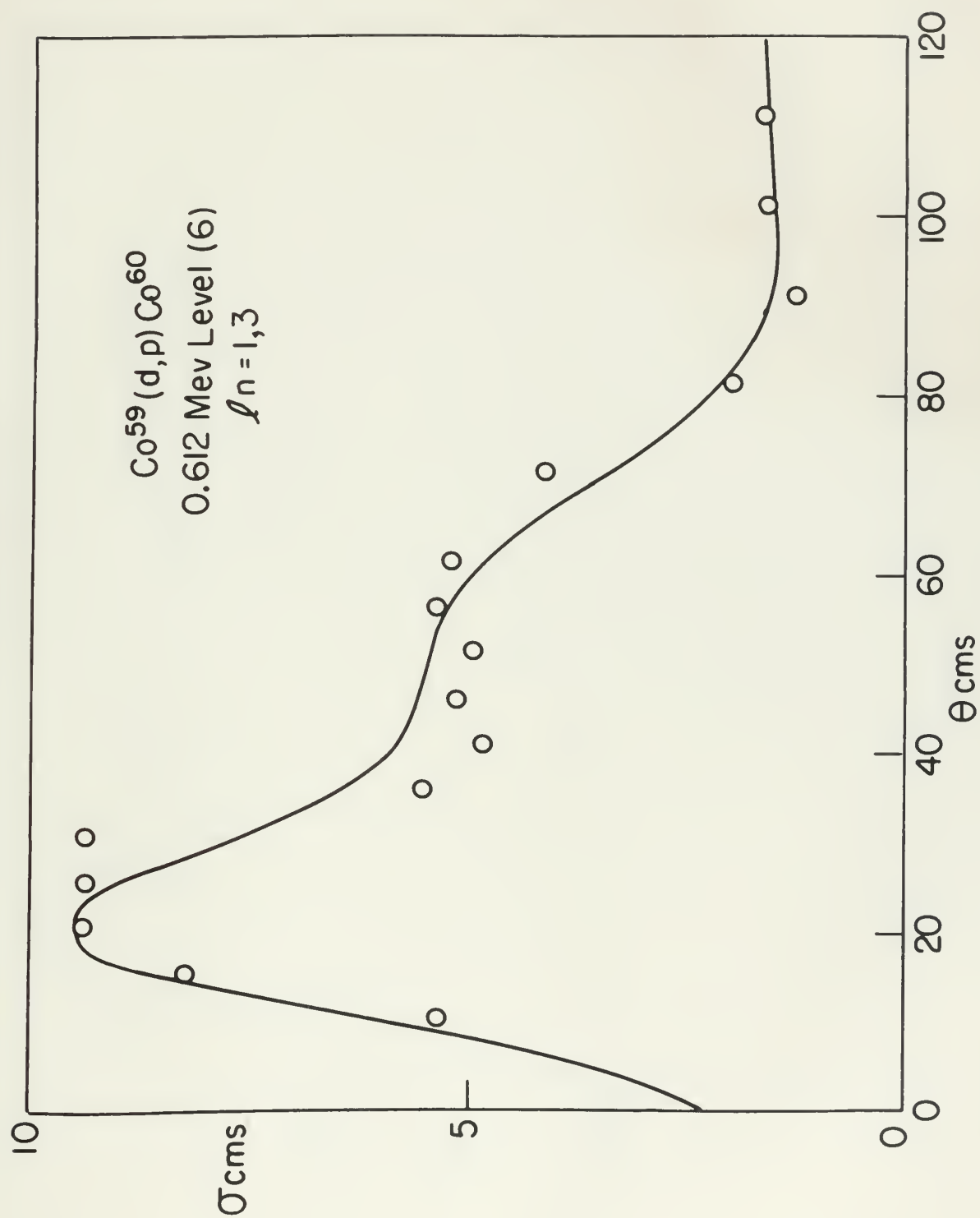


Figure 12

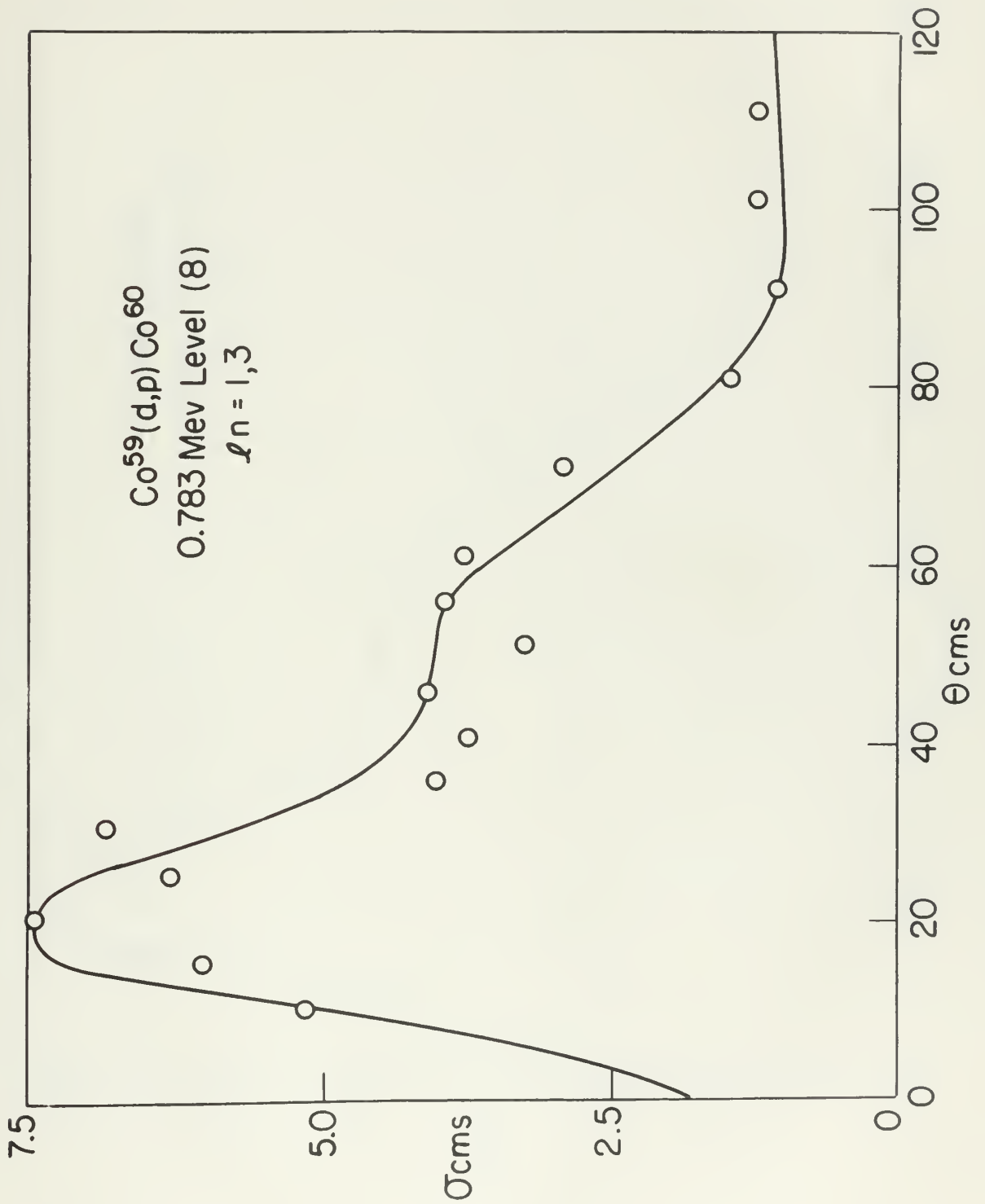


Figure 13

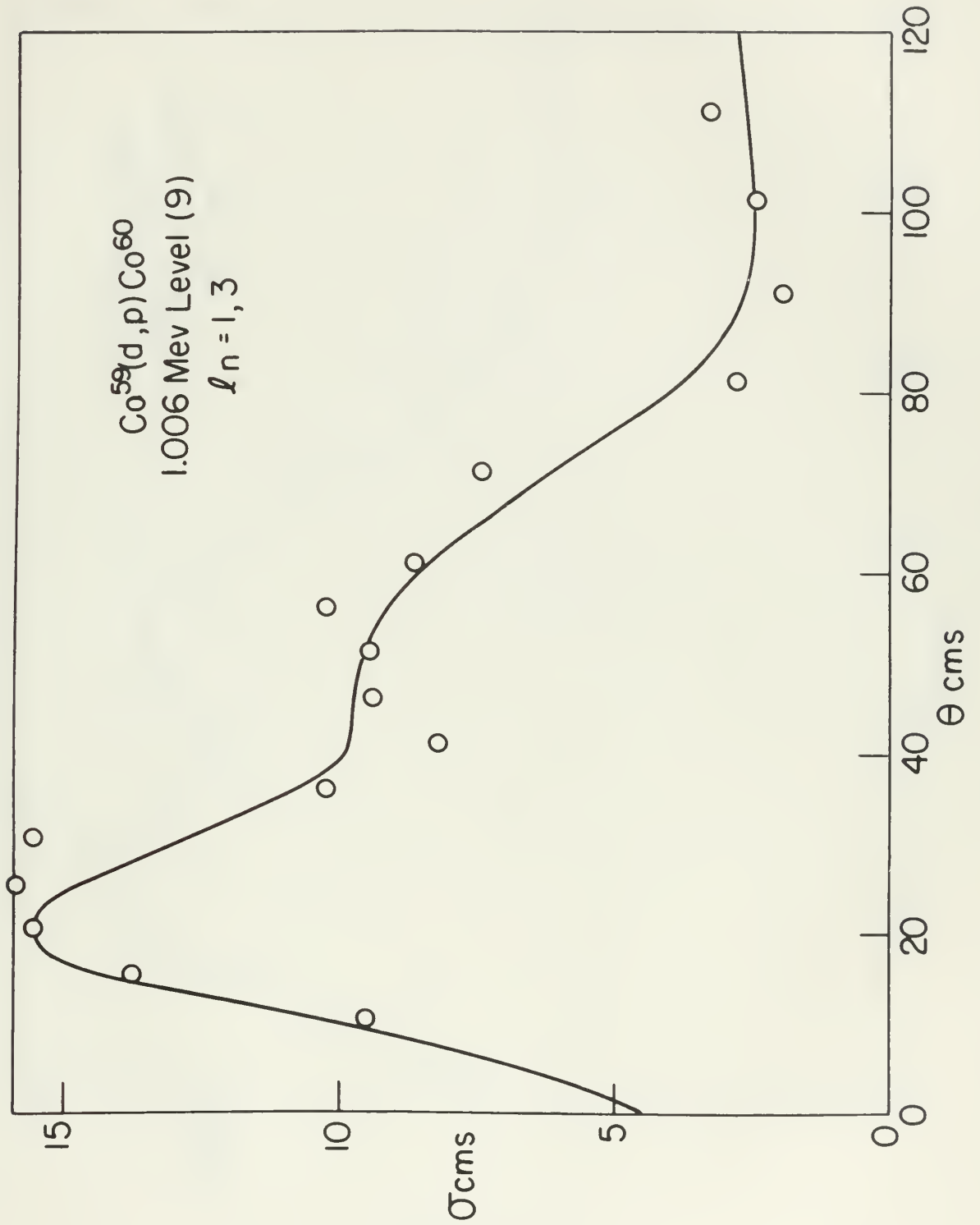


Figure 14

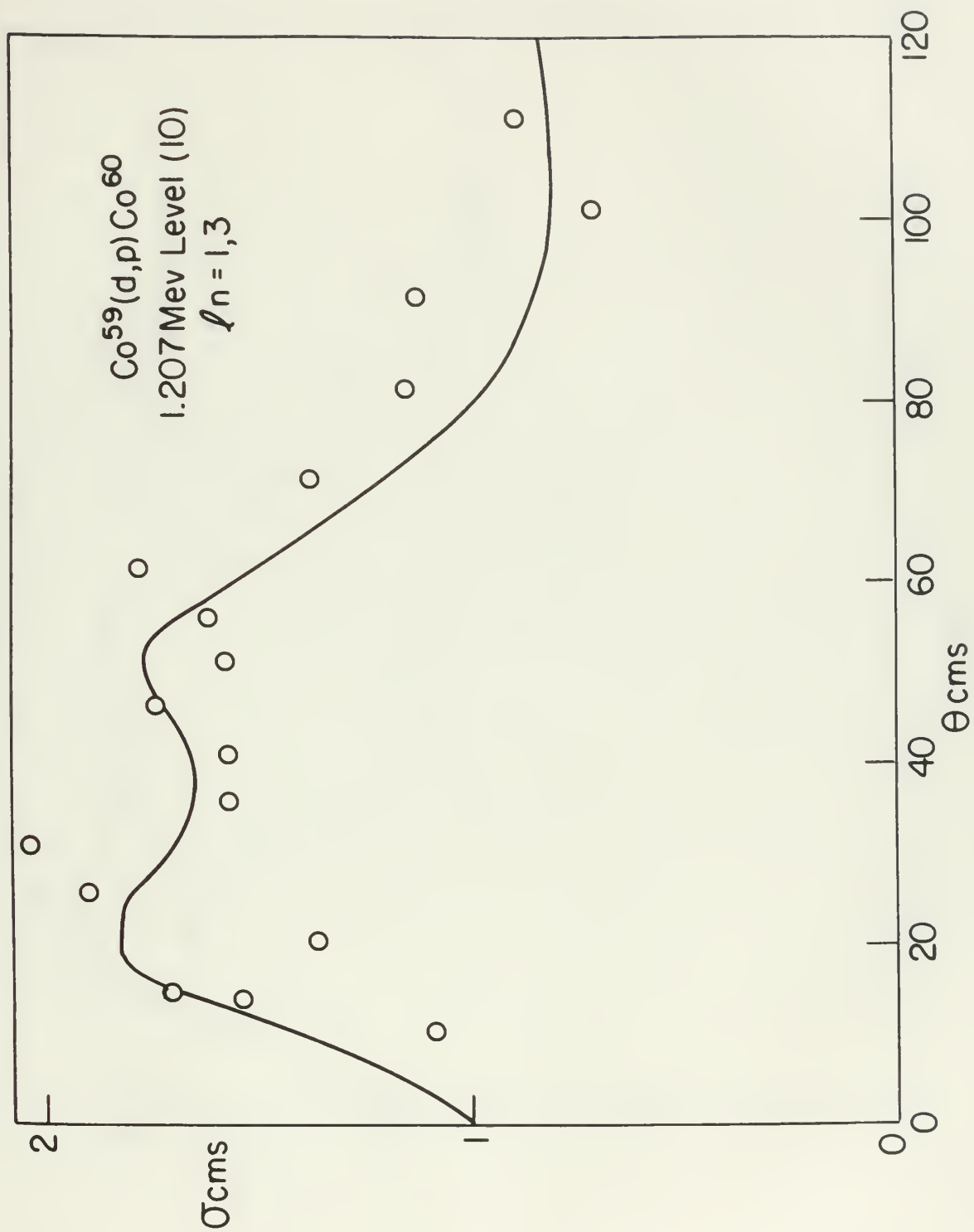


Figure 15

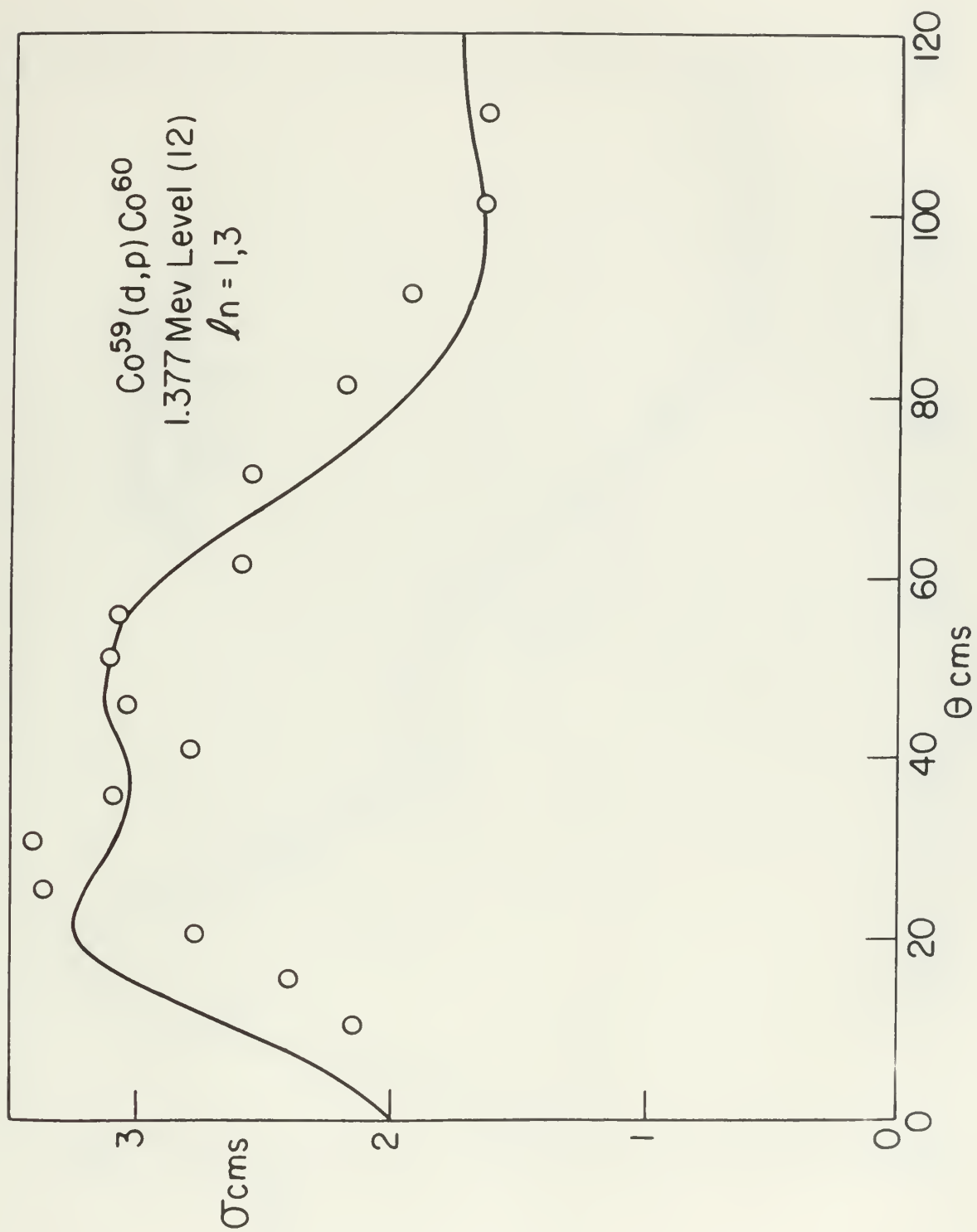


Figure 16

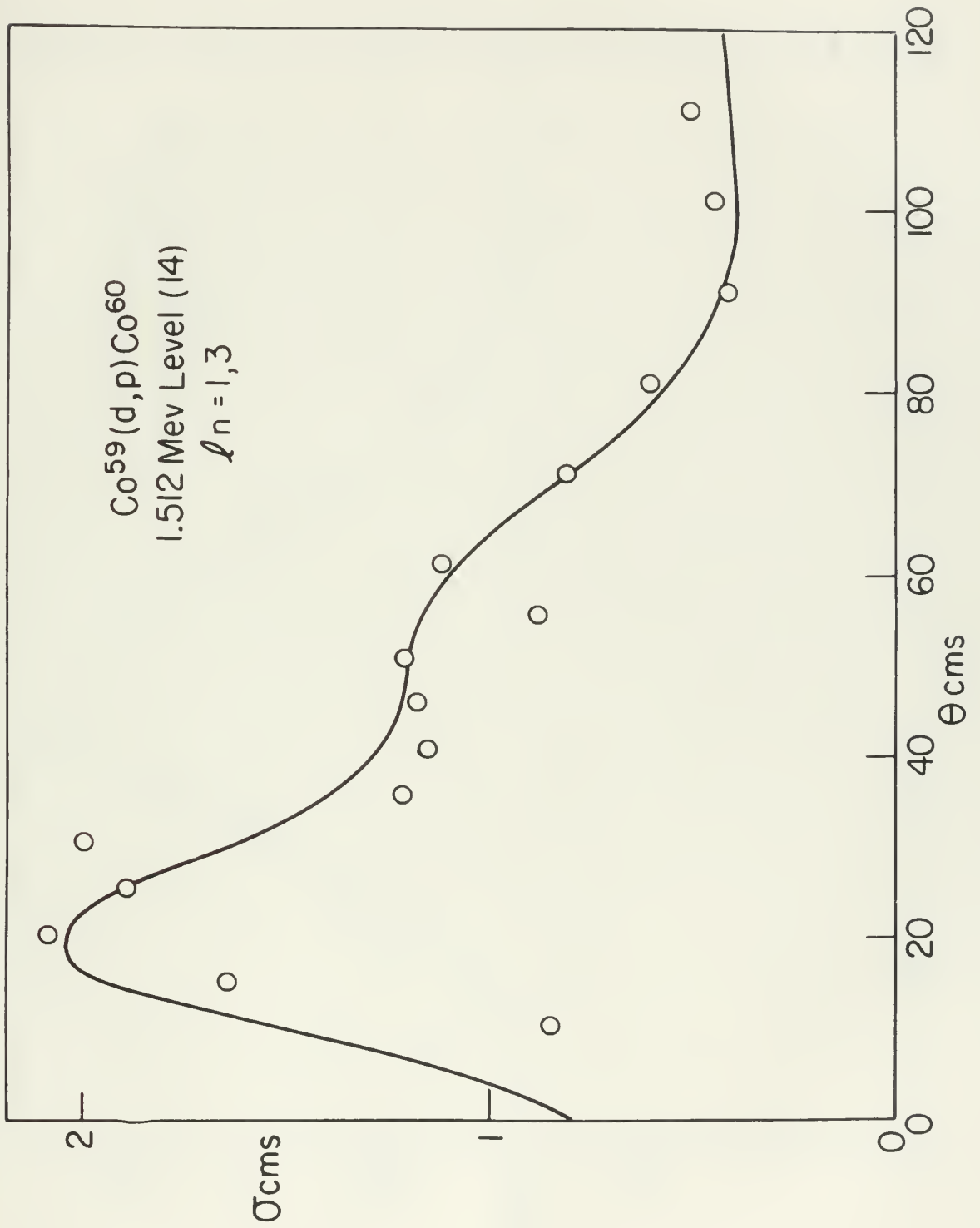


Figure 17

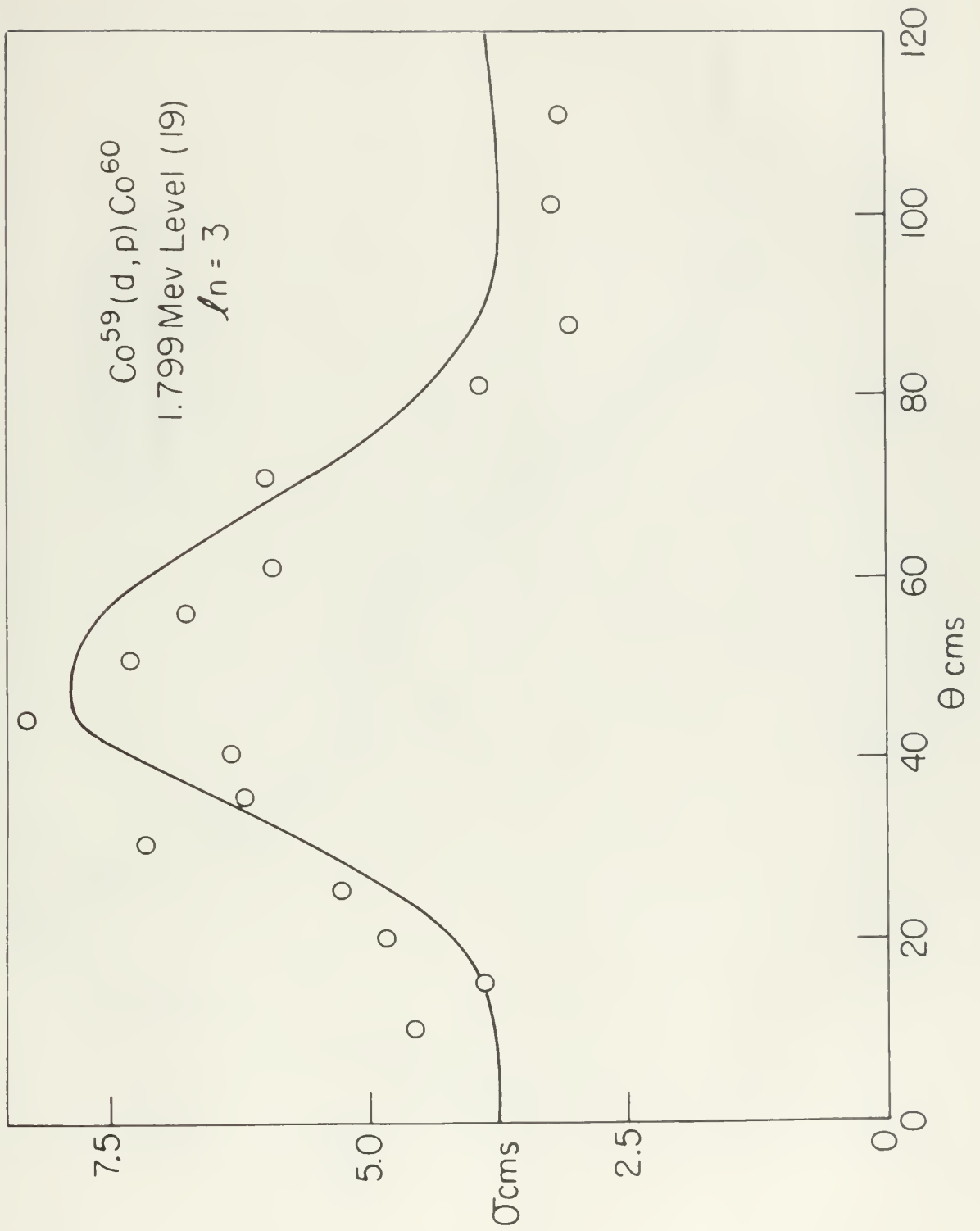


Figure 18

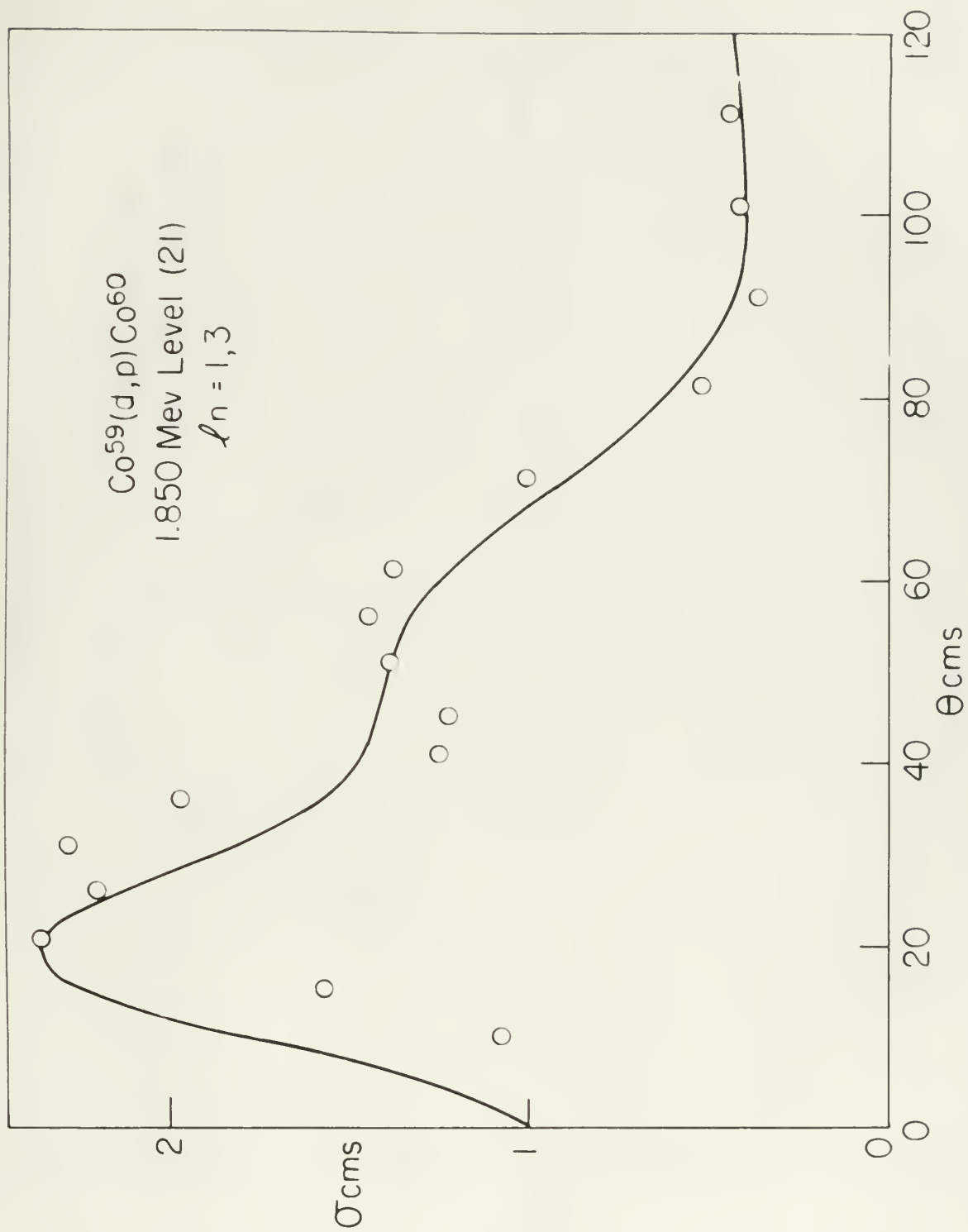


Figure 19

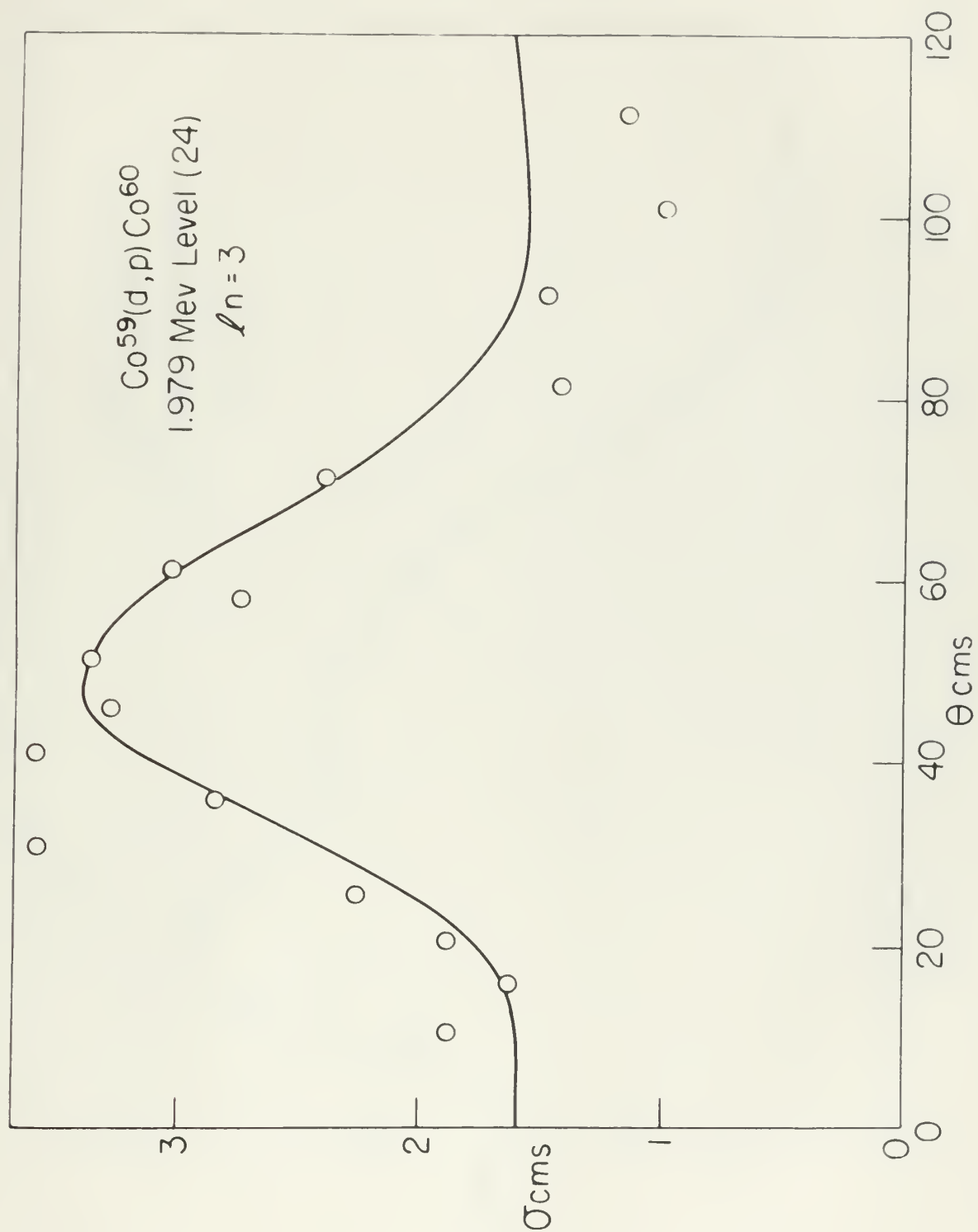


Figure 20

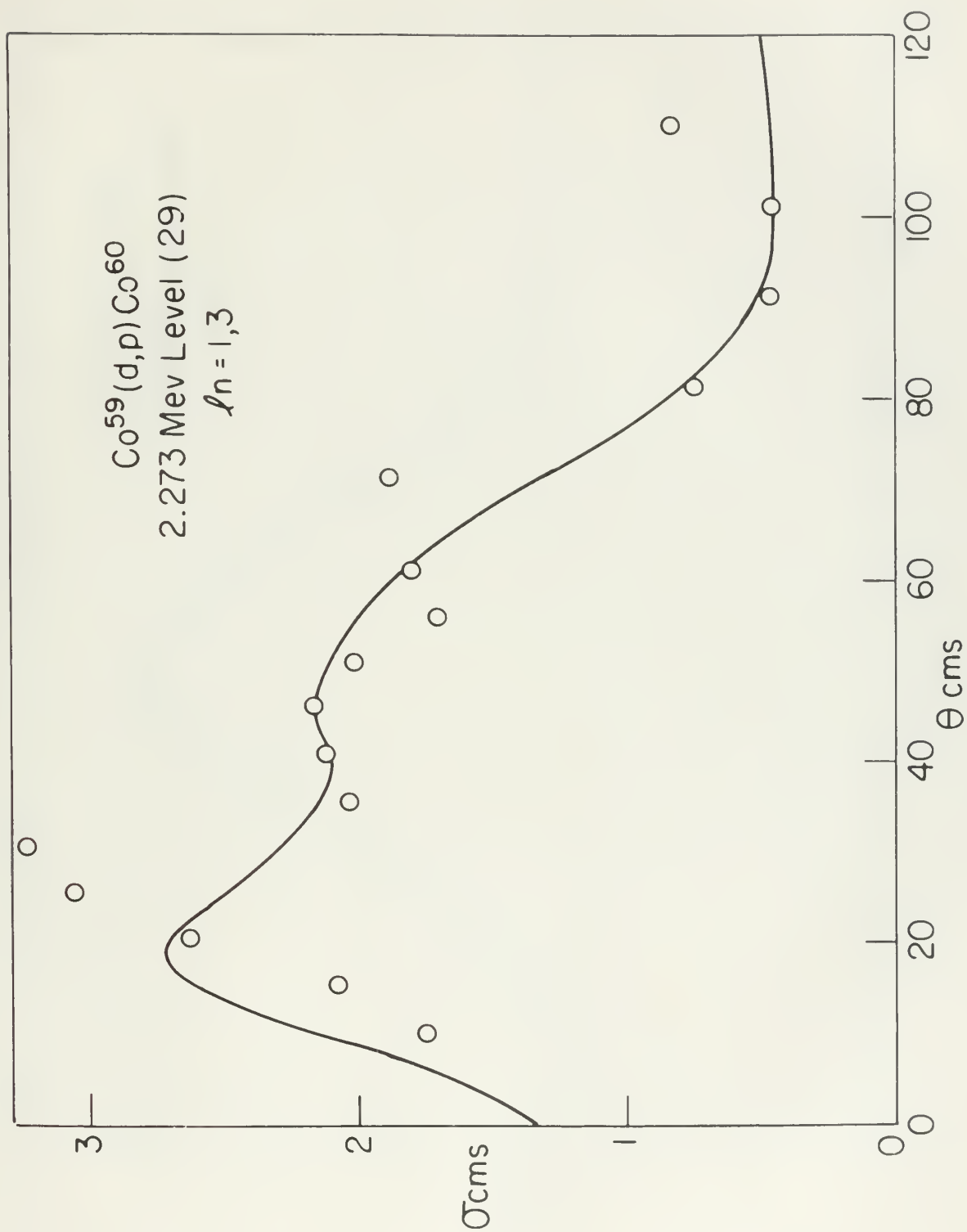


Figure 21

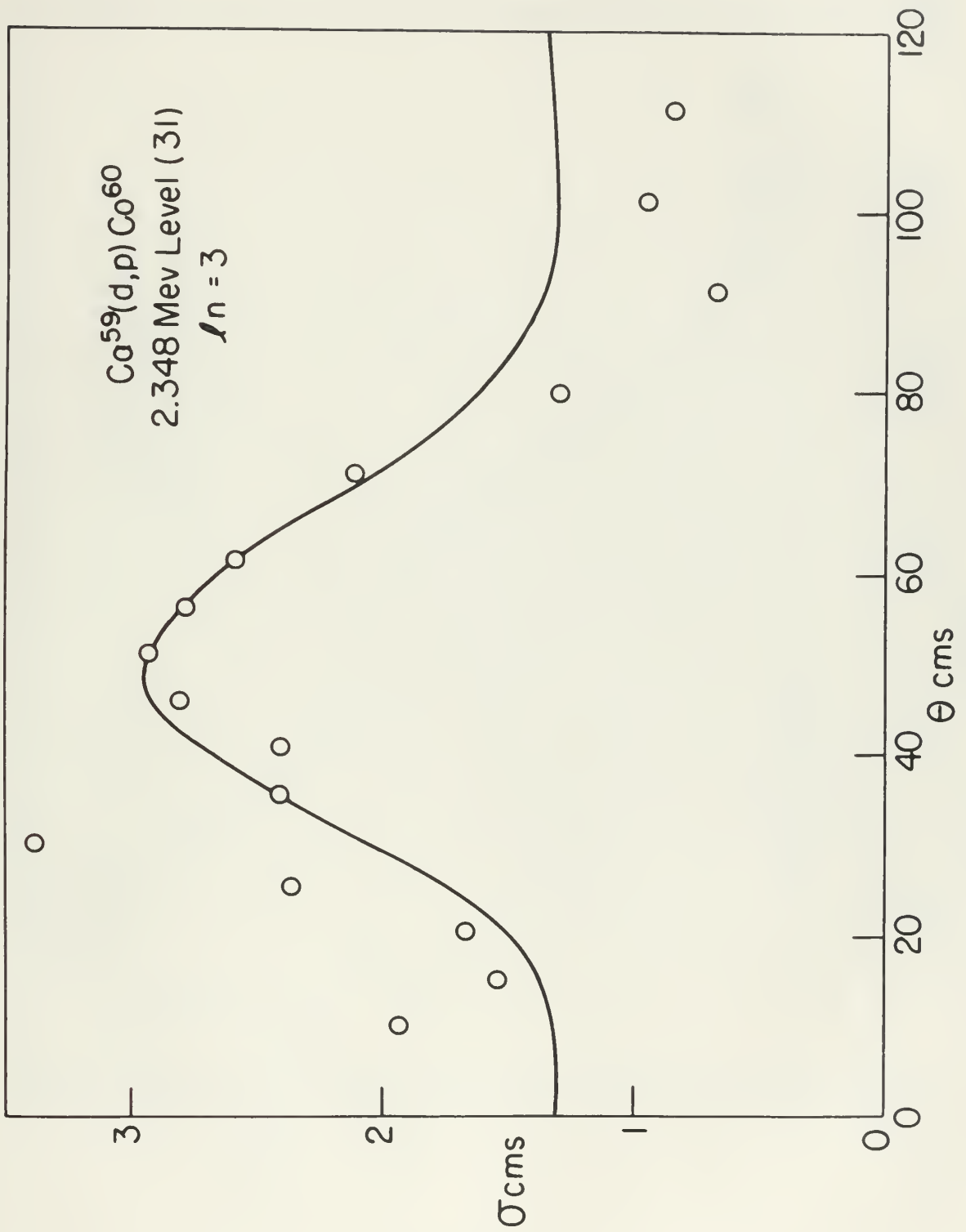


Figure 22

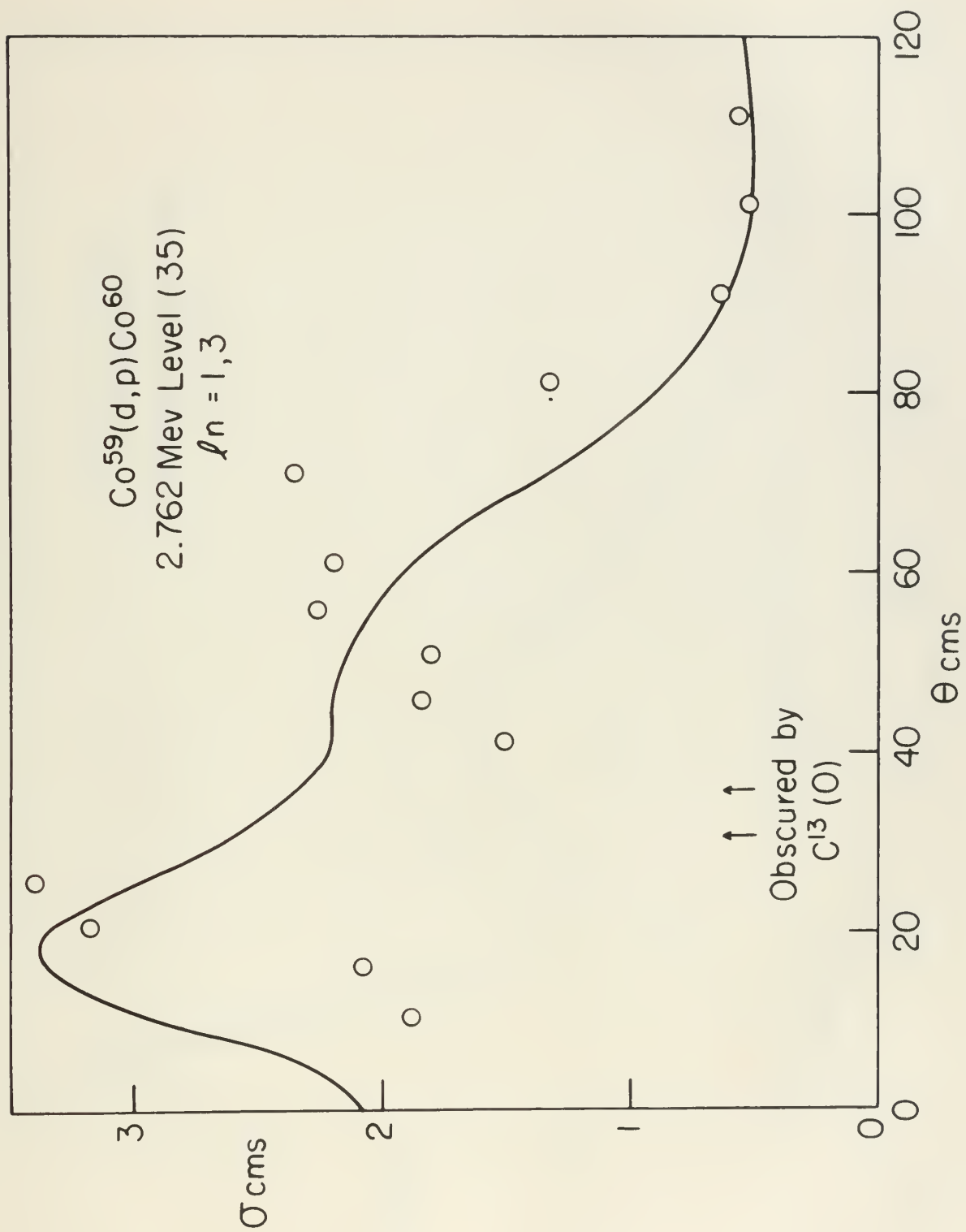


Figure 23

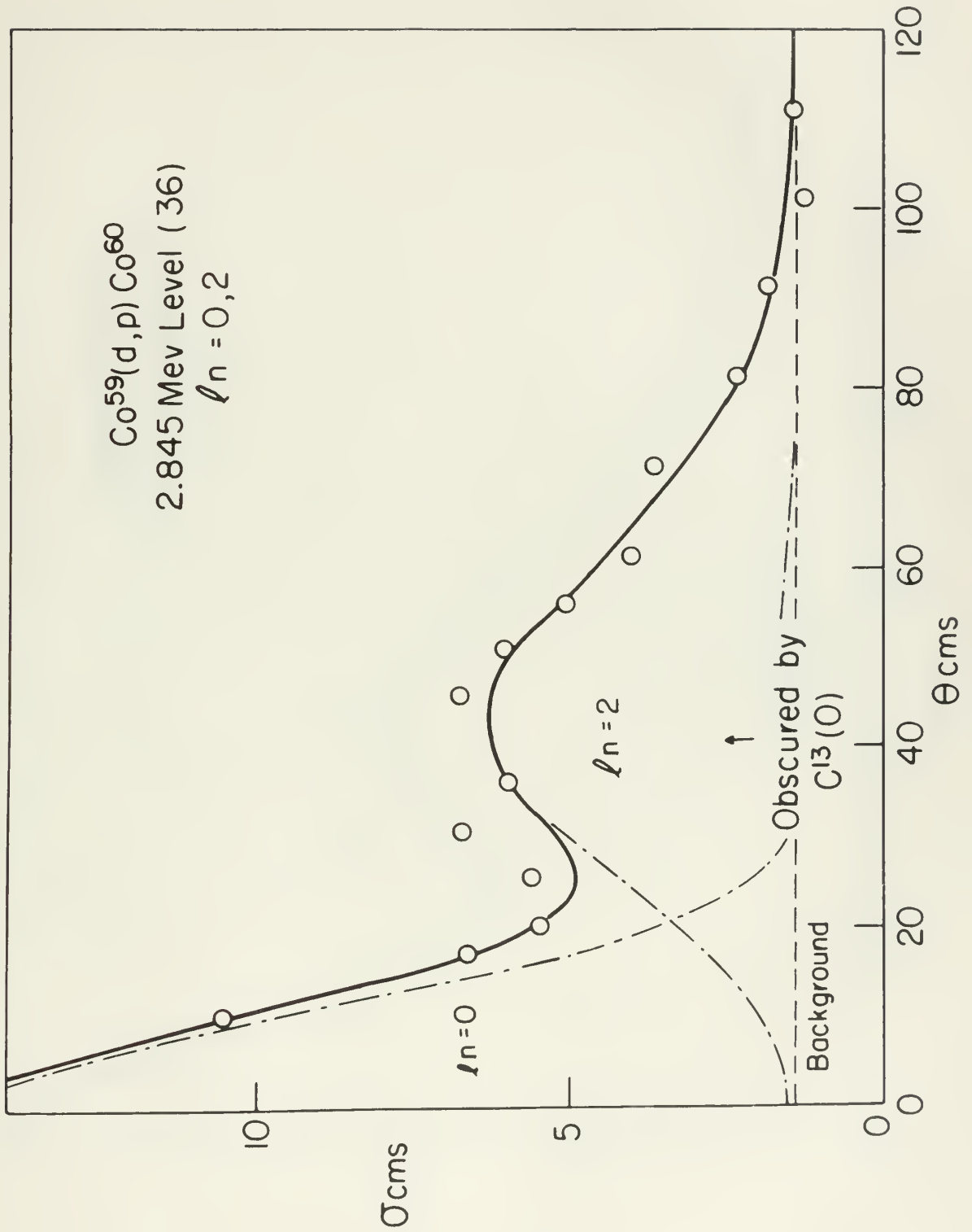


Figure 24

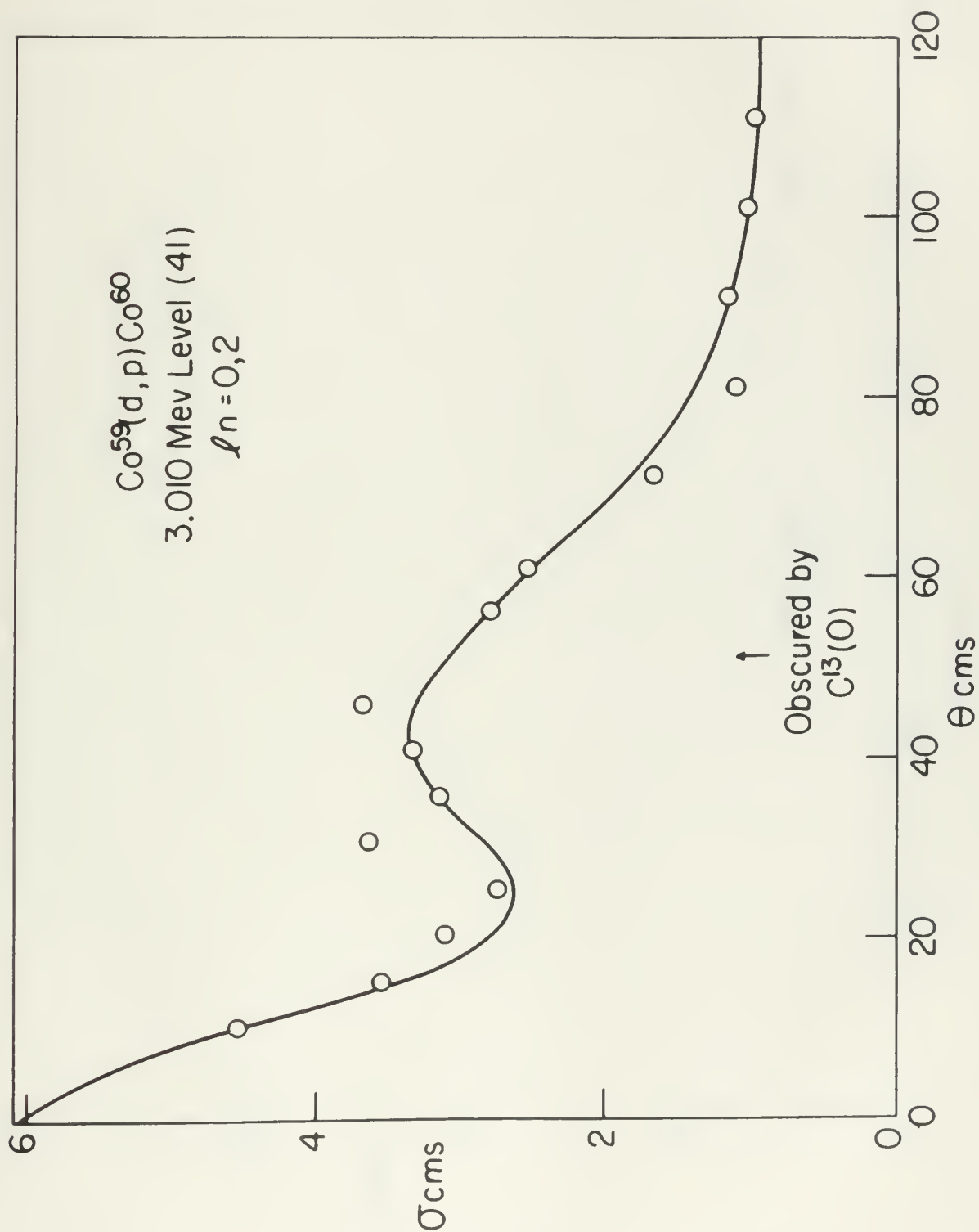


Figure 25

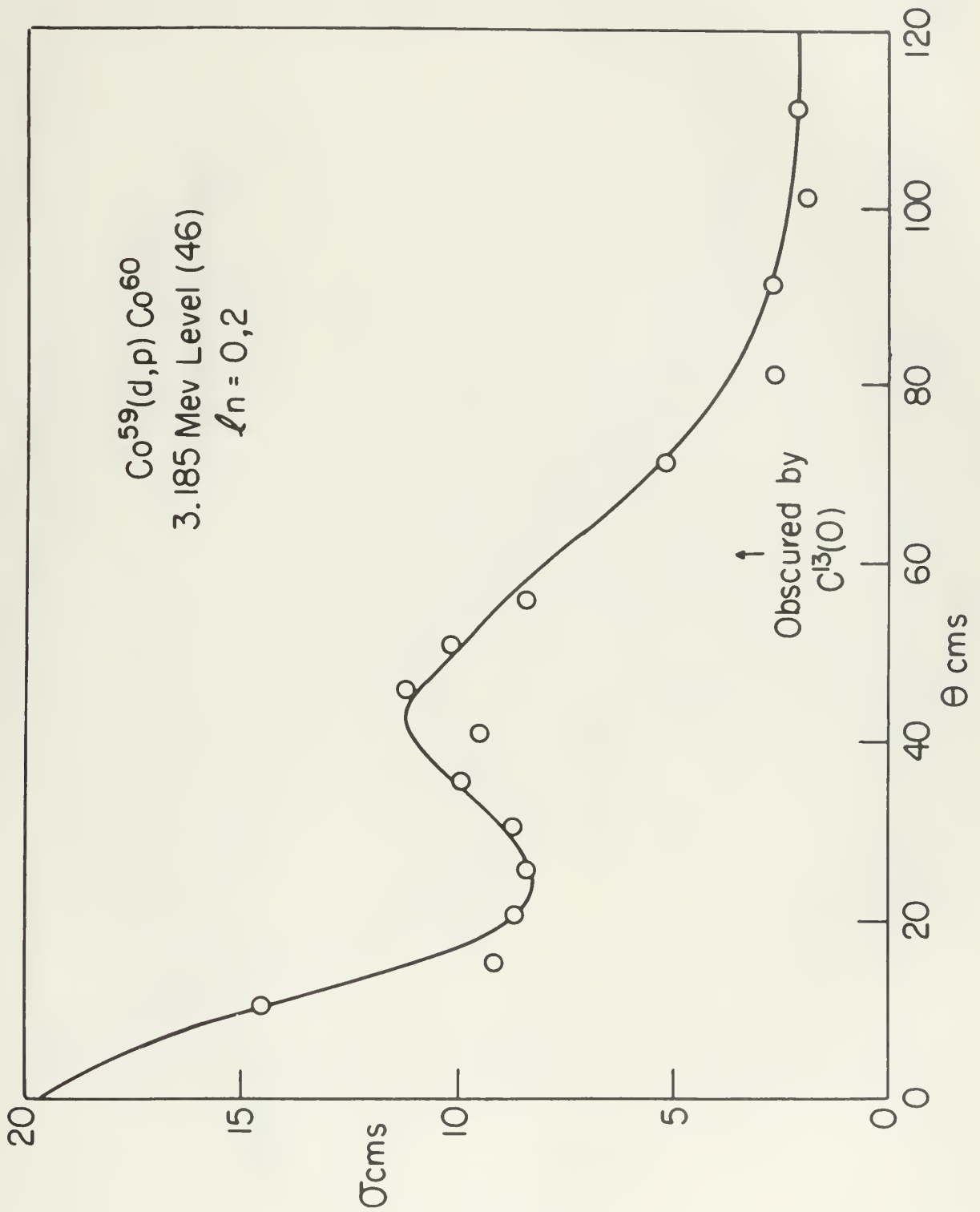


Figure 26

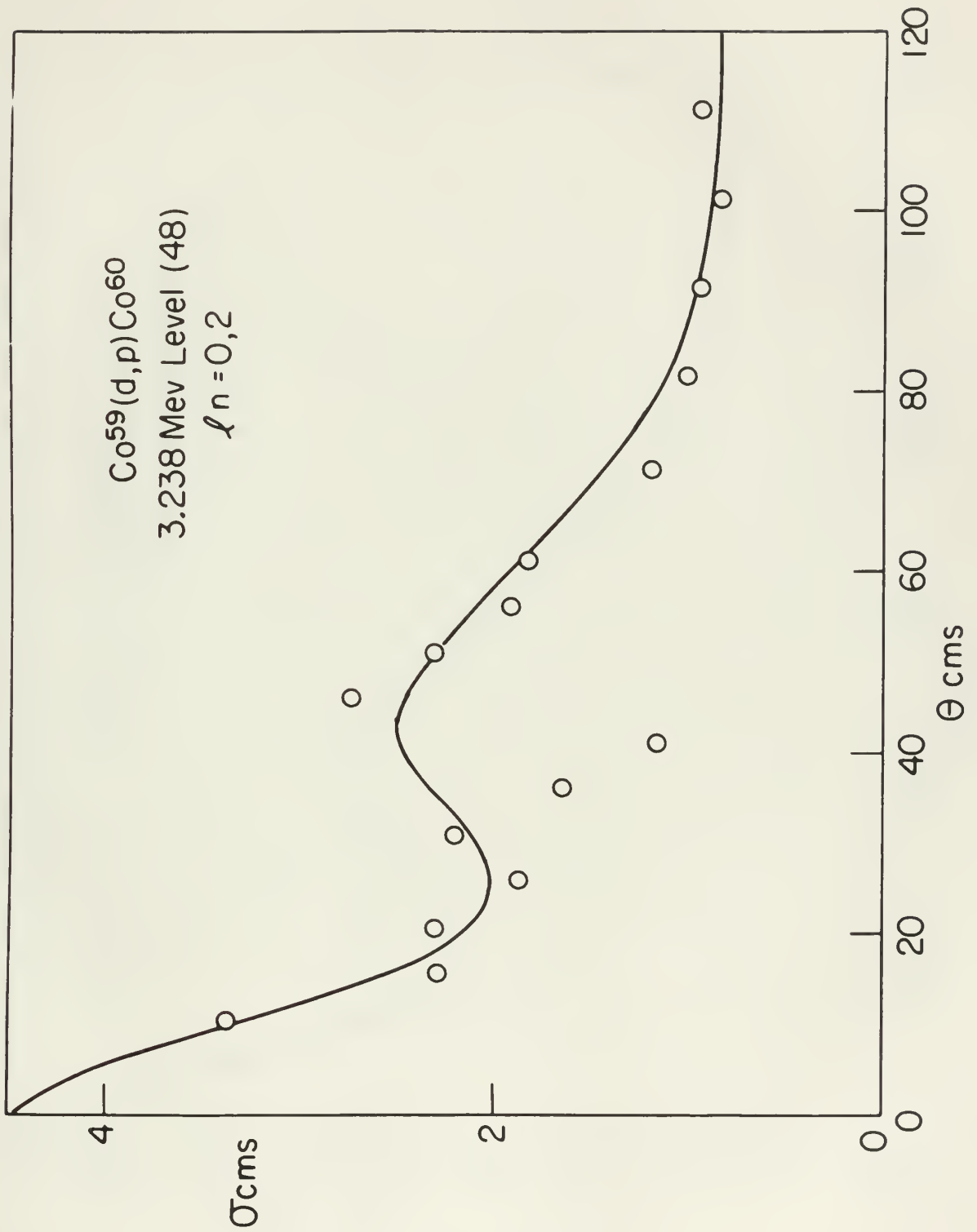


Figure 27

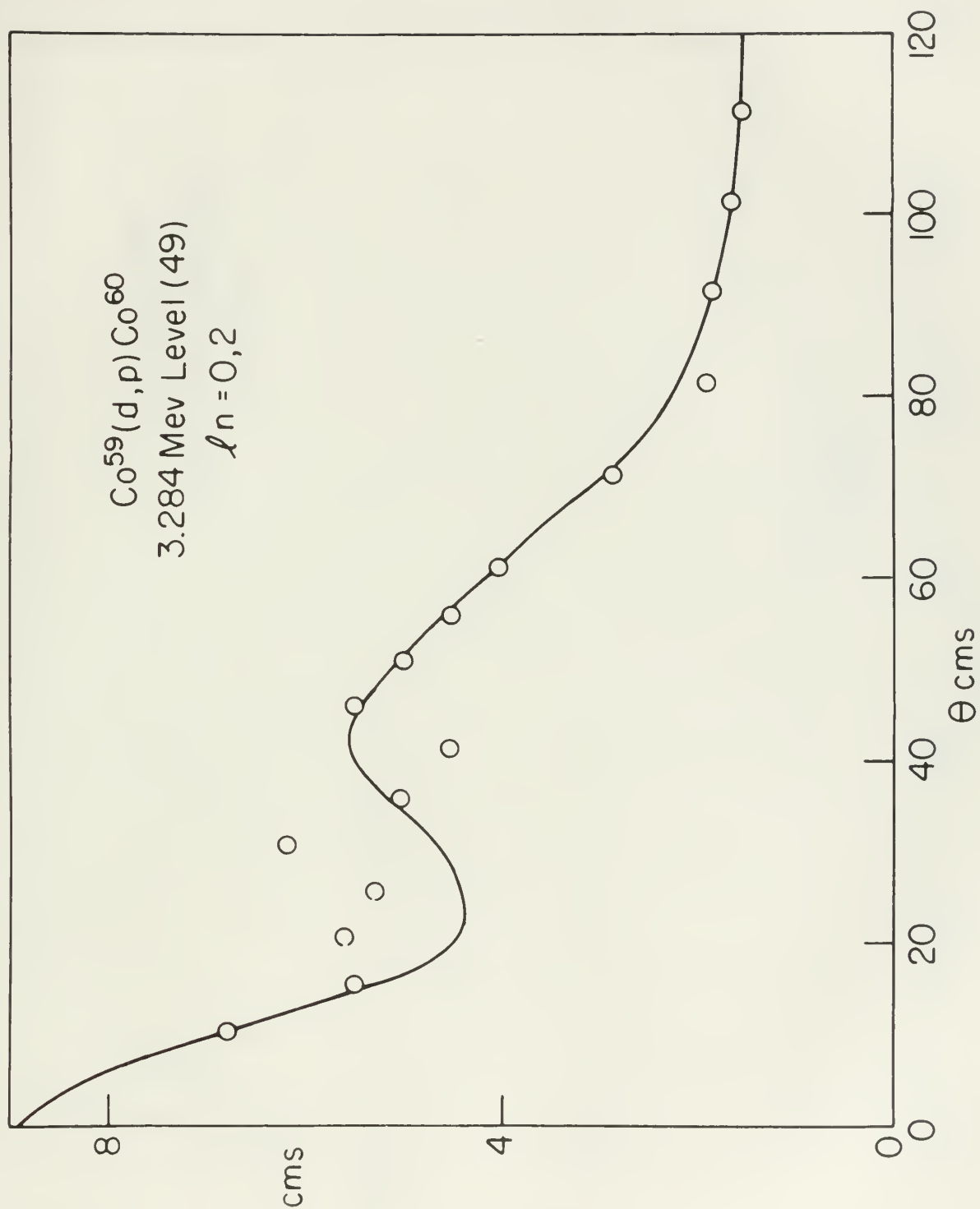


Figure 28

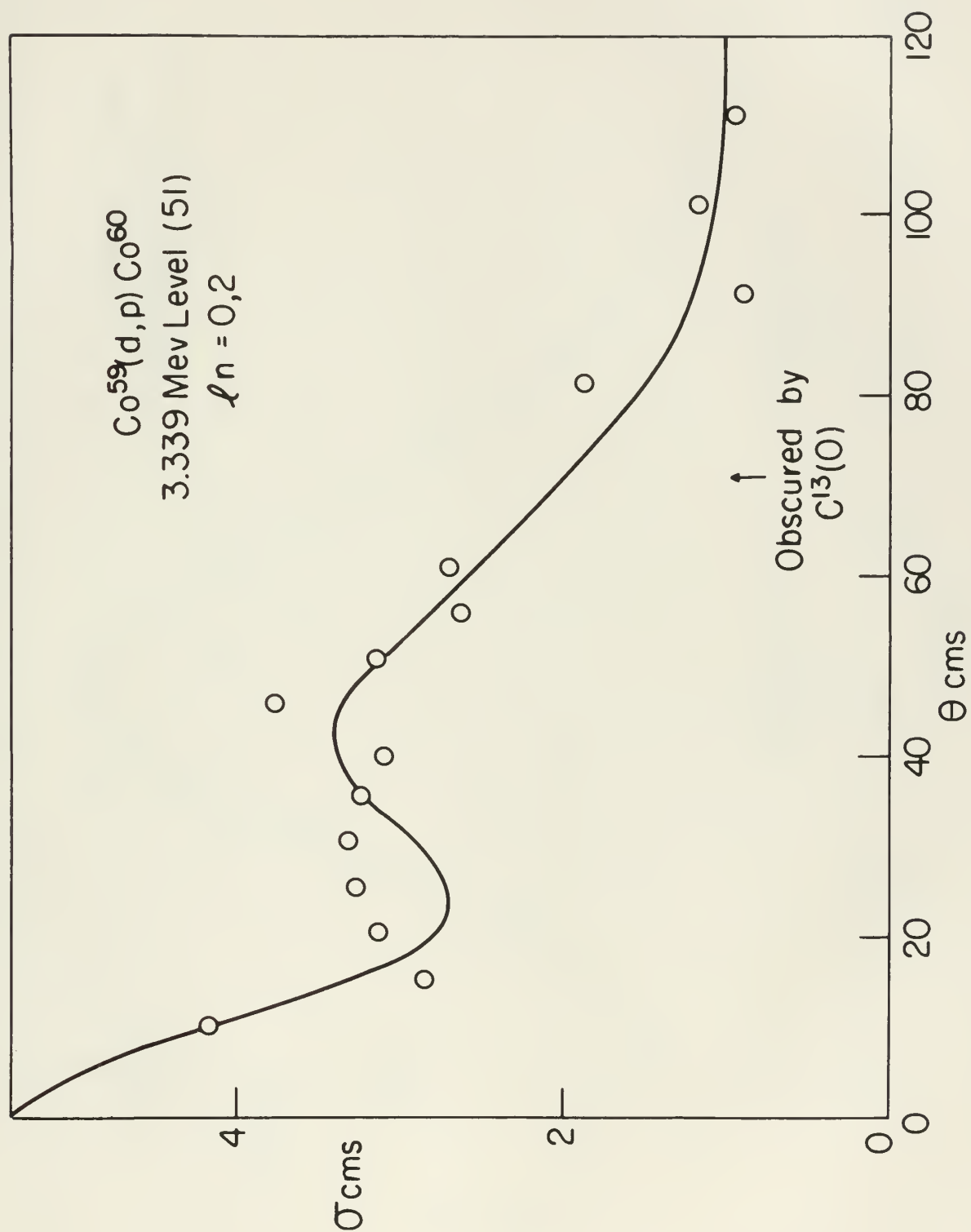


Figure 29

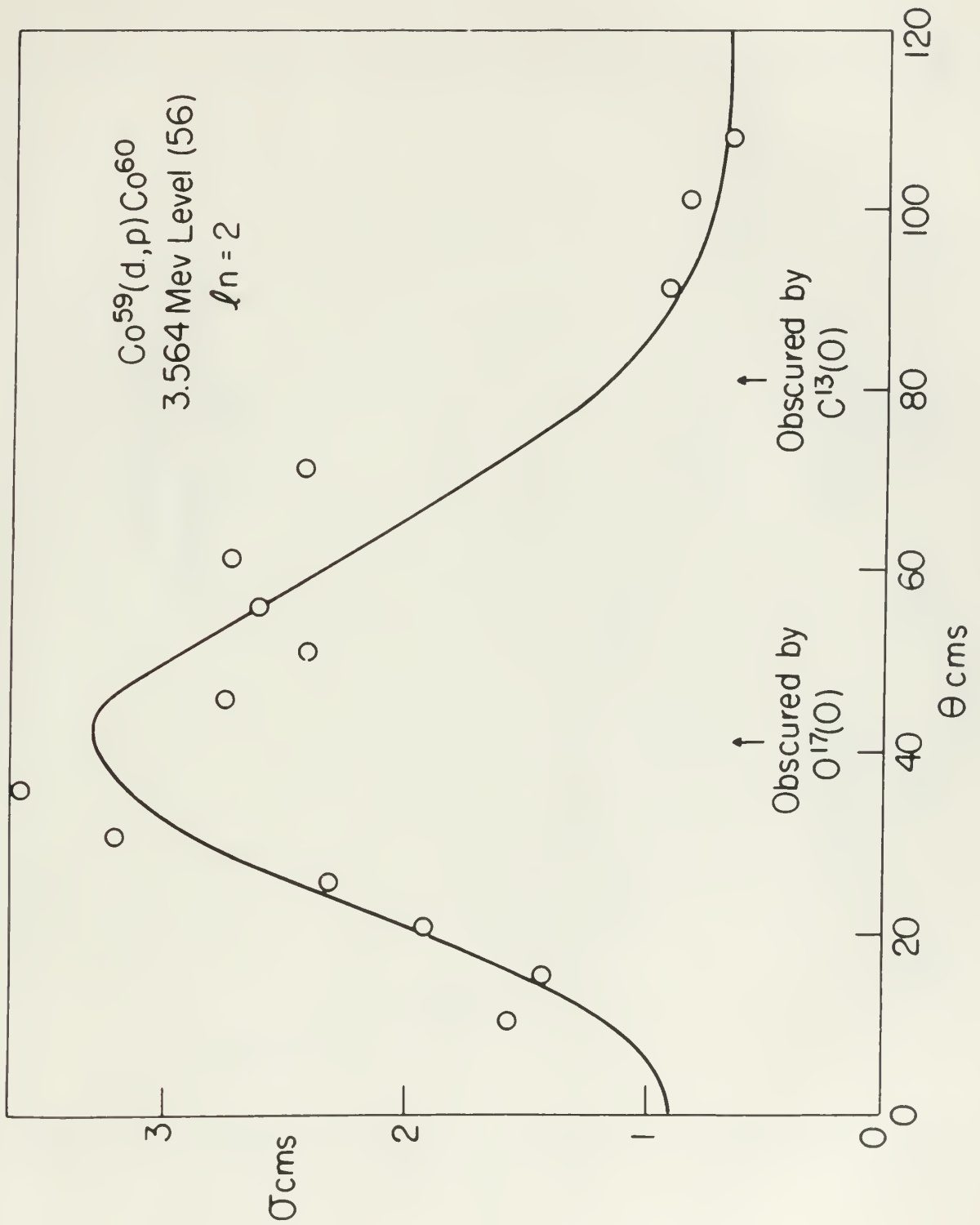


Figure 30

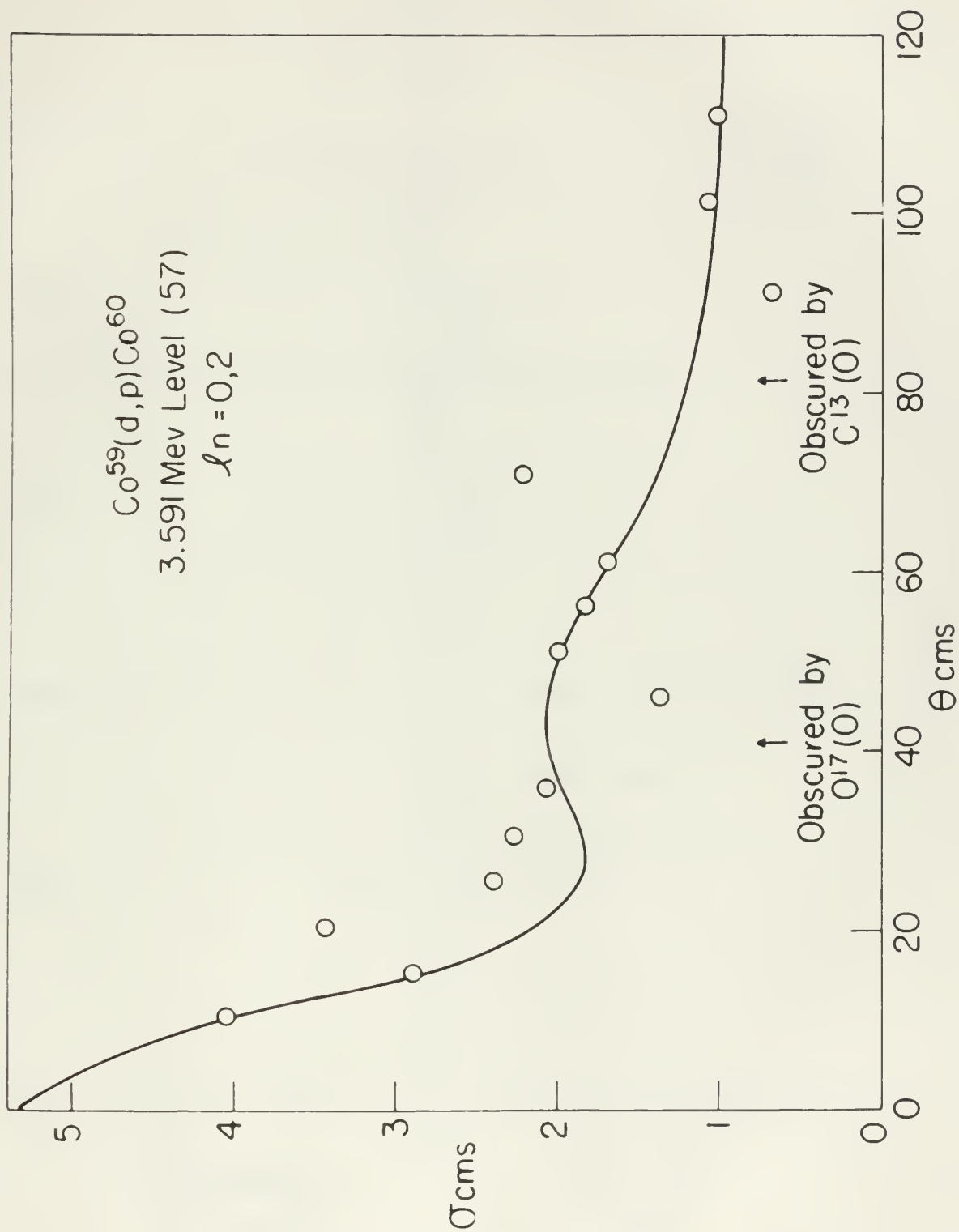
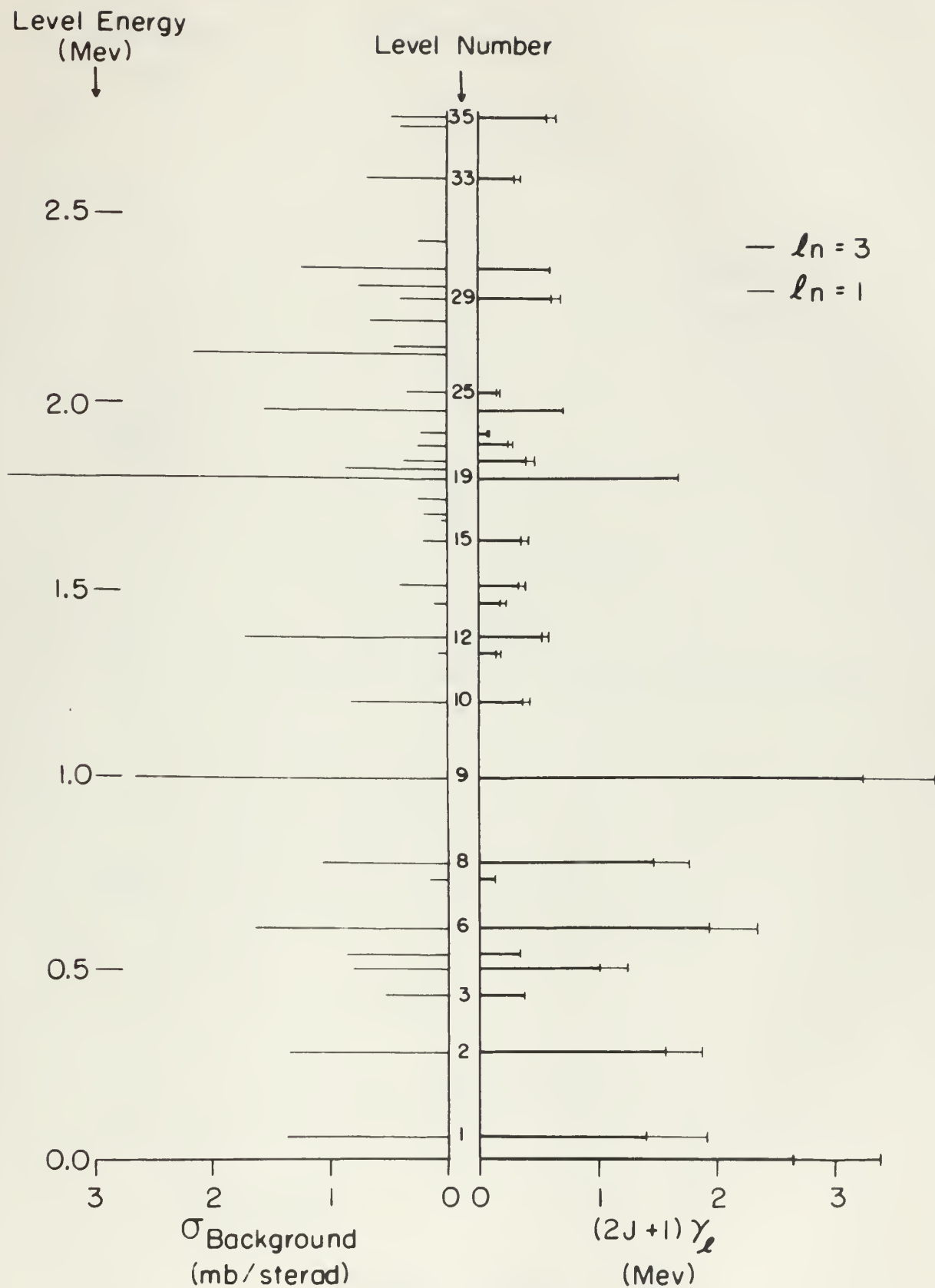


Figure 31



EXCITED LEVELS OF Co^{60}

Figure 32

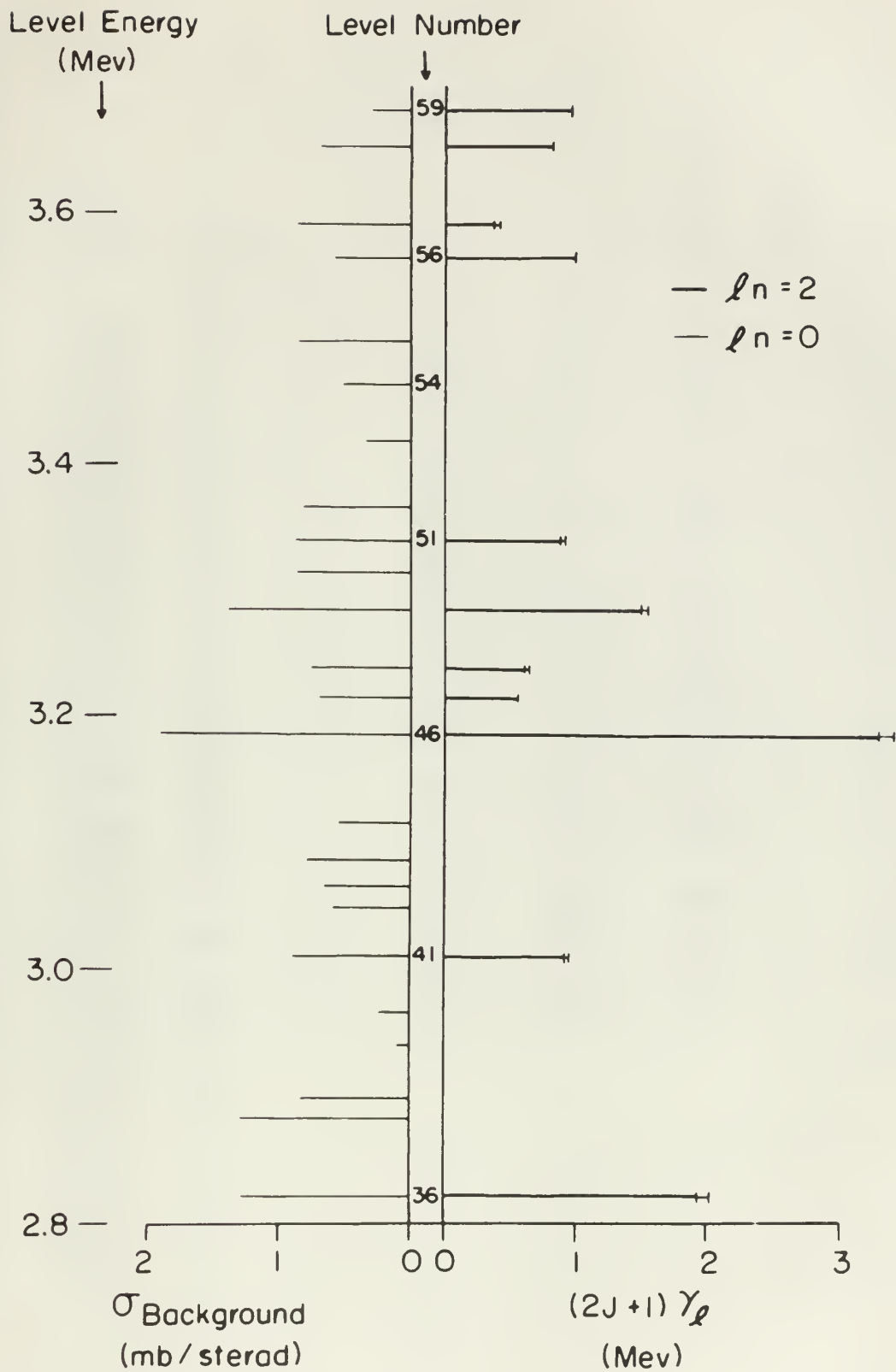


Figure 33

TABLE VII
Summary of Calculations

<u>Level No.</u>	<u>Excit. Energy</u>	<u>σ_{bkgnd}</u>	<u>ℓ_n</u>	<u>$(2J+1)\gamma_3$</u>	<u>$(2J+1)\gamma_1$</u>	<u>γ_1/γ_3</u>	<u>Par- ity</u>	<u>(a)</u>
0	0	3.00	1,3	2.635	0.726	0.276	+	1.155
1	0.058	1.38	1,3	1.472	0.453	0.308	+	1.15
2	0.282	1.34	1,3	1.558	0.322	0.206	+	1.12
3	0.432	0.58	3	0.382	0	0	+	1.11
4	0.501	0.83	1,3	1.021	0.230	0.225	+	1.105
5	0.541	0.88	3	0.347	0	0	+	1.105
6	0.612	1.65	1,3	1.949	0.386	0.198	+	1.10
7	0.738	0.17	1,3	0.130	0.014	0.108	+	
8	0.783	1.08	1,3	1.468	0.302	0.206	+	1.08
9	1.006	2.65	1,3	3.248	0.581	0.179	+	1.06
10	1.207	0.84	1,3	0.397	0.042	0.105	+	1.05
11	1.337	0.08	1,3	0.158	0.023	0.144	+	
12	1.377	1.71	1,3	0.643	0.062	0.097	+	1.035
13	1.447	0.12	1,3	0.190	0.028	0.148	+	

TABLE VII

Summary of Calculations

Level	Height	On	ft	(51+1)Y3	(51+1)Y1	Y1/13	Y2	(a)
0	0	3.00	1.3	5.232	0.150	0.510	+	1.122
1	0.028	1.38	1.3	1.115	0.153	0.308	+	1.12
2	0.585	1.31	1.3	1.228	0.355	0.500	+	1.15
3	0.132	0.28	3	0.385	0	0	+	1.11
4	0.201	0.13	1.3	1.051	0.530	0.522	+	1.102
5	0.211	0.15	3	0.311	0	0	+	1.102
6	0.015	1.02	1.3	1.015	0.388	0.128	+	1.10
7	0.132	0.11	1.3	0.130	0.011	0.120	+	
8	0.183	1.08	1.3	1.188	0.305	0.500	+	1.09
9	1.000	5.02	1.3	3.513	0.281	0.112	+	1.00
10	1.501	0.01	1.3	0.321	0.015	0.102	+	1.02
11	1.331	0.08	1.3	0.120	0.053	0.111	+	
12	1.311	1.11	1.3	0.013	0.003	0.031	+	1.032
13	1.111	0.15	1.3	0.120	0.055	0.110	+	

<u>Level No.</u>	<u>Energy</u>	<u>σ_{bkgnd}</u>	<u>ℓ_n</u>	<u>$(2J+1)\gamma_3$</u>	<u>$(2J+1)\gamma_1$</u>	<u>γ_1/γ_3</u>	<u>Par- ity</u>	<u>(a)</u>
14	1.512	0.41	1,3	0.347	0.065	0.189	+	1.025
15	1.638	0.22	1,3	0.364	0.048	0.131	+	
16	1.684	0.06						
17	1.707	0.20						
18	1.748	0.27						
19	1.799	3.75	3	1.700	0	0	+	1.000
20	1.829	0.87						
21	1.850	0.40	1,3	0.407	0.073	0.178	+	0.995
22	1.887	0.26	1,3	0.259	0.034	0.131	+	
23	1.923	0.24	1,3	0.077	0.020	0.259	+	
24	1.979	1.56	3	0.726	0	0	+	0.985
25	2.031	0.35	1,3	0.170	0.032	0.190	+	
26	2.131	2.17						
27	2.150	0.48						
28	2.217	0.38						
29	2.274	0.44	1,3	0.639	0.074	0.115	+	0.970
30	2.310	0.77						
31	2.348	1.25	3	0.618	0	0	+	0.960
32	2.427	0.26						
33	2.591	0.70	1,3	0.299	0.058	0.193	+	
34	2.734	0.42						
35	2.762	0.47	1,3	0.592	0.086	0.145	+	0.935

Level No.	Interval	Co-ordinates	n	$\Sigma y(1+y)$	$\Sigma y(1+y)^2$	Σy^2	Sign	(a)
14	1.215	0.41	1.3	0.341	0.008	0.186	+	1.082
15	1.434	0.55	1.3	0.364	0.009	0.171	+	
16	1.654	0.00						
17	1.701	0.50	1.3				+	
18	1.748	0.51	1.3				+	
19	1.795	2.12	3	1.100	0	0	+	1.000
20	1.852	0.41						
21	1.850	0.40	1.3	0.101	0.013	0.114	+	0.252
22	1.921	0.54	1.3	0.524	0.034	0.131	+	
23	1.983	0.54	1.3	0.411	0.050	0.522	+	
24	1.925	1.20	3	0.150	0	0	+	0.202
25	2.021	0.52	1.3	0.110	0.035	0.120	+	
26	2.127	5.11					+	
27	2.150	0.48	1.3				+	
28	2.211	0.28	1.3				+	
29	2.254	0.44	1.3	0.633	0.054	0.112	+	0.210
30	2.310	0.11						
31	2.340	1.22	3	0.618	0	0	+	0.200
32	2.451	0.26						
33	2.521	0.40	1.3	0.532	0.059	0.123	+	
34	2.534	0.45						
35	2.545	0.41	1.3	0.222	0.004	0.122	+	0.232

Level No.	Energy	σ_{bkgnd}	ℓ_n	$(2J+1)\gamma_2$	$(2J+1)\gamma_0$	γ_0/γ_2	Par- ity	(a)
36	2.845	1.30	0,2	1.930	0.032	0.0425	-	0.930
37	2.834	1.30						
38	2.899	0.83						
39	2.942	0.13						
40	2.967	0.26						
41	3.010	0.90	0,2	0.917	0.032	0.0340	-	0.917
42	3.048	0.60						
43	3.065	0.66						
44	3.086	0.80						
45	3.115	0.56						
46	3.185	1.95	0,2	3.300	0.107	0.0324	-	0.905
47	3.215	0.71	2	0.570	0	0	-	
48	3.238	0.77	0,2	0.610	0.022	0.0362	-	0.903
49	3.284	1.40	0,2	1.491	0.045	0.0303	-	0.900
50	3.314	0.88						
51	3.339	0.90	0,2	0.890	0.027	0.0304	-	0.896
52	3.367	0.82						
53	3.419	0.34						
54	3.464	0.53						
55	3.498	0.89						
56	3.564	0.59	2	1.002	0	0	-	0.881
57	3.591	0.88	0,2	0.382	0.028	0.0734	-	0.880
58	3.653	0.71	2	0.836	0	0	-	
59	3.682	0.32	2	0.972	0	0	-	

(a) = solid angle correction to σ in Figures 6 - 31.

Level	Station	Height	Distance	Angle	Time	Remarks	Notes
36	101.1	1.30	0.00	0.00	0.00		
37	101.1	1.30	0.00	0.00	0.00		
38	101.1	1.30	0.00	0.00	0.00		
39	101.1	1.30	0.00	0.00	0.00		
40	101.1	1.30	0.00	0.00	0.00		
41	101.1	1.30	0.00	0.00	0.00		
42	101.1	1.30	0.00	0.00	0.00		
43	101.1	1.30	0.00	0.00	0.00		
44	101.1	1.30	0.00	0.00	0.00		
45	101.1	1.30	0.00	0.00	0.00		
46	101.1	1.30	0.00	0.00	0.00		
47	101.1	1.30	0.00	0.00	0.00		
48	101.1	1.30	0.00	0.00	0.00		
49	101.1	1.30	0.00	0.00	0.00		
50	101.1	1.30	0.00	0.00	0.00		
51	101.1	1.30	0.00	0.00	0.00		
52	101.1	1.30	0.00	0.00	0.00		
53	101.1	1.30	0.00	0.00	0.00		
54	101.1	1.30	0.00	0.00	0.00		
55	101.1	1.30	0.00	0.00	0.00		
56	101.1	1.30	0.00	0.00	0.00		
57	101.1	1.30	0.00	0.00	0.00		
58	101.1	1.30	0.00	0.00	0.00		
59	101.1	1.30	0.00	0.00	0.00		
60	101.1	1.30	0.00	0.00	0.00		
61	101.1	1.30	0.00	0.00	0.00		
62	101.1	1.30	0.00	0.00	0.00		
63	101.1	1.30	0.00	0.00	0.00		
64	101.1	1.30	0.00	0.00	0.00		
65	101.1	1.30	0.00	0.00	0.00		
66	101.1	1.30	0.00	0.00	0.00		
67	101.1	1.30	0.00	0.00	0.00		
68	101.1	1.30	0.00	0.00	0.00		
69	101.1	1.30	0.00	0.00	0.00		
70	101.1	1.30	0.00	0.00	0.00		
71	101.1	1.30	0.00	0.00	0.00		
72	101.1	1.30	0.00	0.00	0.00		
73	101.1	1.30	0.00	0.00	0.00		
74	101.1	1.30	0.00	0.00	0.00		
75	101.1	1.30	0.00	0.00	0.00		
76	101.1	1.30	0.00	0.00	0.00		
77	101.1	1.30	0.00	0.00	0.00		
78	101.1	1.30	0.00	0.00	0.00		
79	101.1	1.30	0.00	0.00	0.00		
80	101.1	1.30	0.00	0.00	0.00		
81	101.1	1.30	0.00	0.00	0.00		
82	101.1	1.30	0.00	0.00	0.00		
83	101.1	1.30	0.00	0.00	0.00		
84	101.1	1.30	0.00	0.00	0.00		
85	101.1	1.30	0.00	0.00	0.00		
86	101.1	1.30	0.00	0.00	0.00		
87	101.1	1.30	0.00	0.00	0.00		
88	101.1	1.30	0.00	0.00	0.00		
89	101.1	1.30	0.00	0.00	0.00		
90	101.1	1.30	0.00	0.00	0.00		
91	101.1	1.30	0.00	0.00	0.00		
92	101.1	1.30	0.00	0.00	0.00		
93	101.1	1.30	0.00	0.00	0.00		
94	101.1	1.30	0.00	0.00	0.00		
95	101.1	1.30	0.00	0.00	0.00		
96	101.1	1.30	0.00	0.00	0.00		
97	101.1	1.30	0.00	0.00	0.00		
98	101.1	1.30	0.00	0.00	0.00		
99	101.1	1.30	0.00	0.00	0.00		
100	101.1	1.30	0.00	0.00	0.00		

which was not resolved from the background²⁷. Others could not be identified as stripping reactions because of large statistical or experimental fluctuations in the distributions. The background reported for these was based on a mean of the counts of all angles. This, in general, will be greater than that of a similar distribution with a stripping shape consistent enough for analysis, in which case the background is the minimum value at the higher angles.

In order to calculate the curves, a first approximation of the nuclear radius R was made by the Gamow-Critchfield formula:²⁹

$$R \approx (1.7 + 1.22 A^{1/3}) \times 10^{-13} \text{ cm}$$

which yields 6.5×10^{-13} cm for Co^{60} . The value or values of l_n for each level was determined from the angle of the maxima of the distribution in accordance with the following approximate criterion derived from experience with the curves:

l_n	0	1	2	3
Angle (low excitation)	0°	20°	42°	49°
Angle (high excitation)	0°	17°	41°	48°

All the terms in the theoretical cross-section formula are then calculated for each angle, except the parameter $(2J + 1)\gamma_l$. This term is then used to normalize the curve with the correct value of l_n to the data points at their maximum and minimum. Since 10 degrees was the smallest angle at which protons could be counted, it was used as the normalization point for $l_n = 0$.

which was not resolved from the background. Defects could not be identified as stripping reactions because of large statistical or experimental fluctuations in the distributions. The background reported for these was based on a mean of the counts at all angles. This, in general, will be greater than that of a similar distribution with a stripping shape consistent enough for analysis, in which case the background is the minimum value at the higher angles.

In order to calculate the curves, a first approximation of the nuclear radius R was made by the Gamow-Cricfield formula:²⁹

$$R = (1.7 + 1.25 A^{1/3}) \times 10^{-13} \text{ cm}$$

which yields 6.5×10^{-13} cm for Co^{60} . The values of values of ϵ_n for each level was determined from the spin of the maxima of the distribution in accordance with the following approximate criterion derived from experience with the curves:

ϵ_n	0	1	2	3
Angle (for excitation)	0°	20°	40°	60°
Angle (100% excitation)	0°	15°	40°	60°

All the curves in the theoretical cross-section formula were then calculated for each angle, except the parameter $(2\epsilon + 1)^{-1/2}$. This term is then used to normalize the curve with the correct value of ϵ_n to the data points at their maximum and minimum. Since 10 degrees was the smallest angle at which protons could be counted, it was used as the normalization point for $\epsilon_n = 0$.

The radius was then adjusted by trial and error to give the best fit to the distributions found for the levels with the largest cross sections and the lowest excitation energies at which each value of ℓ_n appeared. The radius was found to be 6.0×10^{-13} cm for $\ell_n = 0$ and $\ell_n = 1$; 4.0×10^{-13} cm for $\ell_n = 2$; and 5.5×10^{-13} cm for $\ell_n = 3$. For the levels with higher excitation energies, it was found that a smaller radius would give a better fit. This is particularly noticeable in levels numbered 12, 14, 21, 29, and 35 (Figures 16, 17, 19, 21, and 23, respectively). Because of the numerous and tedious trial-and-error calculations required and the lack of levels with small statistical fluctuations, no attempt was made to vary the radius with excitation energy.

A majority of levels investigated exhibited a mixture of two ℓ values, either 0 and 2 or 1 and 3. In order to obtain a fit for these levels, the two curves were added together. The normalization was as described above, except that a weighting factor $\gamma_\ell + 2/\gamma_\ell$ also must be determined algebraically. The true reduced width γ is a constant of the final state, but it has been placed inside the summation symbol of the cross-section equation. There it acts as a weight factor giving the relative probability of finding the neutron in one or the other of the two orbits¹⁵.

These results, which require the superposition of two curves with different ℓ_n values, have been encountered before²⁷. It was noted that some could possibly be due to the formation of a doublet level with different ℓ_n values or to the overlapping of a weak group by a stronger one or to a stripping reaction with two ℓ_n values.

The results were then adjusted by trial and error to give the best fit to the distributions found for the levels with the largest number of observations and the lowest excitation energies at which each value of ϵ appeared. The results were found to be 0.0×10^{-13} for $\epsilon = 0$ and 0.1×10^{-13} for $\epsilon = 1$; 0.0×10^{-13} for $\epsilon = 2$ and 0.5×10^{-13} for $\epsilon = 3$. For the levels with higher excitation energies, it was found that smaller results would give a better fit. Table 1, particularly columns 12, 13, 14, 15, 16, 17, 18, 19, and 20, summarizes the results of the numerous and tedious trial-and-error calculations required and the lack of levels with small excitation energies, no attempt was made to very the results with excitation energy.

A majority of levels investigated exhibited a mixture of two ϵ values, either 0 and 1 or 1 and 2. In order to obtain a fit for these levels, the two curves were added together. The normalization was as described above, except that a weighting factor $\gamma_1 + \gamma_2$ also must be determined algebraically. The true reduced width γ is a constant of the final state, but it has been placed inside the summation symbol of the cross-section equation. There is now a weight factor giving two relative probabilities of finding one neutron in one or the other of the two levels 1_2 . These results, which require the superposition of two curves with different ϵ values, have been summarized below. It was noted that some could readily be due to the formation of a doublet level with different ϵ values as in the case of a weak group by a stronger one or to a vibrating resonance with two ϵ values.

Also, it was noted that the experimental points which deviated from the curves had no consistent characteristics, except that points at 30 degrees were high for all but one of the twenty-six levels shown.

In Figures 6 and 24, the dashed lines show the individual curves calculated for each value of ℓ_n . The solid line is the sum of the two separate curves.

It was noted that the experimental points which deviated from the curves had no consistent explanation, except that some of the points were high and some low.

In Figure 6 and 7, the dashed lines show the calculated curves obtained for each value of β . The solid line is the sum of the two calculated curves.

V. CONCLUSIONS

The present investigation of the $\text{Co}^{59}(\text{d},\text{p})\text{Co}^{60}$ reaction, using the broad-range magnetic spectrograph, has resulted in the detection of several excited levels not previously reported. The Q-value of the ground level has been redetermined and agreement with previous (n,γ) results is good. An explanation for the disagreement with the previous (d,p) determination for the ground and first nine excited levels has been offered. Comparison of the excitation energies found in this investigation with those of previous (n,γ) values shows good agreement and serves to confirm the assumption that Bartholomew and Kinsey were measuring gamma rays to the ground level of Co^{60} , not the metastable level.

Agreement with Butler stripping theory seems adequate to assign values of ℓ_n with some assurance to the ground level and to twenty-five excited levels, shown in the included curves. In addition, assignments were tentatively made to eleven weaker levels. In most of the distributions analyzed, the experimental points required the superposition of two curves calculated for different values of ℓ_n . This is not surprising, because odd-odd nuclei may have quite complicated coupling of the angular momentum of the odd neutron and odd proton.

The observed values of orbital angular momentum, ℓ_n , agree with the values allowed by the coupling rules for the reported spins, J , of 5^+ and 2^+ of the ground and first excited level. It must be

V. CONCLUSIONS

The present investigation of the $Co^{59}(d,p)Co^{58}$ reaction, using the direct-range magnetic spectrograph, has resulted in the determination of several excited levels and previously reported levels. The Q -value of the ground level has been redetermined and agreement with previous results is good. An explanation for the disagreement with the previous Q -value determination for the ground and first two excited levels has been offered. Comparison of the excitation energies found in this investigation with those of neutron (n,p) values shows good agreement and serves to confirm the assumption that Bartholomew and Kinsey were measuring Q -values to the ground level of Co^{58} , not the metastable level.

Agreement with earlier stripping theory seems adequate to assign values of J^π with some assurance to the ground level and to twenty-five excited levels, shown in the included curves. In addition, assignments were tentatively made to eleven weaker levels. In most of the distributions analyzed, the experimental points required the superposition of two curves calculated for different values of J^π . This is not surprising, because odd-odd nuclei are known to exhibit excited coupling of the angular momentum of the odd neutron and odd proton.

The observed values of orbital angular momentum, l , agree with the values allowed by the coupling rules for the reported spins, J , of 2^+ and 2^- of the ground and first excited level. It must be

noted that, when several different values of ℓ_n are allowed by the coupling rules, the lowest value of ℓ_n can be determined, but higher values may be missed. This is explained by the behavior of the cross section for the stripping reaction, which decreases rapidly as ℓ_n increases.

The J-values derived from the coupling rules, using the known value $I = 7/2^-$ for Co^{59} and the observed ℓ_n , agree with the J-values allowed by the shell model for the thirty-third neutron being accepted into a $p_{3/2}$ state for $\ell_n = 1$. Agreement is also found for acceptance of the thirty-third neutron into the $p_{1/2}$, $p_{3/2}$, or $f_{5/2}$ states for observed $\ell_n = 1$ or 3.

The observed values $\ell_n = 0, 2$ are consistent with the assignment of the accepted neutron into the $g_{9/2}$ state. With $\ell_n = 0$, the J-values are limited to 3 or 4 from coupling rules.

It is noted that the values of $(2J + 1)\gamma_\ell$ are found to be larger for the $\ell_n = 3$ or 2 when these appear in combination with an $\ell_n = 1$ or 0, respectively.

The survey of the assignments of J-values to the ground and first excited levels was reviewed in the Introduction. Using the values for $(2J + 1)\gamma_3$ of 2.635 and 1.472, respectively, as reported in Table VII, simple calculations were made to test these assignments. If the ground level was assumed to have $J = 5$, the first excited level is found to have $(2J + 1) = 6.15$, instead of 5 as required by the $J = 2$ assignment. This represents an error of 23 percent. Now, if $J = 4$ is assumed for the ground level, the $(2J + 1)$

noted that, when several different values of δ are allowed by the coupling rules, the lowest value of δ can be determined, and higher values may be missed. This is explained by the behavior of the cross section for the stripping reaction, which decreases rapidly as δ increases.

The δ -values derived from the coupling rules, using the known value $I = \sqrt{2}$ for 60° and the observed δ , agree with the δ -values allowed by the shell model for the first three states being assigned with a $\sqrt{2}$ factor for $\delta = 1$. Agreement is also found for assignments at the higher-order states into the $2\frac{1}{2}^+$, $3\frac{1}{2}^+$, or $4\frac{1}{2}^+$ states for observed $\delta = 1$ or 2 .

The observed values $\delta = 0, 2$ are consistent with the assignment of the assigned numbers into the $2\frac{1}{2}^+$ state, with $\delta = 0$, for δ -values are limited to 1 or 2 from coupling rules.

It is noted that the values of $(2i + 1)^2$ are found to be larger for the $\delta = 3$ or 2 than those given in combination with $\delta = 1$ or 0 , respectively.

The survey of the assignments of δ -values in the ground and first excited levels was reviewed in the Introduction. Using the values for $(2i + 1)^2$ of 2.00, 3.00, and 4.00, respectively, as reported in Table VII, simple calculations were made to test these assignments. In the ground level we assume $i = 2$, the first excited level is found to have $(2i + 1)^2 = 3.00$, instead of 2 as reported by the $i = 1$ assignment. This represents an error of 50 percent. Now, if $i = 1$ is assumed for the ground level, the $(2i + 1)^2$

term for the first excited state is found to be 5.22, instead of the 3 which would correspond to $J = 1$. This error is about 68 per cent. Since these errors are a measure of the departure of the observed (d,p) cross sections from theory, the present work clearly supports the assignments to the ground and first excited level of $J = 5^+$ and 2^+ , rather than 4^+ and 1^+ , respectively.

No conclusive assignments of J -values or of γ , could be made on the basis of the observed results.

on the basis of the observed results.

B I B L I O G R A P H Y

1. Mazari, Sperduto, and Buechner, Annual Progress Report, LNS, MIT,
May 31, 1956.
2. G. M. Foglesong and D. G. Foxwell, Phys. Rev. 96, 1001, (1954).
3. G. A. Bartholomew and B. B. Kinsey, Phys. Rev. 89, 386 (1953).
4. Elementary Theory of Nuclear Shell Structure, M. G. Mayer and
J. Hans D. Jensen, John Wiley + Sons, New York, 1955.
5. H. E. Walchli, ORNL Report 1469 (1953), quoted in Mayer and
Jensen, reference 4.
6. Dobrowski, Jones, and Jeffries, Phys. Rev. 101, 1001 (1956).
7. Wheatley, Huiskamp, Diddens, Steenland, and Tolhoek, Physica,
21, 841 (1955).
8. G. L. Keister and F. H. Schmidt, Phys. Rev. 93, 140 (1954).
9. M. Deutsch and G. Scharff-Goldhaber, Phys. Rev. 83, 1059
(L)(1951).
10. J. L. Wolfson, Can. J. Phys. 34, 256 (1956).
11. S. T. Butler, Proc. Roy. Soc. (London) A208, 559 (1951).
12. Bhatia, Huang, Huby, and Newns, Phil. Mag. (London) Ser. 7,
43, 340 (1952).
13. P. B. Daitch and J. B. French, Phys. Rev. 87, 900 (1952).
14. F. L. Friedman and W. Tobocman, Phys. Rev. 92, 93 (1953).
15. H. A. Enge and A. Graue, Universitetet i Bergen, Arbok 1955,
Nat. Vitensk. rekke, nr. 13; Rev. Sci. Instr. 27, 1078 (1956).
16. Buechner, Sperduto, Browne, and Bockelman, Phys. Rev. 91, 1502
(1953).

17. C. P. Browne and W. W. Buechner, Rev. Sci. Instr. 27, 899 (1956).
18. Bockelman, Braams, Browne, Buechner, Sharp, and Sperduto, Phys. Rev. 107 (to be published July 1, 1957).
19. Enge, Wahlig, and Aanderaa, Rev. Sci. Instr. 28, 145 (1957).
20. H. A. Enge, Rev. Sci. Instr. 23, 599 (1952).
21. H. A. Enge, Annual Progress Report, LNS, MIT, p. 148 (May 31, 1956).
22. Buechner, Strait, Sperduto, and Malm, Phys. Rev. 76, 1543 (1949).
23. H. A. Enge, Universitetet i Bergen, Arbok 1954, Nat. Vitensk. rekke, nr. 1.
24. The Atomic Nucleus, R. D. Evans, McGraw-Hill, New York, 1955.
25. Sperduto, Buechner, Bockelman, and Browne, Phys. Rev. 96, 1316 (1954).
26. Strait, Van Patter, Buechner, and Sperduto, Phys. Rev. 81, 747 (1951).
27. Progress in Nuclear Physics, R. Huby, Section 7, edited by O. R. Frisch, Pergamon Press (London) 1953. Vol. 3.
28. D. H. Wilkinson, Phys. Rev. 105, 666 (1957).
29. Theory of Atomic Nucleus and Nuclear Energy Sources, G. Gamow and C. L. Critchfield, p. 11, Oxford University Press (Oxford) 1949.

17. G. E. Brown and W. W. Macmillan, *Rev. Sci. Instr.* 27, 634 (1956).
18. Macmillan, Brown, Macmillan, Smith, and Spedding, *ibid.*

Rev. 101 (to be published July 1, 1957).

19. Macmillan, Smith, and Spedding, *Rev. Sci. Instr.* 28, 115 (1957).
20. H. A. Brown, *Rev. Sci. Instr.* 23, 539 (1952).
21. H. A. Brown, *Annual Progress Report, LSC, MIT, E. 115 (Nov. 20,*

1956).

22. Macmillan, Smith, Spedding, and Smith, *Phys. Rev.* 104, 1213 (1957).
23. H. A. Brown, *Unpublished Report, Brookhaven Nat. Lab.*

Volume 1, 1.

24. *The Atomic Bomb*, W. W. Macmillan, McGraw-Hill, New York, 1952.
25. Spedding, Macmillan, and Brown, *Phys. Rev.* 96, 1316

(1954).

26. Smith, Van Lier, Macmillan, and Spedding, *Phys. Rev.* 91, 147

(1951).

27. *Progress in Nuclear Physics*, W. W. Macmillan, Editor, Vol. 3.

G. E. Brown, Pergamon Press (London) 1953.

28. D. H. Wilkinson, *Phys. Rev.* 102, 664 (1957).

29. *Theory of Atomic Nuclei and Nuclear Energy Sources*, G. Brown

and W. W. Macmillan, P. H. Macmillan University Press (Oxford)

1952.

JA 17 58
7 Sept. 59

BINDERY
INTERLIB
AEC

Thesis
J296

Jarrell

35887

Angular distribution of
protons from the

$\text{Co}^{59}(\text{d},\text{p})\text{Co}^{60}$ reaction.

JA 17 58
7 Sept. 59

BINDERY
INTERLIB
AEC

The
J29

Thesis
J296

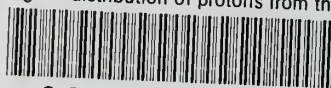
Jarrell

35887

Angular distribution of pro-
tons from the $\text{Co}^{59}(\text{d},\text{p})\text{Co}^{60}$
reaction.

thesJ296

Angular distribution of protons from the



3 2768 002 10034 9

DUDLEY KNOX LIBRARY